ANGULAR DISTRIBUTIONS OF ALPHA PARTICLES SCATTERED BY LIGHT NUCLEI

Harry J. Watters

ANGULAR DISTRIBUTIONS OF ALPHA PARTICLES SCATTERED BY LIGHT NUCLEI

by

Harry J. Watters
Lieutenant Commander, U. S. Navy
B. S. Purdue University (1949)
M. S. Massachusetts Institute of Technology (1953)

SUBMITTED IN PARTIAL FULFILLMENT OF THE
REQUIRSMENTS FOR THE DEGREE OF
DOCTOR OF PHILOSOPHY

at the

MASSACHUSETTS INSTITUTE OF TECHNOLOGY
1956

ANGULAR DISTRIBUTIONS OF ALPHA PARTICLES SCATTERED BY LIGHT NUCLEI

Harry J. Watters

Submitted to the Department of Physics on 9 January 1956 in partial fulfillment of the requirements for the degree of Doctor of Philosophy

ABSTRACT

A study has been made of the angular distributions obtained in the (α,α) and (α,α') interactions on Li^6, C^{12}, and Mg^{24}. The M.I.T. cyclotron was utilized to obtain the 31.5-Mev alpha particles used in the bombardment of these target materials. Separation of the alpha particles from other products of the alpha induced reactions was accomplished by the use of a particle selection technique developed at the cyclotron laboratory. This equipment permitted the detection of groups of inelastically scattered alpha particles which were identified with known levels of excitation of the target nuclei.

Inelastic angular distributions were obtained for the following interactions:

$Li^6(\alpha,\alpha')Li^{6*}$	Q = -2.18 Mev	$C^{12}(\alpha,\alpha')C^{12*}$	Q = -7.65 Mev
$Li^6(\alpha,\alpha')Li^{6*}$	Q = -4.5 Mev	$Mg^{24}(\alpha,\alpha')Mg^{24*}$	Q = -1.37 Mev
$C^{12}(\alpha,\alpha')C^{12*}$	Q = -4.43 Mev	$Mg^{24}(\alpha,\alpha')Mg^{24*}$	Q = -4.12 Mev

The experimental results are shown to be in agreement with the angular distributions predicted for a direct surface interaction model.

The angular distributions of alpha particles elastically scattered by Li^6, C^{12}, and natural Mg were also obtained. These data lend support to the increasing evidence that the nuclear elastic scattering of charged particles can be interpreted in terms of an optical model represented by a complex scattering potential.

In addition, it was determined that the excitation of isotopic spin prohibited levels in Li^6 and in N^{14} occurred with a probability of less than about 5 percent that observed in the excitation of isotopic spin allowed levels of the same nuclei.

Thesis Supervisor: M. Stanley Livingston

Title: Professor of Physics

ANGULAR DISTRIBUTIONS OF ALPHA PARTICLES
SCATTERED BY LIGHT NUCLEI

Barry J. Watkins

Submitted in the Department of Physics in a January 1958 in
partial fulfillment of the requirements for the degree of
Doctor of Philosophy

ABSTRACT

A study has been made of the angular distributions observed in the (α,α) and (α,α') interactions on Li^6, C^{12}, and Mg^{24}. The R.I.U. cyclotron was utilized to obtain the 1.5-Mev alpha particles used in the bombardment of these target materials. Separations of the alpha particles from other products of the alpha induced reactions were accomplished by the use of a partially automatic technique developed at the exploratory. This equipment permitted the detection of groups of inelastically scattered alpha particles which were identified with known levels of excitation of the target nuclei.

Invariate angular distributions were obtained for the following interactions:

$Li^6(\alpha,\alpha')Li^6_{0+}$ $Q = -3.10$ Mev $C_{JE}(\alpha,\alpha)C_{JE}$ $E = -7.65$ Mev

$Li^6(\alpha,\alpha')Li^6_{0+}$ $Q = -4.8$ Mev $Mg^{24}_{0+}(\alpha,\alpha')Mg^{24}_{2+}$ $Q = -1.37$ Mev

$C^{12}_{JE}(\alpha,\alpha')C^{12}_{2+}$ $Q = -4.41$ Mev $Mg^{24}_{0+}(\alpha,\alpha')Mg^{24}_{2+}$ $Q = -4.12$ Mev

The experimental results are shown to be in agreement with the angular distributions predicted for a direct surface interaction model.

The angular distributions of alpha particles elastically scattered by Li^6, C^{12}, and natural Mg were also obtained. These data lend support to the interesting evidence that the nuclear elastic scattering of charged particles can be interpreted in terms of an optical model represented by a complex scattering potential.

In addition, it was determined that the excitation of isotope with closely spaced levels in Li^6 and in Mg^{24} occurred with a probability of less than 3 percent that observed in the excitation of isotope with widely spaced levels of the same nuclei.

Thesis Supervisor: W. Preston Slichter

Title: Professor of Physics

ACKNOWLEDGMENT

The author wishes to thank his advisor, Prof. M. S. Livingston, for his valuable advice and counsel throughout the course of this investigation. He is also grateful to Prof. V. F. Weisskopf for many informative discussions and to Prof. Martin Deutsch for his frequent suggestions and for a critical analysis of the theoretical implications of the results of this experiment.

Sincere appreciation is extended to Prof. S. D. Drell, Dr. N. S. Wall, Dr. A. M. Lane, Dr. J. W. Haffner, and Mr. L. S. Rodberg for their continued interest and advice and for many helpful suggestions.

To Mr. E. White, Mr. F. Fay, and Mr. A. Nummela, of the M.I.T. cyclotron crew, the author wishes to express his most sincere gratitude for their continual efficient and untiring assistance.

Thanks is also due to Mr. J. B. Bulkley, Executive Officer of the Radioactivity Group, for his able assistance in initiating the preliminary research of this experiment.

Above all, the author would like to thank his wife whose patience, understanding, and encouragement were of invaluable assistance during the conduct of this investigation.

TABLE OF CONTENTS

TABLE OF CONTENTS

LIST OF FIGURES

1. Geometric theory of diffraction (GTD) 1

Appendix 8

2. Comparison of experimental measurements 24

3. Experimental determination of far-field scattering matrix . . . 24

4. Illustration of multiplicative convergence of numerical algorithm for calculating matrix [Z] 32

5. Graphs comparing GTD-only and hybrid solutions 33

6. Graphs showing the GTD-only solution, known to differ from exact solution, and hybrid solutions 37

7. Typical errors resulting in approximating wave-front of reflected field by tangent sphere 38

8. Graphs of radar cross section versus aspect angle for determination of focus region 39

9. Graphs of radar cross section versus aspect angle for determination of focus region 40

10. Geometry of right circular cylinder 41

11. Comparison of experimental measurements of TE_z^i and TM_z^i scattering by right circular cylinder 42

12. Comparison of experimental measurements of TE_z^i and TM_z^i scattering by right circular cylinder 43

13. Comparison of experimental measurements of TE_z^i and TM_z^i scattering by right circular cylinder . . . . .

LIST OF TABLES

I. INTRODUCTION

It has long been recognized that a direct experimental study of the scattering of charged particles by atomic nuclei provides a valuable source of information concerning the force field of the nucleus (B1). Subsequent to the classical investigations of Rutherford (R1) and Geiger and Marsden (G5), the alpha particles from radioactive substances were used intensively in studying this and other nuclear properties (B2, R3, D1). A renewal of interest in the scattering of alpha particles has been occasioned by the high energies to which they may be accelerated in the various types of particle accelerators. The stable 31.5-Mev high intensity alpha-particle beam, recently obtained at the M.I.T. cyclotron, has proven to be of great value in extending the scope of these investigations.

The primary object of this experiment is to obtain information concerning the inelastic scattering process. Relatively little data are available concerning the (α,α') interaction due to the experimental difficulties involved. The presence of elastically scattered alpha particles, as well as the reaction products from the (α,p), (α,d), and (α,t) interactions, makes identification of the inelastically scattered particles a major problem. This difficulty is

overcome by the use of a particle selection technique developed by Aschenbrenner (A1). After suitable choice of target material (see Sec. IIIC), this technique permits the observation of separate alpha particle groups, each of which can be identified with a specific level of excitation in the target nucleus. The angular distributions of the inelastically scattered alpha particles can then be compared with those predicted by a theoretical treatment of the scattering process.

Nuclear interactions were, until recently, generally described by the compound nucleus model for nuclear reactions. This model was emphasized by Bohr in 1936 and has since been verified for a large class of nuclear reactions. It is assumed that when a target nucleus is bombarded by a charged particle, the two coalesce to form a compound nucleus in a state of excitation determined by the energy of the bombarding particle. A strong interaction between all the nucleons in the compound nucleus is assumed; the incident particle loses its independent identity and the total energy of the excited compound nucleus is shared in some way by all the nucleons present. It is postulated that the properties of the compound nucleus are independent of the mode of formation. Dissociation can occur in a great number of ways and competition among the various modes of dissociation does not

depend on the manner in which the compound nucleus was formed. Recent evidence has indicated that nuclear excitation may occur by processes which do not involve the formation of a compound nucleus. The results of the present experiment are not compatible with any known theory based on the compound nucleus interaction model.

Three interaction models are currently used to describe the excitation of atomic nuclei which results from a bombardment by charged particles (P2).

1. The statistical theory for nuclear reactions was proposed in 1940 (W4) and numerous experiments were designed to test its validity. Many of these experiments supported the theoretical predictions (B3, B4, D2). However, numerous reports such as those compiled by Cohen (C1) have disclosed discrepancies which are not explained by the statistical approach. This theory, whose model is the formation of a compound nucleus, predicts angular distributions which are symmetric about 90 degrees in the center-of-mass coordinates (H3) if:

(a) the excitation levels of the compound nucleus are so closely spaced that they may be treated statistically or,

(b) the levels are so widely separated that only one excitation level in the compound nucleus is involved in the interaction.

is involved in the interaction.

In certain special circumstances, the angular distribution need not be symmetric about 90 degrees in reactions involving formation of a compound nucleus.

2. A second model (H4, M3) is used to describe a reaction in which the target nucleus is excited through an electromagnetic interaction with the incident charged particle. The theory predicts angular distributions which depend on the energy of the incident particle and the multipole order involved in the transition.

3. As early as 1952 it was proposed (M2) that a model involving a direct interaction at the nuclear surface could be used to explain some of the experimental results which were not explained by either of the preceding theories. This concept was used with some success in studying the angular distributions obtained in (n,p) and (n,α) reactions. The theory (A4) is analogous to the deuteron stripping calculations of S. T. Butler, and predicts the differential cross section for a reaction in which the residual nucleus is excited to a specific level. The angular distribution of the reaction products depends on the angular momenta and parity of initial and final levels of the residual nucleus. This direct interaction model, with certain modifications, has been used by others (B5, C2, G1, H2) in explaining experimental results which are not in agreement with the compound

nucleus or electric excitation models. Recent evidence of a direct interaction in the inelastic scattering process is illustrated in the $Fe^{56}(p,p')Fe^{56*}$ data obtained by G. Schrank et al. (S2). The inelastic alpha-particle angular distributions obtained in the present investigation give strong support to the direct interaction process of nuclear excitation.

The properties of two of the nuclei chosen for investigation in this experiment permitted a test of the applicability of the isotopic spin selection rule in the (α,α') interaction. One of the conclusive verifications of the charge independence of nuclear forces is the validity of this selection rule in nuclear reactions (A5). Since the alpha particle and the ground levels of Li^6 and N^{14} all have T = 0, according to the isotopic spin selection rule the low-lying T = 1 levels of these nuclei should not be excited appreciably. The probability of excitation of these forbidden levels is compared experimentally with the probability for excitation of the allowed levels in the same nuclei to obtain a measure of the validity of this selection rule.

The angular distributions of alpha particles elastically scattered by Li^6, C^{12}, and natural Mg were also obtained in this investigation. Numerous experiments have been performed to observe the elastic scattering of alpha particles by light nuclei (B7, F3, R4, W5). Deviations from coulomb scattering

at angles greater than about 30 degrees were noted in these data but no analyses of the observed structure were attempted. The angular distributions of elastically scattered protons (F3) exhibited a structure suggestive of a diffraction phenomenon. Using the optical model for nucleon scattering and following the method of Feshbach et al. (F4), a theoretical angular distribution was obtained (F5) which compared favorably with the experimental data. Recent progress in interpreting data (B6) obtained in the elastic scattering of alpha particles from heavy nuclei (F1, W3) has revived an interest in the elastic scattering by light nuclei. Diffraction patterns obtained in the elastic scattering of alpha particles by light nuclei have been compared with the diffraction of light by an opaque disc (E1, T2) and by an opaque sphere (F9). In the present investigation, the elastic alpha-particle angular distributions also exhibit a structure similar to that which occurs in optical diffraction. These experimental results are compared with the diffraction of light by an opaque sphere and this interaction model is shown to be consistent with the model employed to describe the inelastic scattering data. It is also shown, however, that the elastic angular distributions are not incompatible with the theoretical predictions for scattering by a square well potential.

II. APPARATUS

A. CYCLOTRON AND EMERGENT BEAM

The high-energy alpha particles used in these experiments were produced in the M.I.T. cyclotron (L1) by accelerating doubly ionized helium atoms to an energy of approximately 31.5 Mev. The cyclotron is surrounded by 4-foot thick concrete walls which act as a radiation shield for personnel and reduce the background radiation in the scattering chamber. The scattering chamber is located in an adjacent room which has 2-foot thick concrete walls providing protection from radiation originating in the chamber. By means of a focusing magnet located in the main cyclotron vault, the external beam is directed into the scattering chamber through a tube which passes through the walls of the main vault. This tube contains a series of tantalum baffles to prevent small angle scattered particles from reaching the target, and a defining and antiscattering slit system at the scattering chamber entrance. After passing through the target, located at the center of the scattering chamber, the beam terminates in the Faraday cup in the beam catcher. The adjustable focus magnet, remotely controlled from the outside area, is set for maximum beam current in the Faraday cup as measured by a sensitive

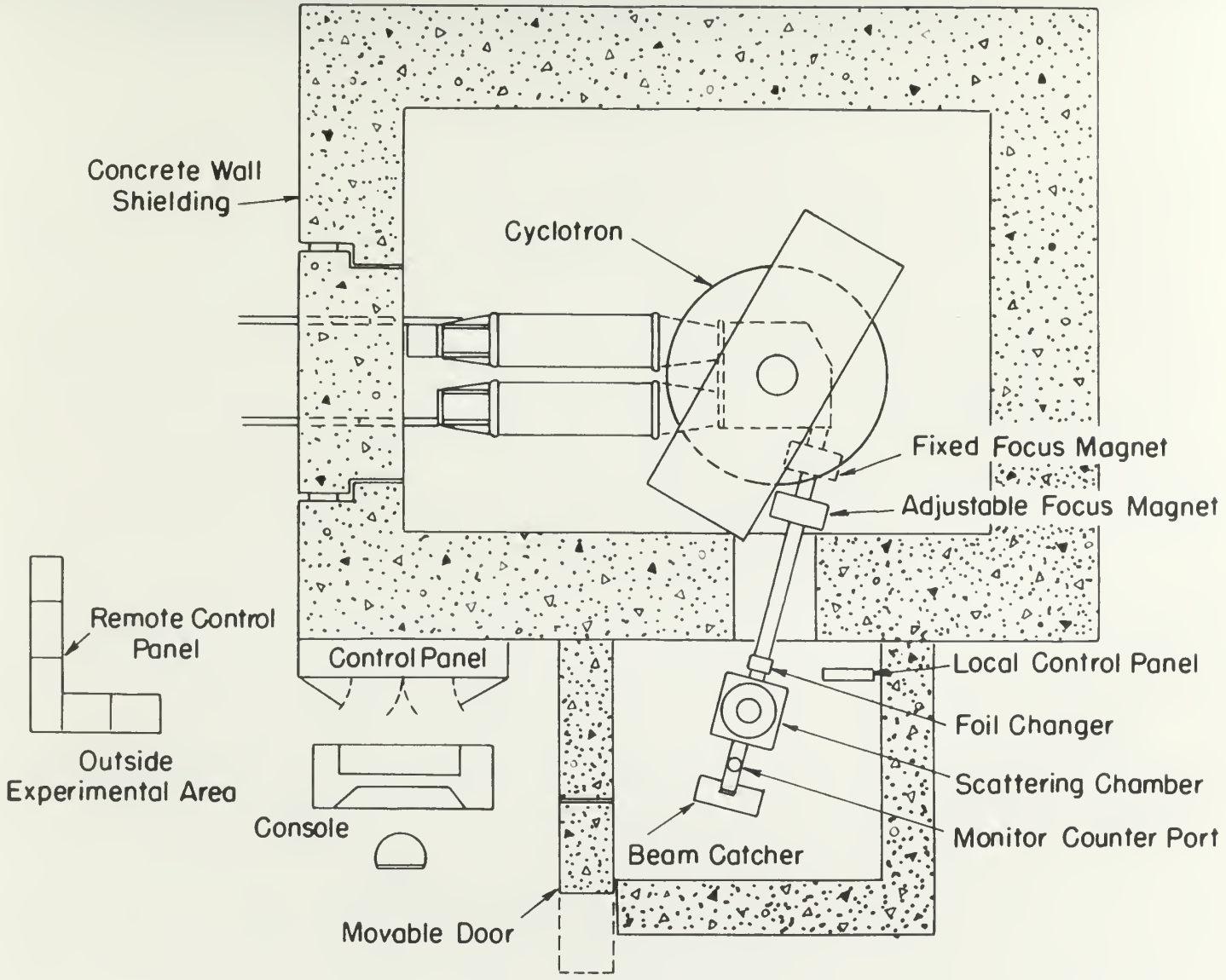
Concrete Wall Shielding
Cyclotron
Fixed Focus Magnet
Adjustable Focus Magnet
Remote Control Panel
Control Panel
Local Control Panel
Foil Changer
Scattering Chamber
Monitor Counter Port
Outside Experimental Area
Console
Beam Catcher
Movable Door

microammeter. The focusing system produces at the center of the target a spot which is 1/4 in. wide and 5/16 in. high. The foil changer contains a series of aluminum absorbers which can be inserted in or removed from the beam path by remote control, when it is desirable to vary the beam energy. A schematic diagram of the cyclotron and scattering chamber is shown in Fig. 1.

B. SCATTERING CHAMBER

A photograph of the scattering chamber, previously described by Haffner (H1), is shown in Fig. 2. The main features of this chamber are:

1. The chamber contains mounting arms for two counters. Each arm can be rotated from 0 degrees to ±175 degrees, with an accuracy of ±0.1 degree. This provides versatility in that the arrangement is excellent for particle-γ coincidence measurements and for angular correlation studies.

2. The target holder has a capacity of four and can be rotated through 360 degrees. Target choice and angular position can be controlled remotely from the outside area. The target holder can be raised into the bell jar hydraulically, in which position the scattering chamber is sealed off, and completely isolated from the bell jar. Targets can be changed

electrometer. The focusing system consists of the anode of the target a post which is 1/4 in. wide and 9/32 in. high. The foil chamber contains a device to change the foils which can be inserted in or removed from the beam path by remote control, when it is desirable to vary the beam energy. A schematic diagram of the evacuation and monitoring chamber is shown in Fig. 5.

B. SCATTERING CHAMBER

A photograph of the scattering chamber, previously described by Bellamy (B1), is shown in Fig. 6. The main features of this chamber are:

1. The rotator contains grinding arms for two monitors. Each arm can be rotated from 0 degrees to 175 degrees, with an accuracy of ±0.1 degree. This provides versatility in that the arrangement is suitable for particle-y coincidence measurements and for angular correlation studies.

2. The target holder has a capacity of four and can be rotated through 180 degrees. Target choice and angular positions can be controlled remotely from the outside area. The target holder can be raised into the well jar hydraulically, in which position the scattering chamber is sealed off, and completely isolated from the well jar. Targets can be changed

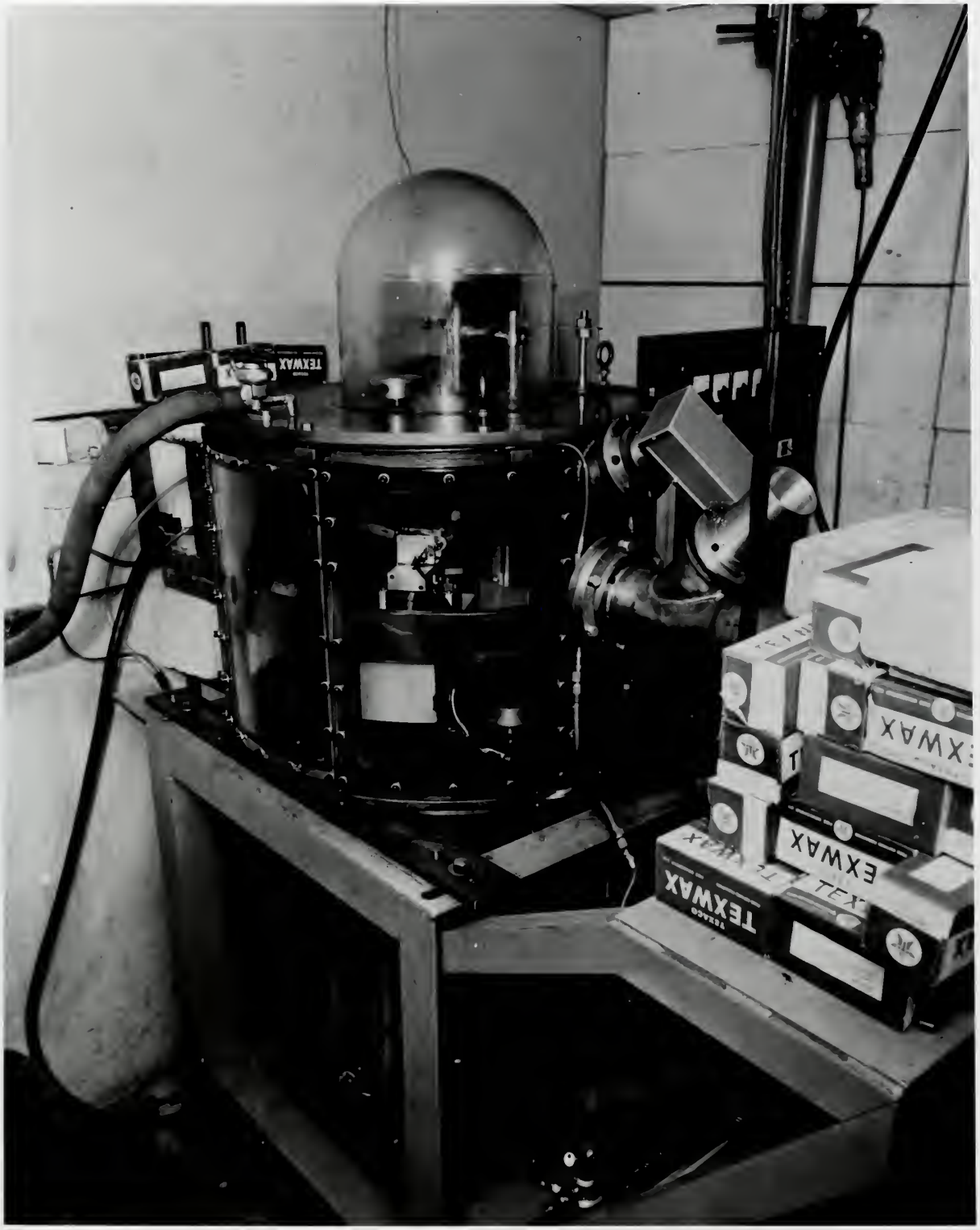

Figure 2

without affecting the scattering chamber vacuum. In addition, an evaporator is contained in the bell jar permitting targets to be made and subsequently bombarded without exposure to air.

3. The angular position of counter arms and target is measured by bridge circuits which contain precision helipots. This provides the positioning accuracy of 0.1 degree previously mentioned.

4. The angular position of counter arm or target and the choice of target can be controlled remotely from the outside area. In addition, these functions can be controlled from within the scattering chamber vault and the plexiglas windows permit visual observation of the scattering chamber interior.

C. BEAM MONITOR

The beam monitor consists of a scintillation counter mounted in a port, at an angle of 45 degrees from the incident beam, between the scattering chamber and the beam catcher. At this point a thin gold foil is fixed in the beam at an angle of 45 degrees, so that only particles scattered 45 degrees by the gold foil are "seen" by the monitor counter.

During the conduct of this experiment, the monitor discriminator was set so that the monitor scaler only counted

the elastic alpha particles scattered at 45 degrees by the gold foil. The optics of this counter is similar to that described by Stoddart and Gove (S1). The scintillation counter consists of a Dumont 6291 photomultiplier tube and a plastic* scintillator.

D. PARTICLE SELECTIVE COUNTER

It is a well established fact that the specific energy loss in traversing matter of a nonrelativistic heavy particle of a given energy is dependent upon its mass. The expression for the specific energy loss given by Livingston and Bethe (L2) can be written

$$-\frac{dE}{dx} = \frac{2\pi z^2 ze^4 NM}{mE} \ln\left(\frac{4mE}{MI}\right)$$

where Ze, M, and E are the charge, mass, and energy of the incident particle, Nz and I are the number of electrons per cm^3 and the average excitation potential of the atom of the material traversed, and m is the electron mass. For a given substance, N, z, m, and e are constant and the logarithm term is practically constant over the energy range under consideration. Therefore to a good approximation, for nonrelativistic particles the above can be written

---

* Pilot "B" - Pilot Chemicals, Inc., 47 Felton Street, Waltham, Mass.

$$\frac{dE}{dx} = \left(\frac{MZ^2}{E}\right)K$$

where K varies only slightly with energy. Then, if both dE/dx and the total energy E are known, the mass M of the particle can be determined.

A particle selection technique has been devised by Aschenbrenner utilizing the above principles. The detector consists of two scintillation counters, each using a Dumont 6291 photomultiplier tube (Fig. 3). The first crystal is a thin plastic (Pilot "B") scintillator which measures the initial specific ionization of the incident particles. The second is a thallium-activated sodium iodide crystal which measures the remaining energy of the particles after traversing the thin scintillator. The pulse height from the first photomultiplier is proportional to dE/dx since all particles traverse the same thickness of plastic scintillator. After amplification and pulse shaping, pulses from the two scintillators are added electronically to give a resultant pulse height proportional to the initial total energy E of the incident particle. The dE/dx and total energy E pulses are then multiplied electronically to give an output pulse proportional to

$$\frac{dE}{dx} = \left(\frac{dE}{dx}\right)_c$$

where E varies only slightly with energy. Then, it pays dE/dx and the total energy E are known, the mass M of the particle can be determined.

A particle selector technique has been devised by Lawrence and Cooksey and Livingston. The detector consists of two scintillation counters, each using a Dumont 6291 photomultiplier tube (Fig. 1). The first counter is a thin plastic (Pilot "B") scintillator which accepts the desired specific ionization of the incident particles. The second is a Cadmium-activated pure Iodide crystal which measures the remaining energy of the particle after traversing the thin scintillator. The pulse height from the first photomultiplier is proportional to dE/dx since all particles traverse the same thickness of plastic scintillator. After amplification the pulse heights, taken from the two scintillators are added electronically to give a resultant pulse height proportional to the total kinetic energy E of the incident particle. The dE/dx and total energy E define the mass multiplied electronically to give an output pulse proportional to

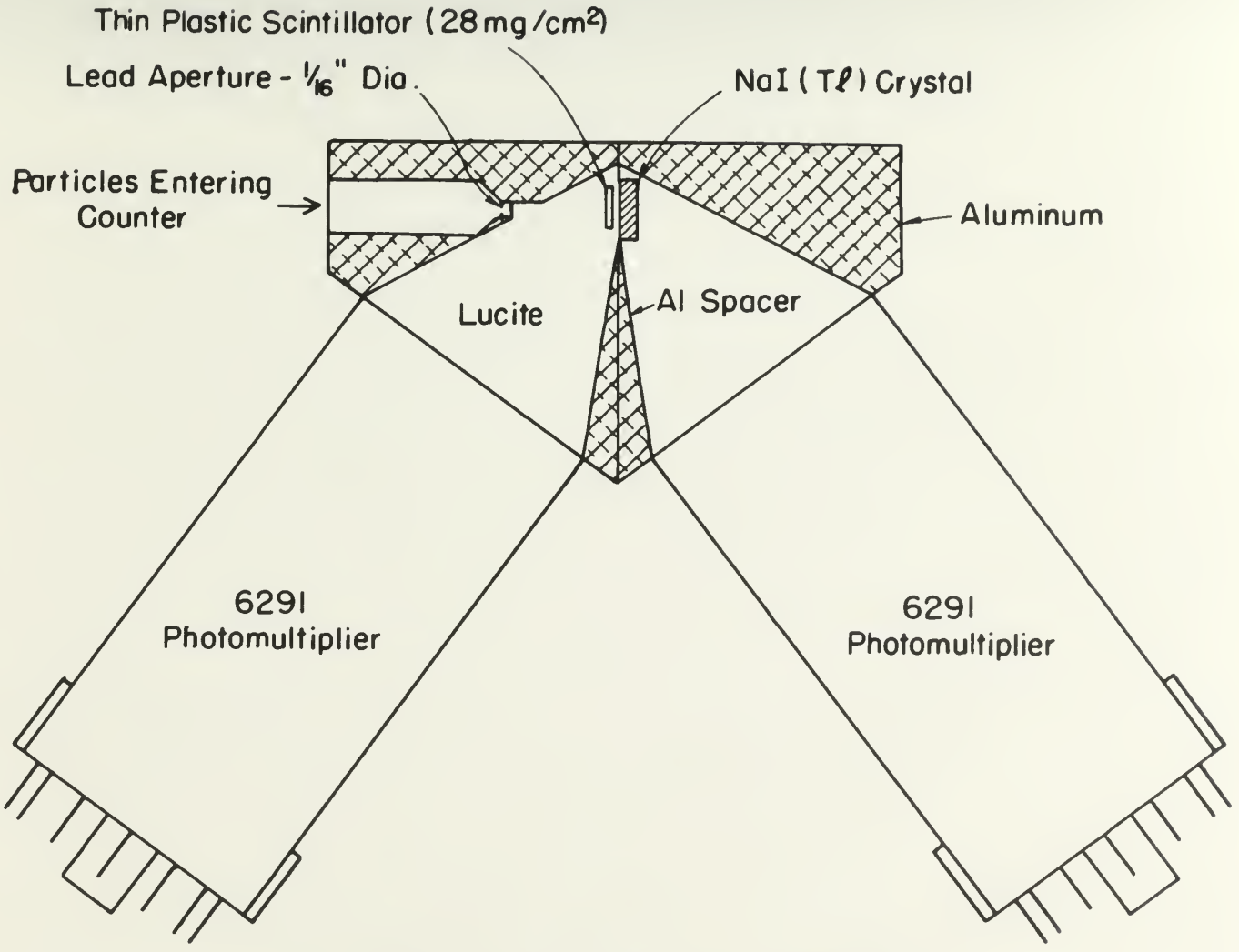

PARTICLE SELECTIVE COUNTER
SCHEMATIC DIAGRAM

$$\frac{dE}{dx} \cdot E = \left(\frac{Mz^2}{E}\right)K \cdot E \propto z^2M$$

Theoretically then, these product pulses should occur in the ratio of 1:2:3:10 for incident protons, deuterons, tritons, and alpha particles of the same energy. Due to the nonlinear response of the plastic and sodium iodide scintillators, and other effects not considered in the approximations made, the observed ratio of pulse heights deviates somewhat from this theoretical ratio. However, since these pulses are used only to identify the reaction products, the deviations do not interfere with the particle selection technique.

E. ELECTRONICS

The functions and over-all method of operation of the electronic equipment will be described for completeness. A detailed description of the electronic components including circuit diagrams has previously been described by Aschenbrenner (A1).

Pulses from the two photomultipliers feed directly into cathode followers (W1) mounted on the counter arm in the scattering chamber. The output signals are then fed to preamplifiers located in the scattering chamber vault. These three-stage preamplifiers invert the signals and the pulses

$$\frac{dx}{dt} + x = \left(\frac{\omega_0^2}{\omega_1^2}\right)\varepsilon + \varepsilon \alpha \left(\frac{\omega_0^2}{\omega_1^2}\right)$$

Theoretically then, these powder pulses should have
if the ratio of inertia for impinging neutrons, deuterons,
tritons, and alpha particles of the same energy. Due to
the destructive responses of the plastic and neutron initiated
scintillators, the alpha effects are considered in the ex-
pressions above, the observed ratio of pulse heights re-
sulted somewhat from this theoretical ratio. However, since
these values are used only to identify the reaction products,
the deviations do not introduce any serious experimental
technique.

E. CONCLUSION

The theories and mathematical method of evaluation of the
electronic equipment will be examined for completeness. A
detailed description of the electronic components including
circuit diagrams has previously been described by Lecompte
[10].

Pulses from the two photomultipliers feed directly into
cathode followers (6J) mounted on the console and to pre-
scattering monitors. The output signals are then fed to pre-
amplifiers located at the scattering chamber unit. These
three-stage transistorized boxes the signals and the pulse

are then conducted to the electronic apparatus located at the outside experimental area. Here, after suitable pulse shaping and linear amplification, the two output pulses are added electronically. This is accomplished by feeding the pulses into the grids of a double triode and superposing the plate currents through a common plate resistor. The adder output pulse is then fed to one side of the pulse multiplier. The shaped amplified pulse from the plastic scintillator provides the second input to the multiplier. Multiplication is accomplished by a 5 × 5 array of matched 6BN6 tubes whose characteristics are such that the plate output pulses are proportional to the product of the pulses fed into the two grids over a range of 0 to 15.5 volts. Phototube high voltage and amplifier gain must be such that the multiplier inputs do not exceed this range. The multiplier output then consists essentially of pulses of three heights corresponding to the alpha particles, deuterons, and protons entering the counter.

The information obtained from the particle selective counter is displayed on an oscilloscope to permit visual observation during adjustment of electronic components. The multiplier output pulses, proportional to Z^2M, are fed through a single channel pulse height analyzer and a coincidence

circuit to the Y axis of the oscilloscope. The shaped amplified NaI scintillator pulses, proportional to particle energy, provide the input to another single channel pulse height analyzer, then feed through the coincidence circuit to the X axis input. The coincidence circuit ensures that only those counts are registered which result from pulses occurring simultaneously at the two analyzer inputs. In addition, the coincidence pulses operate a trigger circuit which operates the intensifying control in the oscilloscope. Thus a particle which traverses the plastic scintillator and is stopped in the NaI crystal registers as a momentary spot on the oscilloscope face, the Y position indicating the mass and the X position the energy of the particle.

By visual observation of the oscilloscope face, the window width and bias of the pulse height analyzers can be set to exclude all but particles of a given mass, or all but particles of a given energy spread. This, of course, includes the possibility of counting all particles of a given mass and any energy or particles of any mass but with an energy which lies in a specific energy interval. Figure 4a is a photograph of the oscilloscope face showing the mass and energy spectrum of particles emitted from a C^{12} target under bombardment by 31.5-Mev alpha particles, observed at an angle of 17 degrees from the direction of the incident beam. The proton

spectrum appears as a low-energy continuum with four distinguishable higher-energy groups of which the highest is the most intense. Three separate deuteron groups and four well separated alpha-particle groups are seen.

When the bias level and window width of the analyzer fed by the multiplier are set to exclude all but pulses due to alpha particles, the spectrum appears as shown in Fig. 4b. This energy spectrum is then scanned using a method in which a single channel pulse height analyzer performs the function of a 20-channel device. By use of an external battery box, a bias range, chosen to include the desired range of pulse heights, is applied to a voltage divider consisting of 20 precision resistors. The window width of the analyzer fed by the NaI scintillator is then adjusted to a value approximately 10 percent greater than one-twentieth of the bias range chosen. This ensures a slight overlap in scanning the energy spectrum. A relay, actuated by the output from the monitor counter scaler, then steps the analyzer window through the 20 individual bias voltage increments in turn, the number of pulses corresponding to each pulse height interval being counted in separate registers. The monitor scaler only counts the alpha particles elastically scattered at 45 degrees by a gold foil. Thus by using the monitor scaler to actuate the stepping relay we ensure that each of the 20 bias increments

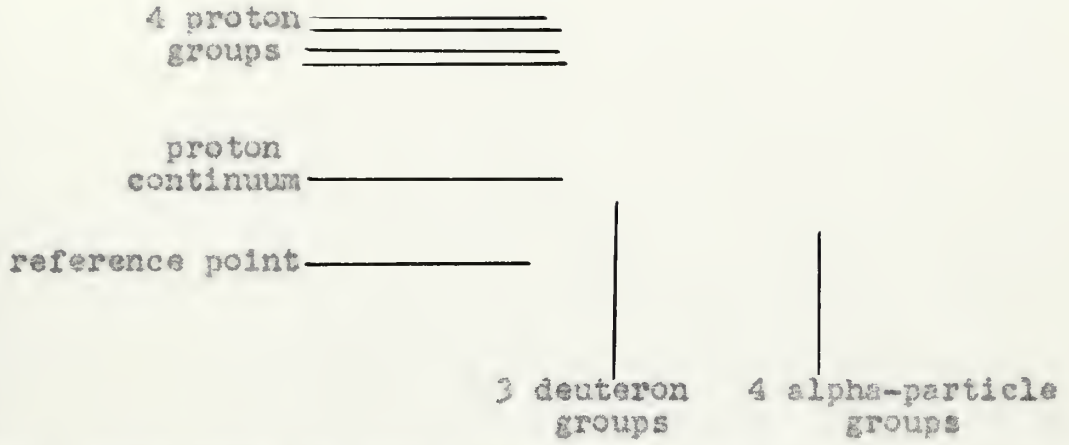

Fig. 4a. Photograph of oscilloscope presentation of mass-energy spectrum of particles emitted from a C^{12} target bombarded by 31.5-Mev alpha particles.

Fig. 4b. Energy spectrum of alpha particles, shown in Fig. 4a, obtained by proper adjustment of bias voltage of multiplier pulse height analyzer.

Fig. 9. Power spectrum of slow variation, minus its 60-cycle component, of linear voltage at plate voltage of multiplier tube during sweep.

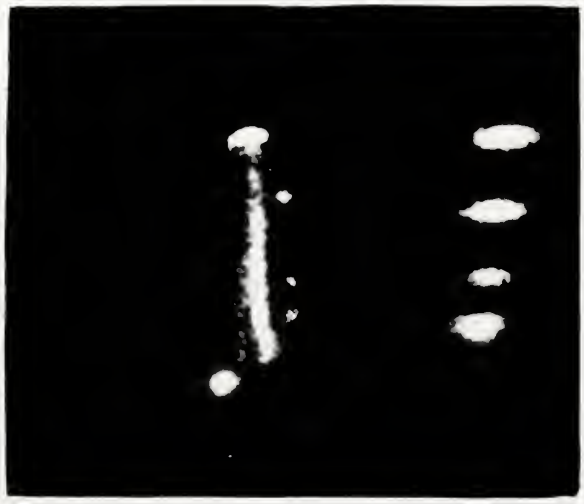

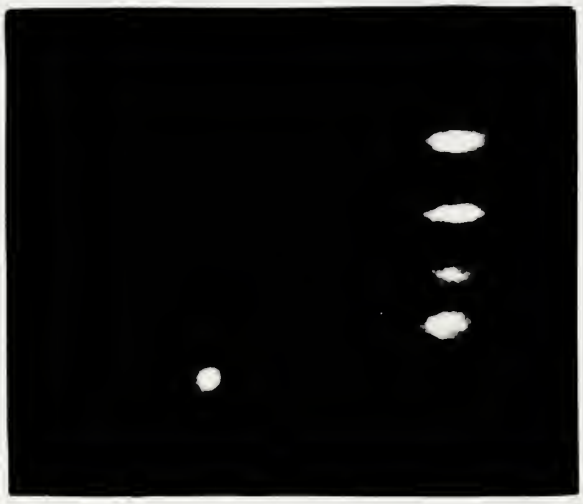

is observed for the same length of time in terms of total number of particles in the incident beam. This automatically compensates for changes in intensity of the beam during a given observation. The experimental assembly of equipment is shown functionally in the block diagram of Fig. 5.

III. PRELIMINARY CONSIDERATIONS

A. BEAM ENERGY DETERMINATION

A 1.4-mil thick natural lithium target was placed in the scattering chamber perpendicular to the beam. The particle selective counter was then used to identify the two proton groups resulting from the reaction $Li^7(a,p)Be^{10}$ $Q = -2.56$ Mev and $Li^7(a,p)Be^{10*}$ $Q = -5.94$ Mev. It was experimentally observed that the intensity of these two groups varied considerably with angle and that the ratio of intensities was smallest at about 28 degrees. The counter was then set at 28 degrees and was used to obtain the energy spectrum of protons after they pass through an aluminum absorber placed in front of the counter aperture. A linear pulse generator was used to calibrate the single channel pulse height analyzer since zero bias on this analyzer does not correspond to zero

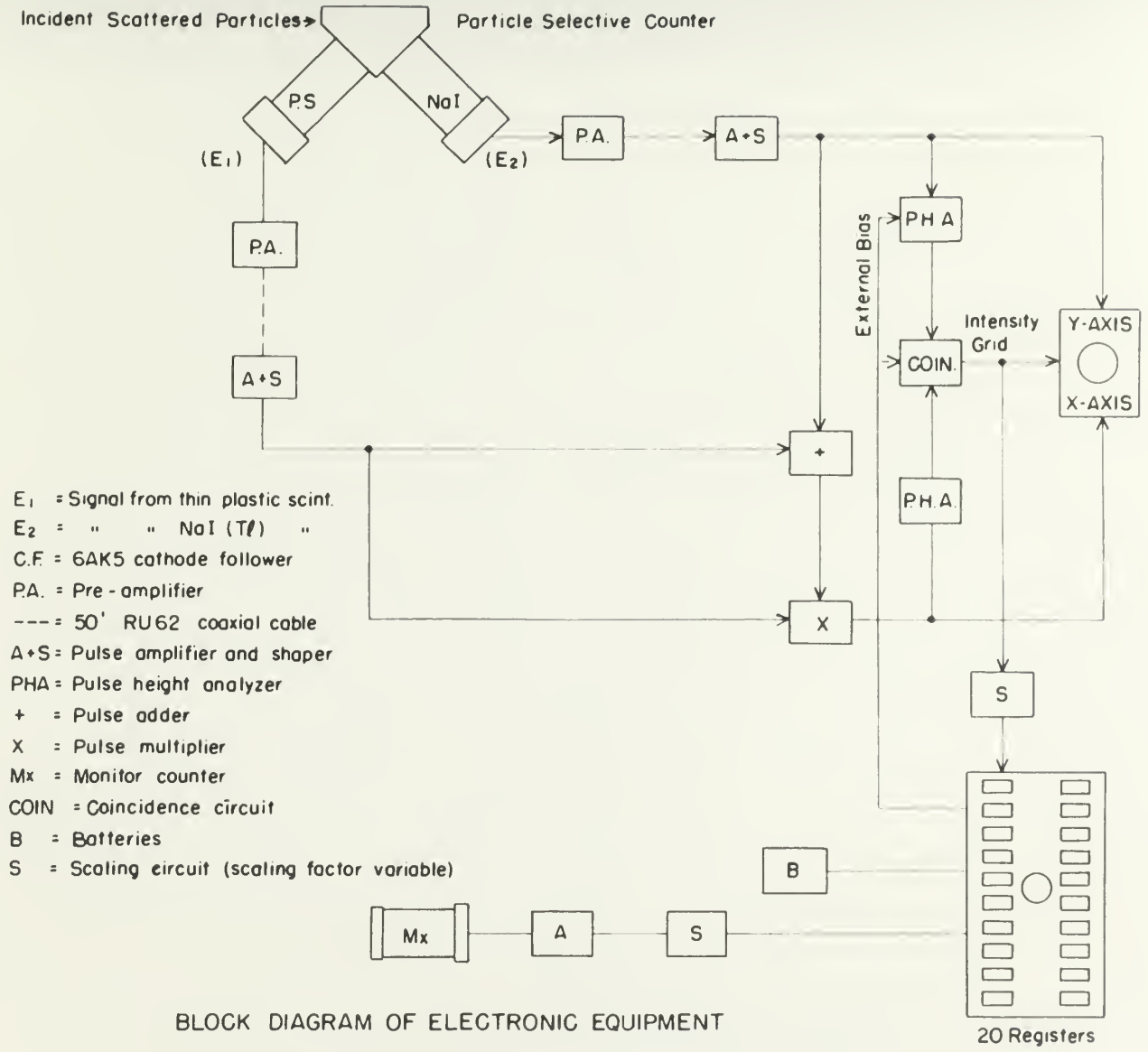

BLOCK DIAGRAM OF ELECTRONIC EQUIPMENT

Figure 5

pulse height. Spectra including these two proton peaks were taken using aluminum absorber of thicknesses 174 mg/cm^2 and 330 mg/cm^2.

If we define E_p and $E_{p'}$ as the energies of the protons incident on the NaI(Tl) crystal from the ground and first excited levels of Be^{10} respectively, then the beam energy can be determined by the ratio $E_p/E_{p'}$ since this ratio varies with beam energy as shown in Fig. 6. The beam energy was measured at frequent intervals and the 64 measurements obtained approximate a normal distribution about 31.5 Mev with 41 measurements falling inside one standard deviation. The error assigned in the energy determination includes the straggling effect in the absorbing material traversed.

B. ENERGY RESOLUTION

Since the particle selective detector consists of two scintillation counters it seemed advisable to determine the highest resolution attainable with the NaI(Tl) crystal and then to determine the effect of introducing the plastic scintillator. The plastic scintillator was removed and the counter positioned at an angle of 30 degrees with the beam. A freshly cleaved NaI(Tl) crystal was used and extreme care was taken so that the crystal had six perfectly cleaved sides

pulse height. Spectra including these two proton peaks were taken using electron observer of thicknesses 2.54 gm/cm^2 and 7.04 gm/cm^2.

If we define E_p^0 and S_p^0 as the energies of the protons incident on the Sn(II) crystal from the stopped and little scaled levels of Sm_{10} respectively, then the beam energy can be determined by the ratio E_p^0/S_p^0 since this ratio varies with beam energy as shown in Fig. 6. The beam energy was measured at frequent intervals and the 34 measurements obtained experimental a normal distribution about 11.5 Mev with 67 measurements falling inside one standard deviation. The error assigned in the energy determination including any straggling effects in the absorbing material traversed.

B. Crystal Conductivity

Since the parallel selective detector consists of two scintillation counters it seemed advisable to determine the highest resolution attainable with the Sn(II) crystal and then to determine the effect of introducing the plastic scintillator. The plastic scintillator was removed and the counter positioned at an angle of 30 degrees with the beam. A freshly cleaved Sn(II) crystal was used and extreme care was taken so that the cleaved and air reacted dirtied atoms

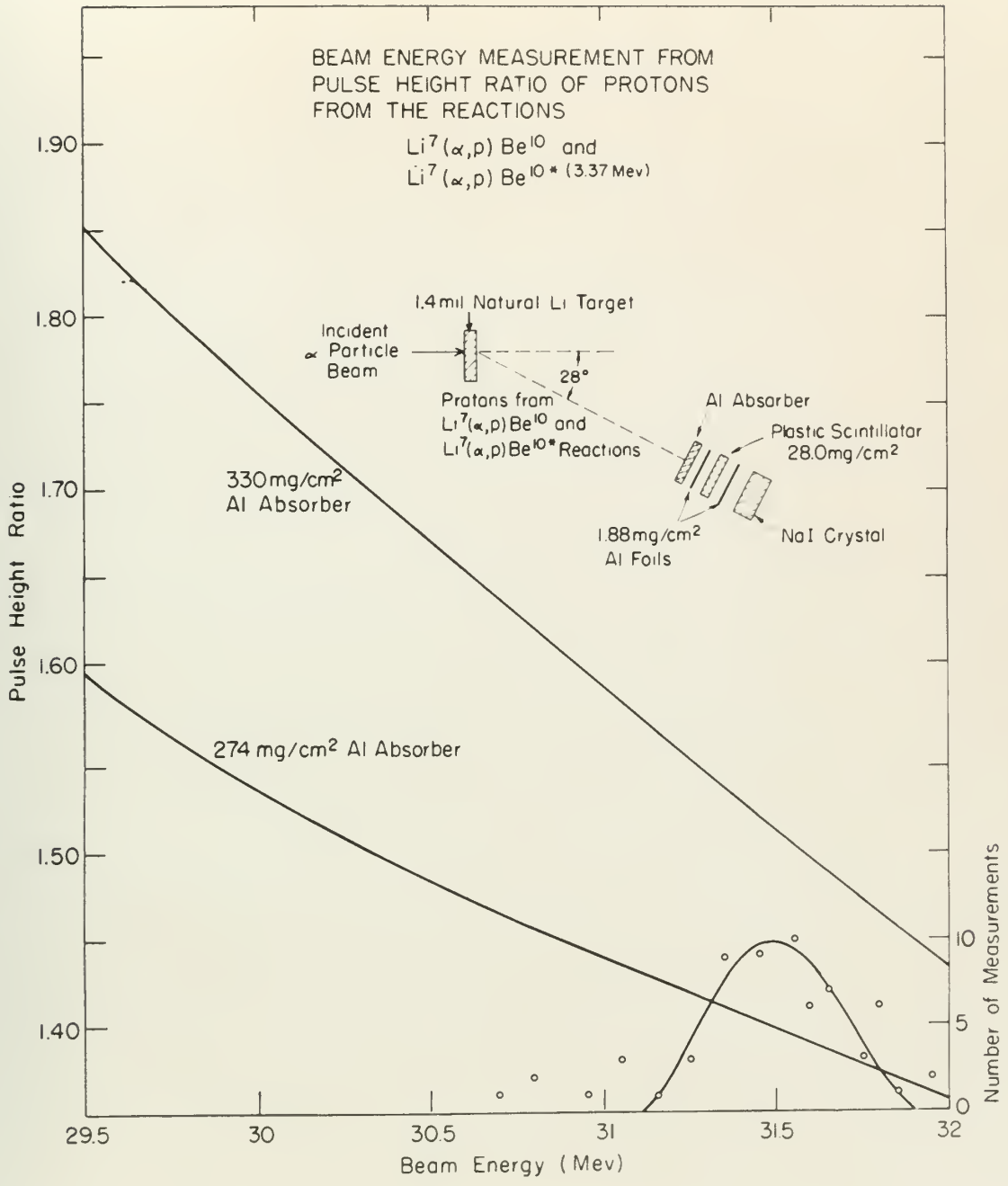
BEAM ENERGY MEASUREMENT FROM
PULSE HEIGHT RATIO OF PROTONS
FROM THE REACTIONS
Li7 (α,p) Be10 and
Li7 (α,p) Be10 * (3.37 Mev)
1.4 mil Natural Li Target
Incident
α Particle
Beam
28°
Protons from
Li7(α,p)Be10 and
Li7(α,p)Be10* Reactions
Al Absorber
Plastic Scintillator
28.0mg/cm2
1.88mg/cm2
Al Foils
NaI Crystal
330mg/cm2
Al Absorber
274 mg/cm2 Al Absorber
Pulse Height Ratio
1.90
1.80
1.70
1.60
1.50
1.40
Number of Measurements
10
5
0
29.5
30
30.5
31
31.5
32
Beam Energy (Mev)

Figure 6

with no visible imperfections of any kind. A thin (0.2 mg/cm^2) gold foil target was then positioned at an angle of 15 degrees with the beam to minimize the target thickness effect on resolution. By use of the linear pulser, the window width of the NaI pulse height analyzer was set to a minimum value which still gave a definite overlap, and the analyzer was calibrated over the 20-channel range. The energy spectrum of alpha particles was then taken and the highest attainable resolution (full width at half maximum) was found to be 1.7 percent. The plastic scintillator was then placed in position in the counter and the spectrum was taken again with identical electronic equipment settings. Under these ideal conditions of target thickness, target angle, and minimum window width, the best resolution attainable was found to be 3.8 percent. A working resolution of 4 percent was assumed which was frequently verified during subsequent experimental work.

C. TARGET CHOICE

The 4-percent energy resolution of the equipment immediately placed a limit on the number and characteristics of the target nuclei to be studied. First of all, the excitation energies of the levels to be investigated must be known. The targets should not consist of compounds but of a single element.

C. Target Choice

The 4-percent energy resolution of the equipment immediately placed a limit on the number and characteristics of the target nuclei to be studied. First of all, the excitation energies of the levels to be investigated must be known. The target should not consist of compounds but of a single element.

The presence of hydrogen contamination was permissible, however, since the elastic scattering of alpha particles from hydrogen does not occur at laboratory angles greater than 14.5 degrees.

Since it was desired to investigate at least two excited levels in each nucleus, the first four energy levels must be separated at least by about 1.2 Mev in order that they might be resolved. Also, depending on the relative positions of the excited levels of the stable isotopes, some targets must consist of a single isotope to permit resolution of the inelastic alpha-particle groups. In addition, the isotopic spin of some of the levels must be known since it was desired to check the validity of the isotopic spin selection rules in these interactions. With these restrictions in mind, the nuclei chosen for investigation were Li^6, C^{12}, N^{14}, and Mg^{24}.

D. TARGET PREPARATION

All targets were 1 1/8 in. by 1 1/8 in. in size, self-supporting, free of any backing material and were mounted in aluminum target frames. It was experimentally determined that a thickness of from 1.0 to 2.0 mils, depending on the target nucleus, gave the best compromise between an acceptable resolution and good counting statistics. Thinner targets

D. TARGET PREPARATION

All targets were 1 1/8 in. by 1 3/8 in. in size, self-supporting, free of any backing material and were mounted in aluminum target frames. It was experimentally determined that a thickness of from 1.0 to 2.0 mils, depending on the target nucleus, gave the best compromise between an adequate resolution and good counting statistics. Thinner targets

would increase the statistical errors in a reasonable counting time and thicker targets made resolution of the separated particle groups less accurate.

1. $\underline{Mg^{24}}$. This was the simplest target to obtain and prepare. A foil of 1.5 mils thickness, 99.8 percent pure magnesium was commercially obtained.* Surface oxidation was removed by lapping in jeweler's rouge and the completed target was either kept under vacuum or in a dry atmosphere. The percent abundance and level structure of the Mg^{25} and Mg^{26} is such that their presence in the target was of no consequence in this experiment.

2. $\underline{Li^{6}}$. The separated isotope was obtained from the Atomic Energy Commission in a pure metallic form. Targets of 1.0 to 1.4 mils thickness were formed by rolling the lithium between sheets of thin aluminum using a set of micrometer-controlled rollers. The material was rolled under dried Nujol to prevent oxidation from exposure to air. The Nujol was removed by immersion in successive baths of thoroughly dried naphtha after which the lithium target was keptin a high vacuum. The targets maintained a bright metallic luster throughout their use indicating the absence of oxidation.

- -

* Magnesium foil obtained from A. D. Mackay, Inc., 198 Broadway, New York 38, N. Y.

3. $\underline{C^{12}}$. The negligible percentage abundance of C^{13} permits the use of natural carbon; however, the problem of preparing a contaminant-free self-supporting thin sheet of carbon of the size required was quite troublesome. Using a pair of hardened steel dies in a 40-ton press, it was possible to form 0.5-mil targets from a special spectroscopic graphite powder.* The resolution obtained with these targets was relatively poor and they were discarded.

After experimenting with several different colloidal graphite dispersions, the "Dag No. 154"** was found to be quite satisfactory, and self-supporting targets of from 0.3 to 1.5 mils were prepared. Dag No. 154 consists of colloidal graphite dispersed in alcohol with a particle size of 1 micron or less and a solid content of less than 10 percent. No contaminant was experimentally observable using targets prepared from this material in the following manner.

(a) The colloid is further diluted by the addition of two parts alcohol (isopropanol). Using an artist's air brush with a fine nozzle*** and a

---

* Special graphite spectroscopic powder (suitable for pelleting) obtained from National Carbon Company.

** Dag dispersion obtained from Acheson Colloids Co., Port Huron, Michigan.

*** Paasche type H air brush and H3 nozzle obtained from S. L. Makepeace, Inc., Boston, Mass.

1. C_{12}. The negligible polarography observed at C_{12} permits the use of mineral oxygen bearing, the problem of preparing a condensation-free salt-supporting film about at ppm of the size required was quite encouraging. Using a pair of matched wheel like in a de-ion jewel, it was possible to form 1.5-mil bridges from a special spectroscopic graphite powder.* The resolution obtained with these bridges was relatively poor and they were discarded.

After experimenting with several different colloidal graphite dispersions, the "Dag No. 154ss" was found to be quite satisfactory, and self-supporting bridges of from 0.1 to 1.5 mils were produced. Dag No. 154 consists of colloidal graphite dispersed in alcohol with a particle size of 1 micron or less and a solid content of less than 1% present. Its composition was approximately observable using targets prepared from this material in the following manner.

(a) The colloid is further diluted by the addition of two parts alcohol (isopropanol). Using an artist's air brush with a fine nozzle and a

---

* Special graphite spectrographic powder (suitable for polishing) obtained from National Carbon Company.

** Dag dispersion obtained from Acheson Colloids Co., Port Huron, Michigan.

*** Passage time 4 air bubbles and 25 seconds obtained from 3. In Instrument, Inc., Dayton, Ohio.

30 psi supply of dry nitrogen, the solution is sprayed so as to uniformly cover the face of a mirror on which a thin film of detergent has been applied and thoroughly dried. The dry nitrogen causes the highly volatile liquie to solidify almost on contact and with practice, uniform layers of almost any desired thickness can be obtained.

(b) An infrared heat lamp is used to thoroughly dry the layer and then the mirror is immersed in water. The thin layer separates from the mirror floating to the surface of the water. The film is transferred directly to a target frame and dried under a heat lamp after which it is ready for use.

4. $\underline{N^{14}}$. This was the only target material used which could not be obtained in pure form. The substance with the highest nitrogen content suitable for use as a target was found to be a melamine formaldehyde resin "Melmac 404"* which is a filler-free thermal setting plastic. It was impossible to mould this material to less than 6 mils thickness because the powder would set before sufficient pressure

---

* Obtained from American Cyanamid Company, Research Division, Stamford, Conn.

(b) An interposed heat layer is used to plasticize the layer and then the mirror is pressed to water. The cold layer separates from the mirror clearing to the surface of the water. The film is transferred directly to a heavy frame and dried under a heat lamp after which it is ready for use.

6. Ex. This was the only factory artificial sand which could not be obtained in pure form. The substance with the highest silicon content suitable for use as a sand was found to be a calcined diatomaceous earth "Celite Corp. which is a filter-free thermal setting plastic. It was impossible to mould this material to less than 6 mils thick because the powder could not before artificial pressure

---

* obtained from Johns-Manville Company, Manville Building, Chicago.

could be applied. However, several pieces of 4-mil thickness, resulting from the "flash" obtained in a bar mould, were lapped down to uniform thicknesses varying from 1.5 to 2.0 mils using various abrasives.*

E. COUNTER ZERO ANGLE DETERMINATION

A 0.2-mg/cm^2 gold target was positioned perpendicular to the beam, the angular position being determined optically. With the cyclotron set to produce a steady beam in the scattering chamber, the energy spectrum of alpha particles scattered by gold was taken. This measurement was repeated at 1.8 degree intervals as the counter was rotated from an angle of approximately 25 degrees to 45 degrees on each side of the assumed direction of the beam. The intensity at each angular setting, as determined by the area under the elastic peak, was then plotted against the setting of the 1000-division helipot which determines the angular position of the counter. The intersection of the curves taken on each side of the assumed beam direction thus located the setting corresponding to zero angle as shown in Fig. 7. This measurement was repeated at frequent intervals during the conduct of the experiment.

---

* Obtained from the Plastics Laboratory, National Bureau of Standards, Washington, D. C.

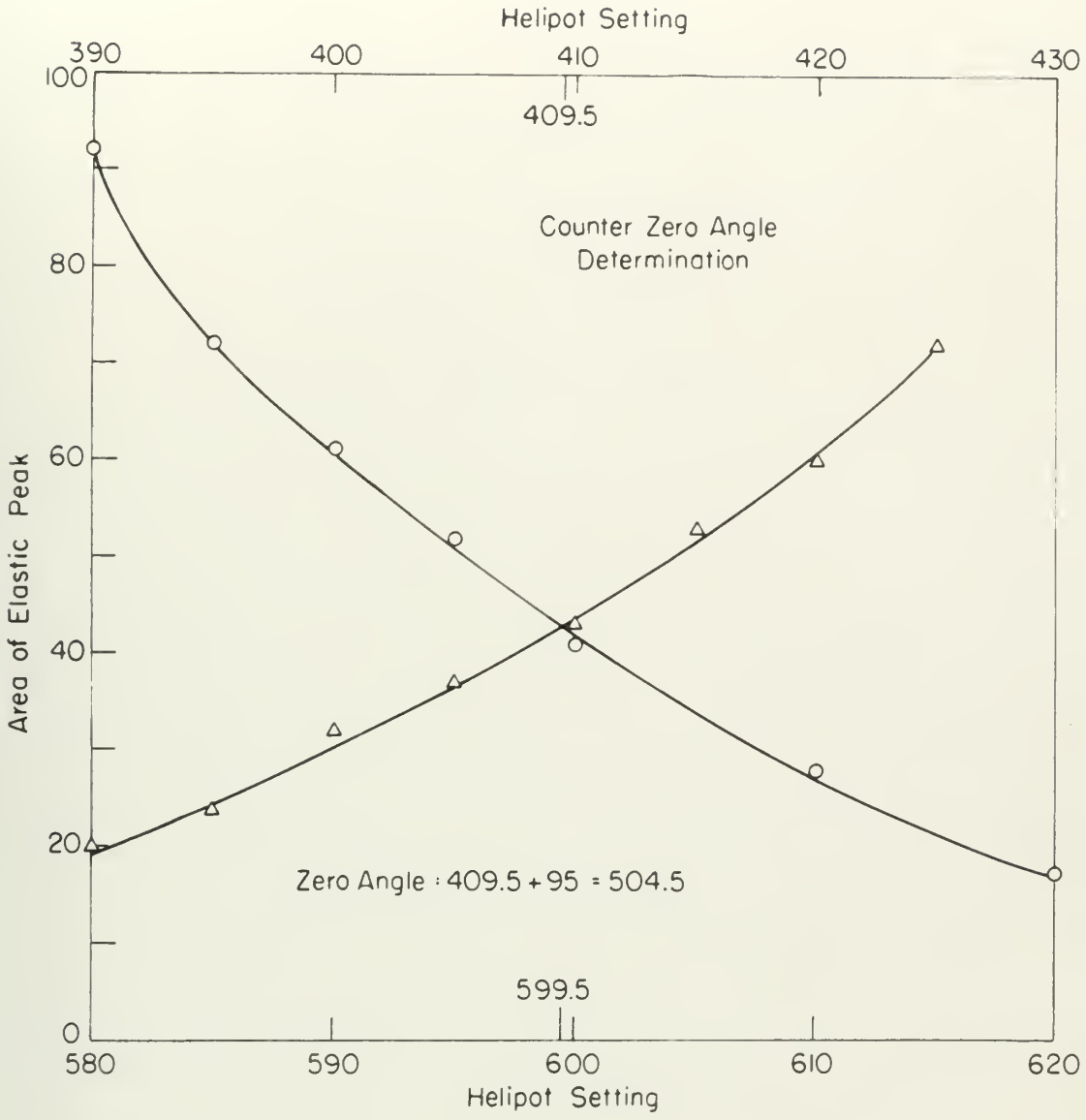
Helipot Setting
390
400
410
420
430
409.5
Counter Zero Angle
Determination
Area of Elastic Peak
100
80
60
40
20
0
Zero Angle : 409.5 + 95 = 504.5
599.5
580
590
600
610
620
Helipot Setting

Figure 7

IV. EXPERIMENTAL PROCEDURE

A. IDENTIFICATION OF ALPHA PARTICLE GROUPS

The theory and method of operation of the particle selective counter were outlined in Sec. IID. There is no difficulty in separating the alpha particles from the protons and deuterons resulting from the bombardment. Figure 8a, b, and c shows the complete mass-energy spectra of particles resulting from the 31.5-Mev alpha particle bombardment of Li^6, C^{12}, and natural magnesium respectively. Figure 9a, b, and c shows only the alpha particle spectra, obtained by proper setting of the bias level of the pulse height analyzer fed by the plastic scintillator. The energies of the separated alpha-particle groups must be determined in order to identify them as being associated with a given level of excitation in the target nuclei.

The bias level of the plastic scintillator analyzer is set to exclude all but alpha particles, as shown in Fig. 9. A bias level and window width, chosen to include at least two alpha-particle groups, is set on the NaI(Tl) pulse height analyzer. The energy pulse height spectrum of the alpha-particle groups is then taken with the counter set at a forward

IV. EXPERIMENTAL PROCEDURE

A. IDENTIFICATION OF ALPHA PARTICLE GROUPS

The theory and method of operation of the particle selective counter were outlined in Sec. III. There is no difficulty in separating the alpha particles from the proton and deuteron resulting from the $B^{10}(n,\alpha)Li^7$ reaction. Figure 8a, b, and c show the complete mass-energy spectra of particles resulting from the 3.2-mev alpha particle bombardment of Ti^{48}, C_{12}, and natural magnesium respectively. Figure 9a, b, and c show only the alpha particle spectra, obtained by proper setting of the bias level of the pulse height analyzer fed by the plastic scintillator. The energies of the monoenergetic alpha-particle groups must be determined in order to identify them as being associated with a given level of excitation in the target nuclei.

The bias level of the plastic scintillator analyzer is set to exclude all but alpha particles, as shown in Fig. 9. A bias level and window width, chosen to include at least the alpha-particle groups, is set on the $Ra(Ti)$ pulse height analyzer. The energy pulse height spectrum of the alpha-particle groups is then taken with the counter set at a forward

Photographs of oscilloscope presentation of mass energy spectra of particles resulting from the 31.5-Mev alpha-particle bombardment of $C1^6$, C^{12}, and natural Mg.

Fig. 8a Li^6

Fig. 8b C^{12}

Fig. 8c natural Mg

natural fit.

CT_6', C_{T6}', and

positions of

slope-barrier

the 1,6-yne

sulfide from

practice re-

sphere of

Fig. 6e CT_6

of seven words

precision

cancellation

>photography of

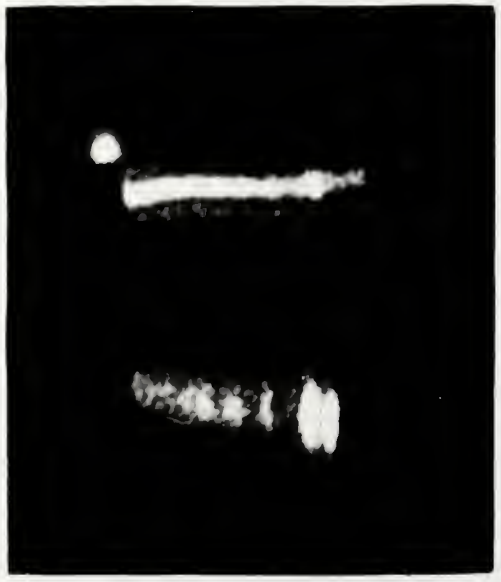

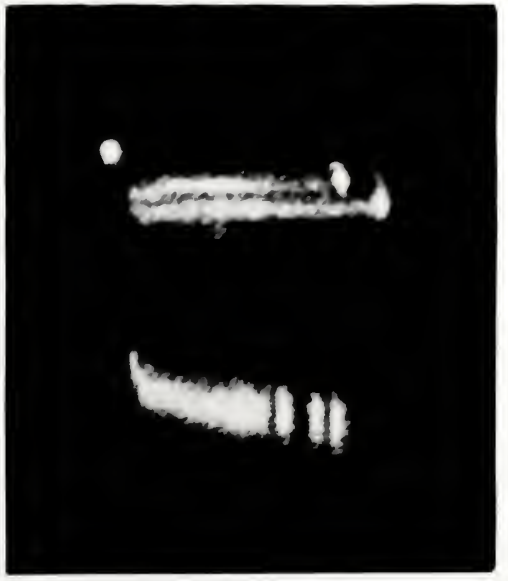

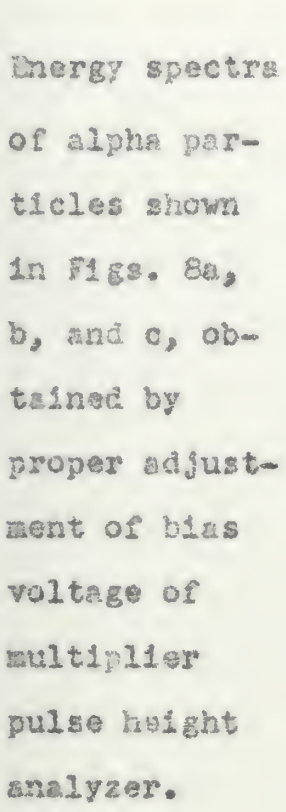

Energy spectra of alpha particles shown in Figs. 8a, b, and c, obtained by proper adjustment of bias voltage of multiplier pulse height analyzer.

Fig. 9a Li^6

Fig. 9b C^{12}

Fig. 9c natural Mg

Fig. 3e T_6

Shield connector

of viper box-

clover sonar

in Fig. 9e?

p' and n' op-

tained at

bipolar voltage-

mand of pins

voltage of

Fig. 8B T_{IX}

multiplex

bytes packet

analyzer.

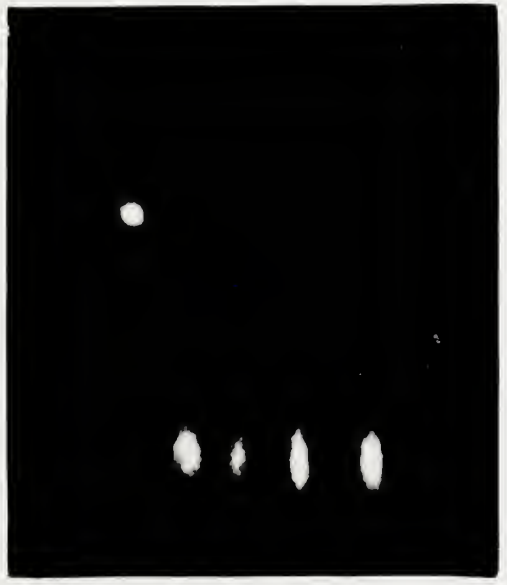

angle chosen such that the intensity ratio of the groups is small. The target is then replaced by a gold foil of approximately equal thickness, in mg/cm^2, and the elastic peak of the alpha particles scattered by gold is obtained. With no change in electronic settings, the effective 20 channels of the NaI(Tl) single channel analyzer are calibrated using a linear pulse generator. The resultant positions of the alpha-particle groups, on a linear voltage scale, then correspond to the energies of the alpha particles at the NaI(Tl) crystal. With the beam energy known, and assuming that the interaction occurs at the center of the target, the energy of the alpha particles elastically scattered by gold at the angle of the counter can be computed. By use of range-energy curves, the resultant alpha-particle energy at the NaI(Tl) crystal is obtained and the energy calibration of the effective 20-channel analyzer is accomplished. Then by extrapolation through known range-energy relationships, the center-of-target energies of the unidentified alpha-particle groups may be found and the groups identified with known levels in the target nucleus. Figure 10 shows the result of such a calibration in the case of Li^6. The computed energies of the alpha particles from the ground, first, and third levels of Li^6 all agree within 2 percent with the calibration against gold. Figure 10 also shows that excitation to the second excited

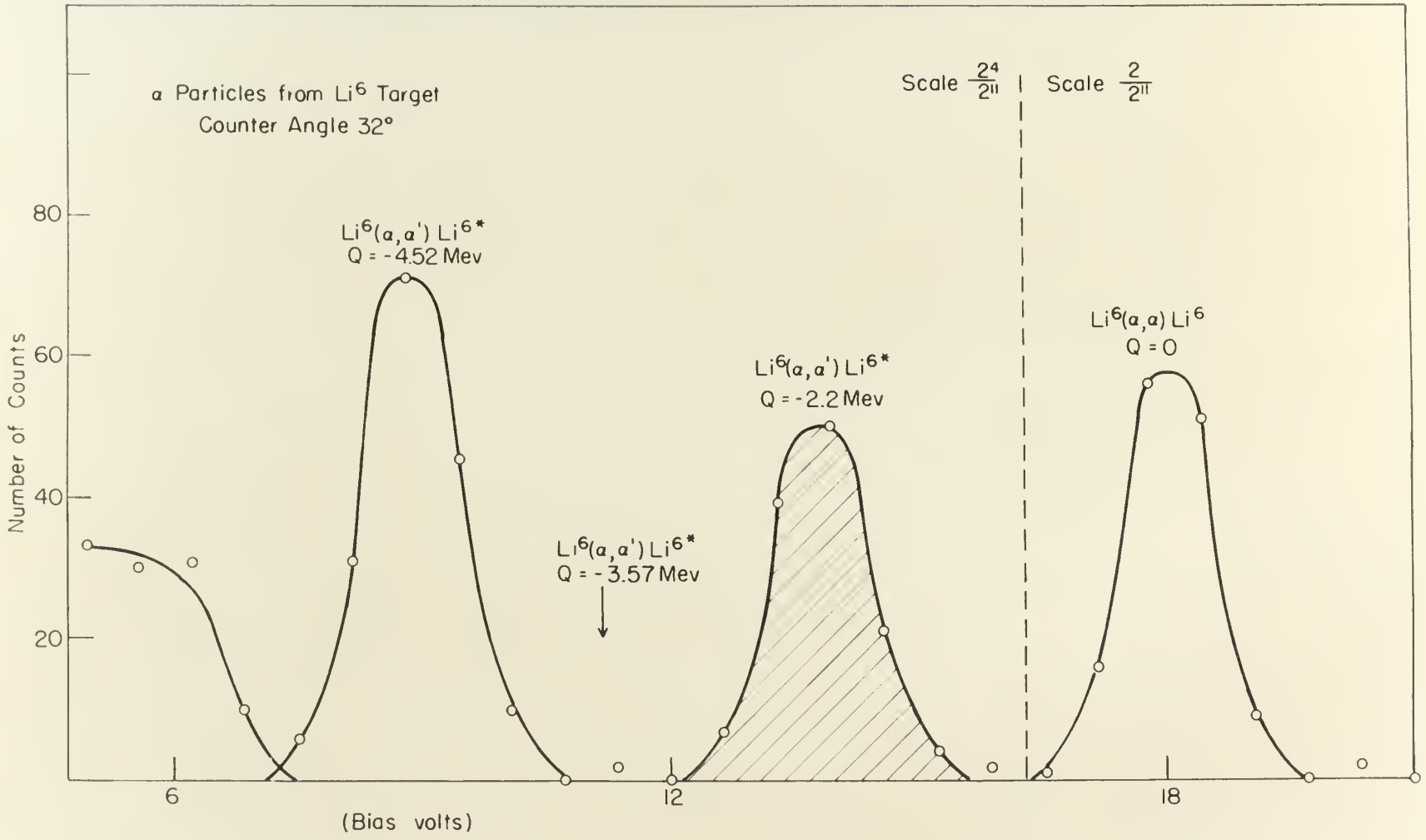
α Particles from Li⁶ Target
Counter Angle 32°
Scale 2⁴/2¹¹
Scale 2/2¹¹
Li⁶(α,α') Li⁶*
Q = -4.52 Mev
Li⁶(α,α') Li⁶*
Q = -3.57 Mev
Li⁶(α,α') Li⁶*
Q = -2.2 Mev
Li⁶(α,α) Li⁶
Q = 0
Number of Counts
80
60
40
20
6
12
18
(Bias volts)

Figure 10

level has an extremely low probability of occurrence.

B. ANGULAR DISTRIBUTION MEASUREMENTS

To obtain an angular distribution one must measure the number of alpha particles of a given energy, corresponding to a specific excitation level of the target nucleus, scattered into unit solid angle at a given mean angle, over a specific angular range. All angular distribution measurements were made with the target normal set at an angle of 45 degrees with the incident beam. This permitted observation of the entire forward quadrant without the necessity of rotating the target. With the bias level of the plastic scintillator pulse height analyzer set to exclude all but alpha particles, as shown in Fig. 4b, the bias voltage range was chosen so that the resulting spectrum would include two peaks. As an example, intensity measurements of the alpha-particle groups corresponding to the elastic and first excited levels were included in one bias range. The peak corresponding to the first excited level was also included in the intensity measurement of the group corresponding to the next higher excited level, etc. This afforded a continuous check on the reproducibility of the measurement, on the linearity over the bias range, and on the stability of the window width.

level may be extremely low especially at resonance.

B. ANGULAR DISTRIBUTION MEASUREMENTS

To obtain an angular distribution one must measure the number of alpha particles of a given energy, corresponding to a specific excitation level of the target nucleus, scattered into unit solid angle at a given mean angle, over a specific angular range. All angular distribution measurements were made with the target normal set at an angle of 45 degrees with the incident beam. This permitted observation of the multiple forward gradient without the necessity of rotating the target. With the thin level of the plastic scintillator pulse height analyzer set to exclude all but alpha particles, as shown in Fig. 4B, the plus voltage range was chosen so that the resulting spectrum would include two peaks. As an example, intensity measurements of the alpha-particle groups corresponding to the elastic and first excited levels were indicated in one plus range. The peak corresponding to the first excited level was also included in the intensity measurement of the group corresponding to the next higher excited level, etc. This allowed a continuous check on the reproducibility of the measurements, on the linearity over the plus range, and on the stability of the electron multi-

Early in the experiment it was found that the intensities of the separated alpha-particle groups varied rapidly with angle. To ensure that none of the structure was missed, intensity measurements were made at angular intervals of 1.8 degrees (5 helipot units). To prevent errors due to pulse pile-up in the multiplier circuit at excessive counting rates, resulting from the rapidly increasing intensity of elastic alpha particles at forward angles, the incident beam intensity had to be decreased to a very low value (< 0.0001 microampere). As a result, one to three hours of steady operation were required to obtain a statistically significant cross section measurement at a forward angle. At large angles, where the scattered intensity was greatly decreased, considerable time was also required to accumulate statistically acceptable data. To ensure proper matching of curves to make up the total angular distribution, all partial curves obtained on different runs were matched over an angular region of at least 9 degrees, chosen so that the intensity permitted a rapid accumulation of data and the intensity variation with angle produced a well defined maximum or minimum to facilitate the matching.

An initial energy spectrum, containing the desired alpha-particle group, was run with the counter set at an angle of 30 degrees. The spectrum was then taken at intervals of 1.8

degrees as far forward as possible without having the particles enter the counter so rapidly that pulse pile-up occurred. The limit was determined to be 1000 particles per second for a maximum acceptable counting error of 1 percent. The counter was then repositioned at 30 degrees and the spectrum verified with the initial measurement. Then the spectrum was taken at intervals of 1.8 degrees as the angle was increased to a value where the lowered intensity of the scattered group necessitated an increase in incident beam intensity. The power level of the cyclotron was then raised, the counter rotated 9 degrees forward to ensure a match with the previous data at the old cyclotron power level, and the measurements continued. The angle of observation was increased in this way until the energy of the alpha group under observation had decreased to a point where the peak could no longer be detected or until the time required for the collection of statistically acceptable data was considered excessive. The cyclotron power level was then decreased until the intensity was well below the initial value, spectrum was again checked at 30 degrees, and the forward angle measurements were made, decreasing the incident beam intensity as necessary and requiring a match of the curves at each new power level. In addition to the numerous checks at 30 degrees and the matching over a 9-degree range, the spectrum was also frequently checked at various angles on the

opposite side of the zero angle of the beam. This verified the zero angle determination previously described and insured that no particles were scattered into the aperture from the asymmetric small angle scattering shield. Each complete angular distribution was taken at least two times and the positions of maxima and minima were verified at least three additional times for each distribution.

When the data for a complete angular distribution had been obtained, the counts recorded in the 20 registers were plotted versus bias voltage for each angle of observation and the areas under the peaks corresponding to the identified alpha-particle groups were taken as a measure of their relative intensities. The areas under the peaks were measured, after graphical resolution where necessary, using a polar planimeter.

The cross-hatched areas shown in Figs. 10-12 correspond to the relative intensities of the indicated groups at the angle specified. The relative intensities were thus obtained as a function of laboratory angle. These data must be corrected for two effects before they are subject to comparison with any theoretical interpretation. Since the solid angle subtended by the counter in the particle or center-of-mass coordinates differs from the angle subtended in the laboratory coordinates and also varies with angle, the observed intensities must be corrected for this effect. In addition, the angles of observation must be transposed from the laboratory to the center-of-mass

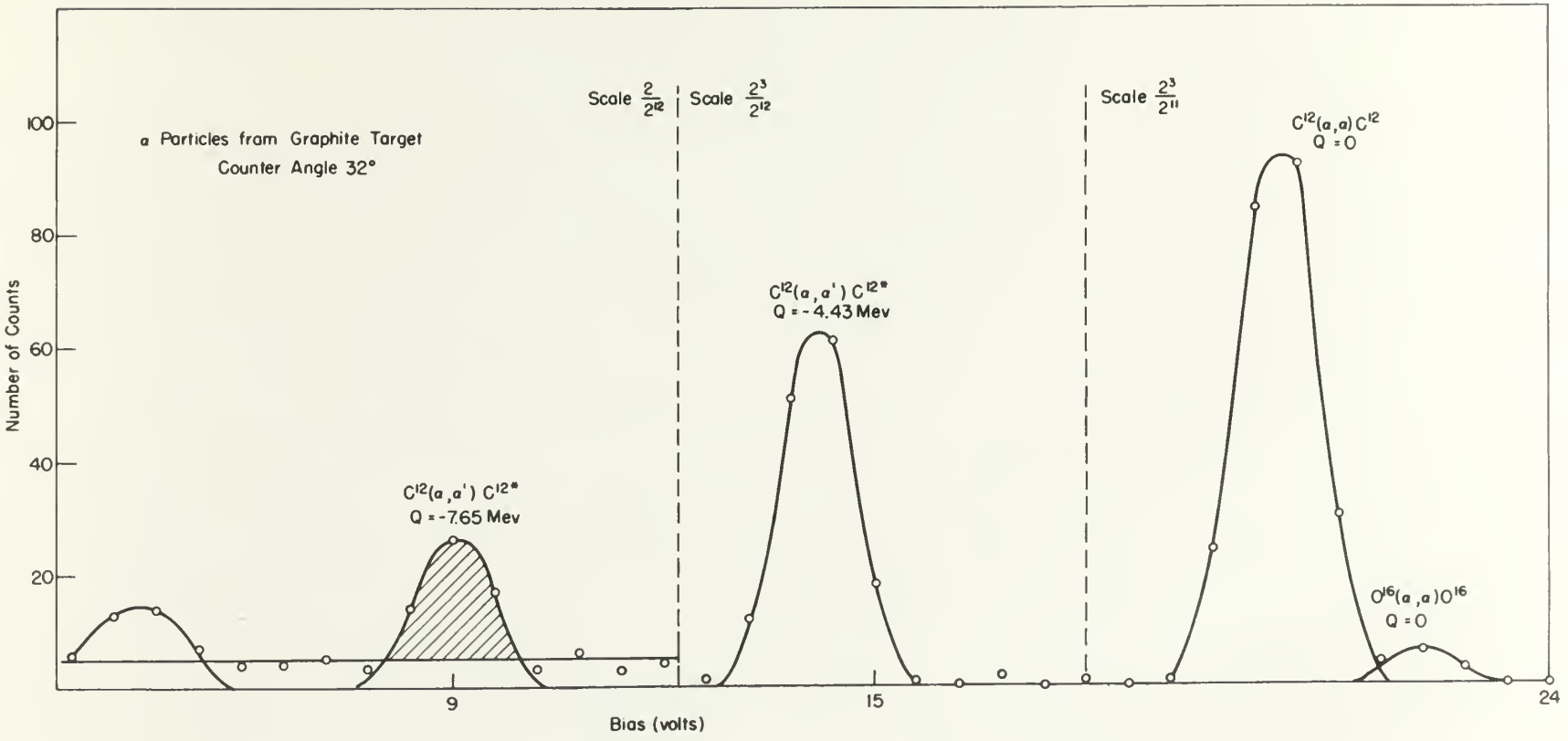
α Particles from Graphite Target
Counter Angle 32°
Scale $\frac{2}{2^{12}}$
Scale $\frac{2^3}{2^{12}}$
Scale $\frac{2^3}{2^{11}}$
$C^{12}(\alpha,\alpha')\,C^{12*}$ Q = -7.65 Mev
$C^{12}(\alpha,\alpha')\,C^{12*}$ Q = -4.43 Mev
$C^{12}(\alpha,\alpha)\,C^{12}$ Q = 0
$O^{16}(\alpha,\alpha)\,O^{16}$ Q = 0
Number of Counts
100
80
60
40
20
9
15
24
Bias (volts)

Figure 11

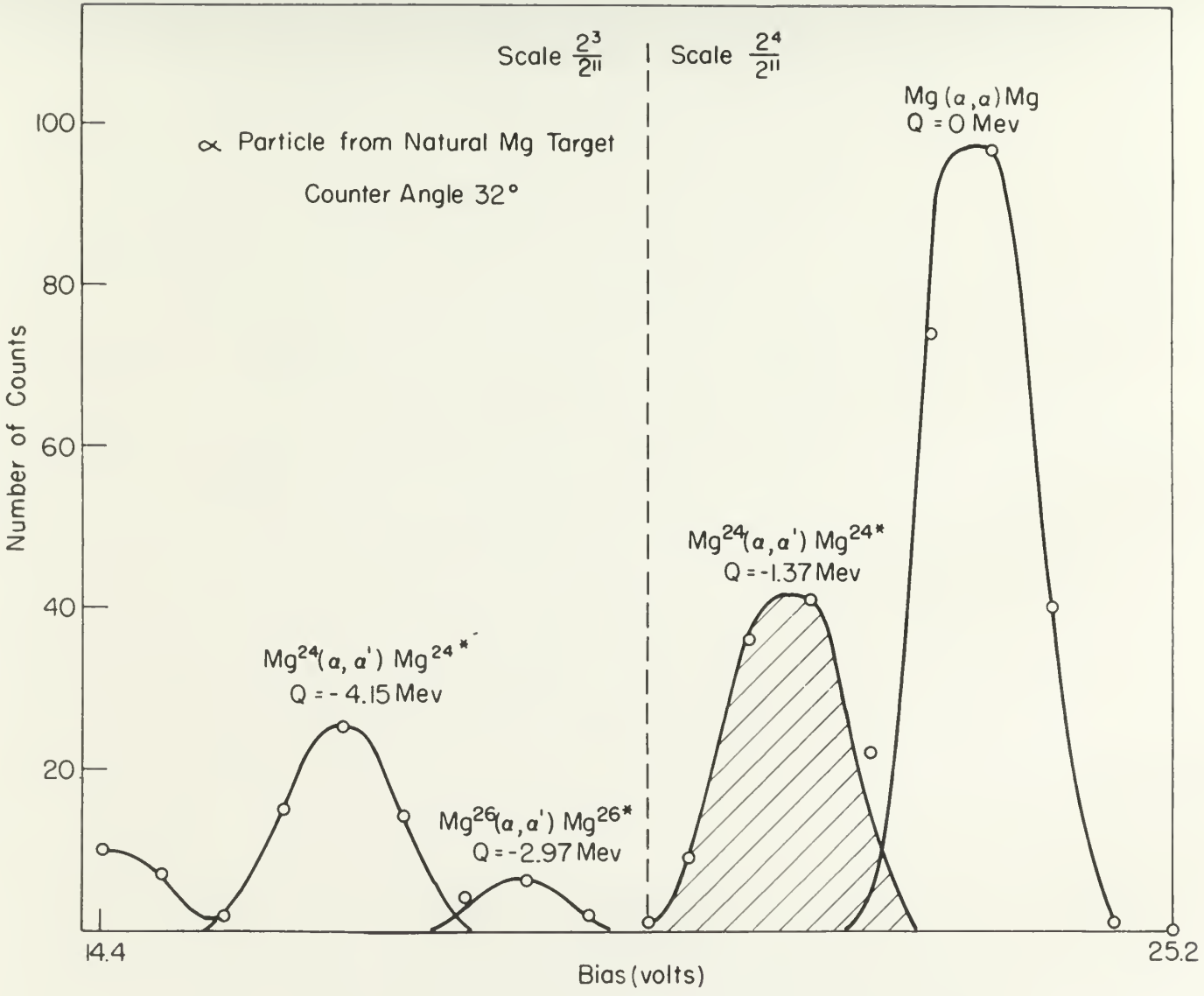
Scale $\frac{2^3}{2^{11}}$
Scale $\frac{2^4}{2^{11}}$
α Particle from Natural Mg Target
Counter Angle 32°
Mg (α, α) Mg
Q = 0 Mev
Mg^{24}(α, α') Mg^{24*}
Q = -1.37 Mev
Mg^{24}(α, α') Mg^{24*}
Q = - 4.15 Mev
Mg^{26}(α, α') Mg^{26*}
Q = -2.97 Mev
Number of Counts
100
80
60
40
20
14.4
25.2
Bias (volts)

coordinate system. These corrections are derived and typical conversion curves are shown in Appendix I. The angular distributions are thus obtained after the data have been corrected for these effects. The relative intensity measurements are converted to an absolute differential cross section by the method described in the following section.

C. CROSS SECTION MEASUREMENTS

As described in Sec. IIC, the beam monitor consists of a plastic scintillator which observes only the particles scattered at an angle of 45 degrees with the incident beam by a thin gold foil. The bias level of the monitor counter is adjusted so that it counts only those pulses of a height corresponding to the elastically scattered alpha particles. Since the monitor counter does not measure the alpha-particle beam directly, the differential cross sections were determined by comparing the intensities of the observed alpha-particle groups with the intensity of the alpha particles elastically scattered by a gold target. Recent experiments (W2, S3) have shown that the elastic scattering of energetic alpha particles from heavy elements agrees with the coulomb differential cross section (R1) at small angles. The angular distribution of 31.5-Mev alpha particles elastically scattered from gold was taken over an angular range of from 14.8 degrees to 60 degrees, and

coordinate system. These corrections are derived and typical corrected curves are shown in Appendix I. The angular distributions were thus obtained after the data have been corrected for these effects. The relative intensity measurements are compared to an absolute differential cross section by the method described in the following section.

6. CROSS SECTION MEASUREMENTS

As described in Sec. IIC, the beam monitor consists of a plastic scintillator which observes only the particles scattered at an angle of 45 degrees with the incident beam by a thin gold foil. The bias level of the monitor counter is so-justed so that it counts only those pulses of a height corresponding to the elastically scattered alpha particles. Since the monitor counter does not measure the alpha-particle beam directly, the differential cross sections were determined by comparing the intensities of the observed alpha-particle group with the intensity of the alpha particles elastically scattered by a gold target. Recent experiments (6, 23) have shown that the elastic scattering of energetic alpha particles from heavy elements agrees with the coulomb differential cross section (RI) at small angles. The angular distribution of 31.5-Mev alpha particles elastically scattered from gold was known over an angular range of from 14.8 degrees to 90 degrees, and

observed intensities were found to agree with the Rutherford scattering equation, within 3 percent, back to 30 degrees. Accordingly, all intensity comparisons used to determine absolute differential cross sections were made at angles smaller than 30 degrees.

An energy spectrum which includes the desired alpha-particle group was taken at an angle of 30 degrees as described in Sec. IVB. The target under investigation was then replaced by a gold foil of approximately the same thickness in mg/cm^2. This limitation on the thickness of the gold foil is necessary for two reasons. The width of the peak in the energy spectrum is dependent on the straggling effect in traversing the target and therefore if targets of different thickness are used, the calibration made by comparing the areas under the peaks would not be correct. In addition, since some small fraction of the beam incident on the counter aperture undergoes significant small angle scattering by the plastic scintillator, a more accurate comparison is obtained if the scattered particles have traversed the same effective scattering thickness of target material. Using the area under the elastic gold peak as a standard, the differential cross section of the alpha-particle group under investigation can be expressed in terms of this standard as follows (A1):

$$\frac{d\sigma}{d\Omega} = \frac{C/N}{C_s/N_s} \frac{A/T}{A_s/T_s} \frac{\cos \varphi}{\cos \varphi_s} \left(\frac{d\sigma}{d\Omega}\right)_s$$

where

$\frac{d\sigma}{d\Omega}$ = differential cross section in millibarns/steradian-atom in the laboratory coordinates

C = area under the differential spectrum curve

N = number of incident alpha particles

A = atomic weight of target material

T = target thickness in mg/cm^2

φ = angle between target normal and direction of incident alpha-particle beam

s = subscript indicates the values applicable to the gold target used as a standard

The ratio N_s/N is determined by the ratio of scaling factors used on the monitor counter. This, of course, assumes that interchanging the two targets does not affect the intensity of the beam incident on the gold foil observed by the monitor. The comparisons were made with both targets at the same angle which eliminated any error in the ratio $\cos \varphi/\cos \varphi_s$, due to errors in the angular positioning of the target.

D. BACK ANGLE INTENSITIES

The report of a recent experiment (R2), involving the bombardment of C^{12} with 22-Mev alpha particles, indicates

$$\frac{d\sigma}{d\Omega} = \frac{e^2}{4\pi\varepsilon_0} \frac{\omega^2}{c^2} \frac{\sin^2\theta}{(1-\beta\cos\theta)^2} \frac{d\sigma}{d\Omega}$$

where:

$\frac{d\sigma}{d\Omega}$ = differential energy radiation per solid angle in the laboratory coordinates

ε_0 = permittivity of free space

ω = angular velocity of charged particle

β = velocity of charged particle / velocity of light

θ = angle between direction of observation and direction of the accelerated charged particle

$\frac{d\sigma}{d\Omega}$ = differential energy radiation per solid angle in the coordinates moving with the charged particle

The ratio $\varepsilon_0^2/2$ is measured by the ratio of emitting power used on the monitor counter. This, of course, assumes that the spectral distribution of the two beams are identical. The absolute value of the beam intensity is measured by the monitor counter. The monitor counter is also used to measure the beam position. The monitor counter is also used to measure the beam position. The monitor counter is also used to measure the beam position.

3. Data reduction

The value of $\frac{d\sigma}{d\Omega}$ is measured (3), knowing the

a strong maximum at 150 degrees in the angular distribution of the inelastic alpha group corresponding to the 4.43-Mev excitation level in the target nucleus. Some equipment modification was necessary to investigate the intensity of alpha particles scattered at back angles in the present experiment.

A particle entering the aperture of the counter must traverse two 1.88-mg/cm^2 aluminum foils, used as light shields, and a 28.8-mg/cm^2 thickness of plastic scintillator, as shown in Fig. 6, before striking the NaI(Tl) crystal. After traversing this thickness of absorbing material, the particle must have sufficient energy remaining to produce a scintillation in the NaI(Tl) crystal which can be distinguished above the γ-ray background, since chance coincidences between γ rays and alpha particles are appreciable at the low end of the energy spectrum. As this investigation involves the bombardment of light nuclei with a relatively heavy particle, the decrease in energy of the inelastically scattered particles as the angle of observation increases is quite rapid. The result of these considerations is that a limitation is placed on the maximum angle of observation permissible using this particular method of particle detection.

The plastic scintillator was removed from the particle selective counter and only the NaI(Tl) scintillator was used

for particle detection. This eliminated 38.9 mg/cm^2 of absorbing material and removed the previous limitation on the maximum permissible angle of observation. The maximum proton and deuteron energies and the energies of the alpha-particle groups resulting from the bombardment of a C^{12} target were computed over the angular range of from 90 degrees to 180 degrees. The response of NaI(Tl) to protons, deuterons, and alpha particles has been determined (Tl). By using these response curves in conjunction with known range-energy relations (A2) it was possible to choose a set of aluminum absorbers such that the percentage change in pulse height, produced by inserting these absorbers in front of the counter aperture, permitted identification of the particle producing the pulse, over this 90-degree angular range. The three alpha-particle groups observed in the bombardment of C^{12} and previously studied with the particle selective counter were identified using this method. Since these peaks were superposed on a background of protons, deuterons, and low-energy alpha particles, the intensity measurements obtained were assigned an experimental uncertainty of 50 percent. Nevertheless, by scanning the back angles, it was possible to ascertain that the differential cross section for scattering of any detectable alpha-particle group at angles greater than 90 degrees was less than 0.9 percent the value of that for

the ground level at 28 degrees, i.e., less than 0.8 millibarns/steradian-atom. From this it appeared that, at least in the case of C^{12}, the scattering is primarily confined to the forward quadrant.

E. ENERGY DEPENDENCE OF ANGULAR DISTRIBUTIONS

The data previously mentioned (R[illegible], P1) indicated a very sensitive energy dependence in the angular distributions of [illegible]-Mev alpha particles scattered by C^{12}. In the present experiment, the beam energy was known to vary as much as 0.4 percent (H1) depending on the power level of the cyclotron. This is largely due to variations in the r.f. heating and the subsequent mechanical motion of the dees. The continuous reproducibility of data, regardless of the cyclotron power level, implied that this strong energy dependence was not a factor in the present work. To verify the insensitivity to small changes in beam energy, angular distributions of the alpha groups corresponding to the ground, first, and second excited levels in both C^{12} and Mg^{24} were also taken with reduced beam energies of 30.9 Mev and 30.4 Mev. The reduction in energy was accomplished by insertion of 3.76-mg/cm^2 and 6.88-mg/cm^2 aluminum absorbers in the beam. Angular distributions obtained at both energies fell within the experimental uncertainties of those taken at 31.5 Mev.

F. EXPERIMENTAL UNCERTAINTIES

Only those sources of error which have an appreciable effect on the experimental data are mentioned. These are discussed with respect to their effect on the experimental measurements made.

1. Errors in Particle Selection. The separation of alpha particles from the protons and deuterons from all of the targets studied was quite satisfactory. Figures 8 and 9 show this separation as observed on the oscilloscope face while Fig. 28 shows the pulse height separation in terms of analyzer bias. Due to the long resolving time required in the coincidence circuit, chance coincidences between alpha particles and γ rays are possible. However, these chance coincidences are appreciable only at the low end of the energy spectrum where the γ-ray intensity is high (Al). The individual alpha-particle groups were, in general, cleanly separated from each other. Thus it was usually possible to graphically eliminate the chance coincidence rate by treating it as a continuous background over the specific low-energy range where it occurred. This procedure is shown in Fig. 11 where the cross-hatched area indicates the relative intensity of the alpha group corresponding to the 7.65-Mev level in C^{12} after background subtraction.

4. [illegible]

[illegible] those devices of strong radiation hardness which are [illegible] effect on the experimental data are considered. These are discussed with respect to their effect on the spectrometer measurements made.

1. Errors in Particle Selection. The separation of alpha particles from the protons and deuterons from all of the isotopes studied was quite satisfactory. Figures 8 and 9 show this separation as achieved on the oscilloscope from which data was taken. By the coincidence circuit, choice of analyzer bias, use of the anticoincidence circuit, and choice of detector bias, particles and X rays are possible. However, there remain coincidences are controllable only at the low end of the energy spectrum where the X-ray intensity is high (41). The initial alpha-particle groups were, in general, already separated from each other. Thus it was usually possible to practically eliminate the coincidence pile up problem it as a continuous background over the specific low-energy range where it occurred. This procedure is shown in fig. 11 where the pulse-height area indicates the relative intensity of the alpha group corresponding to the X-ray level in (1).

2. Errors in Beam Energy Determination. After consideration of all the sources of error, it is estimated that the beam energy measurement is correct to well within ±400 kev. This is approximately twice one standard deviation as indicated in the distribution of energy measurements shown in Fig. 6. The sources of error in the determination of beam energy are:

(a) Errors in thickness measurements of target, plastic scintillator, and aluminum foils in the counter, and the aluminum absorbers used in front of the counter aperture. These measurements were made by two methods. First, the thickness was measured directly with a vernier micrometer and converted to mg/cm^2. Then the various materials were weighed using an accurate analytical balance and the mg/cm^2 thickness determined by dividing this weight by the cross sectional area. The estimated error in determining the thickness of the aluminum foils is ±1.0 percent, but because these foils were extremely thin compared with the other absorbing material, this inaccuracy had a negligible effect on the energy determination. The thickness of the plastic

scintillator was determined to within ±0.3 percent but this inaccuracy is quite small compared with the uncertainty in the plastic scintillator range-energy relations. For the same reason, the small error involved in determining the thickness of the aluminum absorbers may also be neglected.

(b) Errors in range-energy curves. The range-energy curves (A2) were determined as follows. The rate of energy loss was computed from the theoretical formula (L2). Range-energy values were then obtained by numerical integration of the reciprocal of this rate with respect to energy. Low-energy values were based on experimental data rather than theoretical calculation. Range-energy relations for the plastic scintillator were calculated by a method previously described (A1). Due to inaccuracies in these calculations, they are estimated to be correct within 4 percent over the range of proton energies incident on the plastic scintillator. This inaccuracy permits an error of ±100 kev in the beam energy determination.

an error of 5% or so in the mean energy deterioration.

(p) Errors in knock-energy curves. The knock-energy curves (xi) were determined in various ways. The rate of energy loss was computed from the theoretical formula [12]. Knock-energy values were then obtained by numerical integration of the rate-expression of this rate with respect to energy. Low-energy values were based on experimental data without theoretical calculation. Knock-energy relations for the plastic scintillator were calculated by a method previously described (11). Due to inaccuracies in these calculations, they are estimated to be correct within a percent only for the range of proton energies involved on the plastic scintillator. Data concerning helium ion energy loss in the plastic scintillator [13] were determined by numerical integration of the differential form of the Bethe-Bloch equation [14]. For the same reason, the small error committed in determining the thickness of the elements absorbers may also be neglected.

(c) Variation in incident beam energy. The mechanical motion of the dees previously mentioned produced a variation of ±125 kev in the incident alpha-beam energy.

(d) Error in Q values. The proton groups used for this energy calibration were from the reactions $Li^7(\alpha,p)Be^{10}$ and $Li^7(\alpha,p)Be^{10*}$. The Q values for these reactions (A3) are known to within 20 kev and introduce a negligible error in the energy determination.

(e) Nonlinear response of NaI(Tl) crystals. Over the range of proton energies used in this experiment, the response of NaI(Tl) has been shown to be linear within 2 percent (Tl). This is a small error compared with those previously mentioned.

(f) Error in locating the center of the proton peaks. The full width at half maximum of the observed proton peaks was approximately 500 kev. It was therefore possible to locate the maximum to within 50 kev. The nonlinearity of the pulser used to calibrate the energy scale was determined to be negligible.

(c) Error in locating the centre of the circle
chose fortuitously coinciding.
(d) Error in a values. The factor should read
for this reason originally were from the
reference $\int_0^{\infty}(\alpha^3/\beta)e^{-\alpha r}dr$ not $\int_0^{\infty}(\alpha^2/\beta)e^{-\alpha r}dr$.
The f values for these reflexions (r) are
known to within 5% but uncorrected a
negligible error in the second approximation,
[e] Footnote reference at Ia(II) wrongly
made the index of reflexion marginal once in
this edgewise, the reference at Ia(II)
has been shown to be itself within 2 percent
(II). This is a small error considered with
those previously mentioned.
(f) Error in locating the centre of the circle
frame. The full width at half maximum of
the observed proton peaks was approximately
900 sec. It was therefore possible to
locate the maximum to within 5% sec. The
uncertainty of the values used in calculating
the energy levels was determined to be sufficient.

3. Errors in Angular Positioning. The angular position of the counter is determined by balancing a bridge circuit whose variable element consists of a precision helipot connected to the arm on which the counter is mounted. With this method of control, the counter angle can be set to within ±0.1 degree. The method described in Sec. IIIE for determining the zero angle is believed to be correct only to within ±0.3 degree. The finite area of the beam on the target permits a maximum angular uncertainty of ±0.5 degree. The collective effect of these possible errors limits the precision of angles measured relative to the beam to ±0.6 degree. Due to the continuous reproducibility of results, especially when measuring coulomb scattering in the sensitive region of the $\left[\sin^4(\theta/2)\right]^{-1}$ factor, it was concluded that angles could be set relative to one another to well within ±0.3 degree.

Since the target was initially set perpendicular to the beam by optical means, a possible error of ±2 degrees is assigned for this angular position. This error is insignificant, however, when the effect of the resultant error, a change in effective target thickness, is considered. In the few instances where the target angle was changed during an experiment, the correction for effective target thickness invariably fell within the statistical error of the data.

4. Errors in Relative Intensity Measurements. The most important error introduced in the measurement of relative

intensities was that due to the method of comparison. The area under a given peak was measured by a polar planimeter and this measurement is estimated to be correct to within 3 percent. Due to the small area of the target subtended by the beam, errors due to target thickness variations are estimated to be less than 1 percent. Compared to the above, those errors due to monitor discriminator stability and the inherent statistical counting errors are considered to be negligible.

5. Errors in Cross Section Measurement. As previously described in Sec. C, the cross section measurement depends on a comparison of plotted areas which represent relative intensities. The standard of comparison was that area under a peak corresponding to a differential cross section for coulomb scattering. This standard intensity was always obtained in a region where the variation with angle followed the $\left[\sin^4(\theta/2)\right]^{-1}$ relationship within statistical counting error limits. The assumption was made that in this region, the Rutherford differential cross section formula (R1) is correct. Then, consideration of the errors previously described in this section places an upper limit of ± 7 percent on the accuracy of the differential cross section values.

V. EXPERIMENTAL DATA

The nuclei chosen for investigation afforded two opportunities for observing the validity of the isotopic spin selection rule in this experiment. In the reaction $Li^6(\alpha,\alpha')Li^{6*}$, excitation from the T = 0 ground level to the 2.19-Mev and 4.53-Mev levels, both of isotopic spin T = 0, are allowed since the bombarding alpha particle is also T = 0. However, excitation to the T = 1, 3.57-Mev level is prohibited by this selection rule. Figure 10 shows the spectrum of alpha particles, observed at an angle of 30 degrees, which results from the bombardment of a 1.4-mil Li^6 target. It is clearly evident that excitation of the 3.57-Mev level is almost entirely nonexistent. A study of the spectrum at all angles of observation indicates that excitation of this level has a probability of occurrence of less than 4 percent that of either of the two allowed levels which were excited.

A similar investigation was made to determine the probability of excitation of the T = 1, 3.91-Mev level in N^{14} compared with that of the T = 0, 3.95-Mev level. The only target material suitable for the study of nitrogen was melamine (see Sec. IIID), which contained a high percentage of carbon.

Combined with the poor resolution of the equipment, the proximity of the excitation levels of carbon and nitrogen did not permit taking clean angular distributions of the alpha particles scattered by N^{14}. However, it was possible to place an upper limit on the excitation of one forbidden level as follows. The alpha-particle groups elastically scattered by carbon and nitrogen were unresolved as were those groups corresponding to the 4.43-Mev level in C^{12} and the 3.95-Mev allowed level in N^{14}. The unresolved peaks were calibrated, as described in Sec. IVC, in terms of an absolute total differential cross section for both interactions. The C^{12} cross sections, separately obtained using a pure carbon target of a thickness determined by the carbon content of the melamine target, were then subtracted out. By this expedient it was determined that excitation of the isotopic spin prohibited 2.31-Mev level in N^{14} occurred with a probability of less than 6 percent that of the allowed 3.95-Mev level over an angular range of observation of from 14.8 degrees to 64.1 degrees.

Figure 11 shows the alpha-particle groups observed at an angle of 32 degrees with the beam when a carbon target is bombarded by 31.5-Mev alpha particles. The alpha particles elastically scattered by oxygen contamination of the target show up as a clearly separated group just above the elastic C^{12} group.

^{12}C atom.

The alpha-particle spectrum shown in Fig. 12 results from the 31.5-Mev alpha-particle bombardment of a natural magnesium target. The elastic peak includes the elastic scattering from all three stable magnesium isotopes while the inelastic groups are due only to the individual isotopes indicated in the figure.

The angular distributions of alpha particles scattered inelastically by Li^6, C^{12}, and Mg^{24} are shown in Figs. 13-18. The well defined maxima and minima are suggestive of a direct interaction, as discussed later in Sec. VI. The data of G. Schrank et al. (58), obtained for the interaction $Fe^{56}(p,p')Fe^{56*}$, show a similar structure and are interpreted as indicative of a direct interaction. The errors indicated in Figs. 13-18 include all uncertainties affecting a comparison of relative intensities. Where no errors are indicated, the uncertainty lies within the limits of the finite size of the points on the curve. An additional error of 2 percent should be added to account for the uncertainty in absolute differential cross section values. The positions of maxima and minima for each observed inelastic angular distribution are indicated in Table 1.

The angular distributions obtained for the elastically scattered alpha particles are shown in Figs. 19-21 where the calculated coulomb cross sections are indicated by a dashed line.

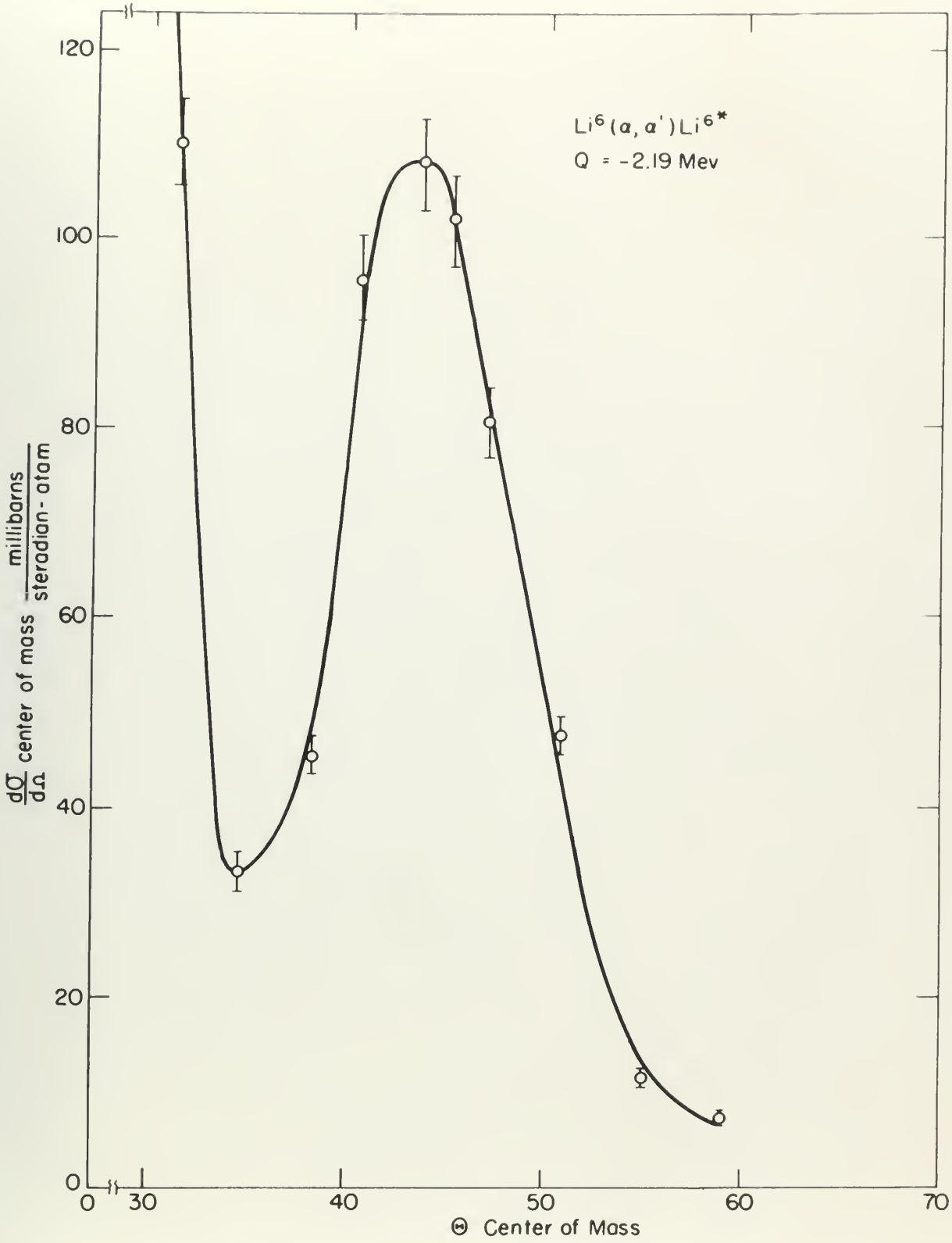
$Li^6(\alpha, \alpha')Li^{6*}$
Q = -2.19 Mev
$\frac{d\sigma}{d\Omega}$ center of mass $\frac{\text{millibarns}}{\text{steradian-atom}}$
120
100
80
60
40
20
0
0
30
40
50
60
70
Θ Center of Mass

Figure 10

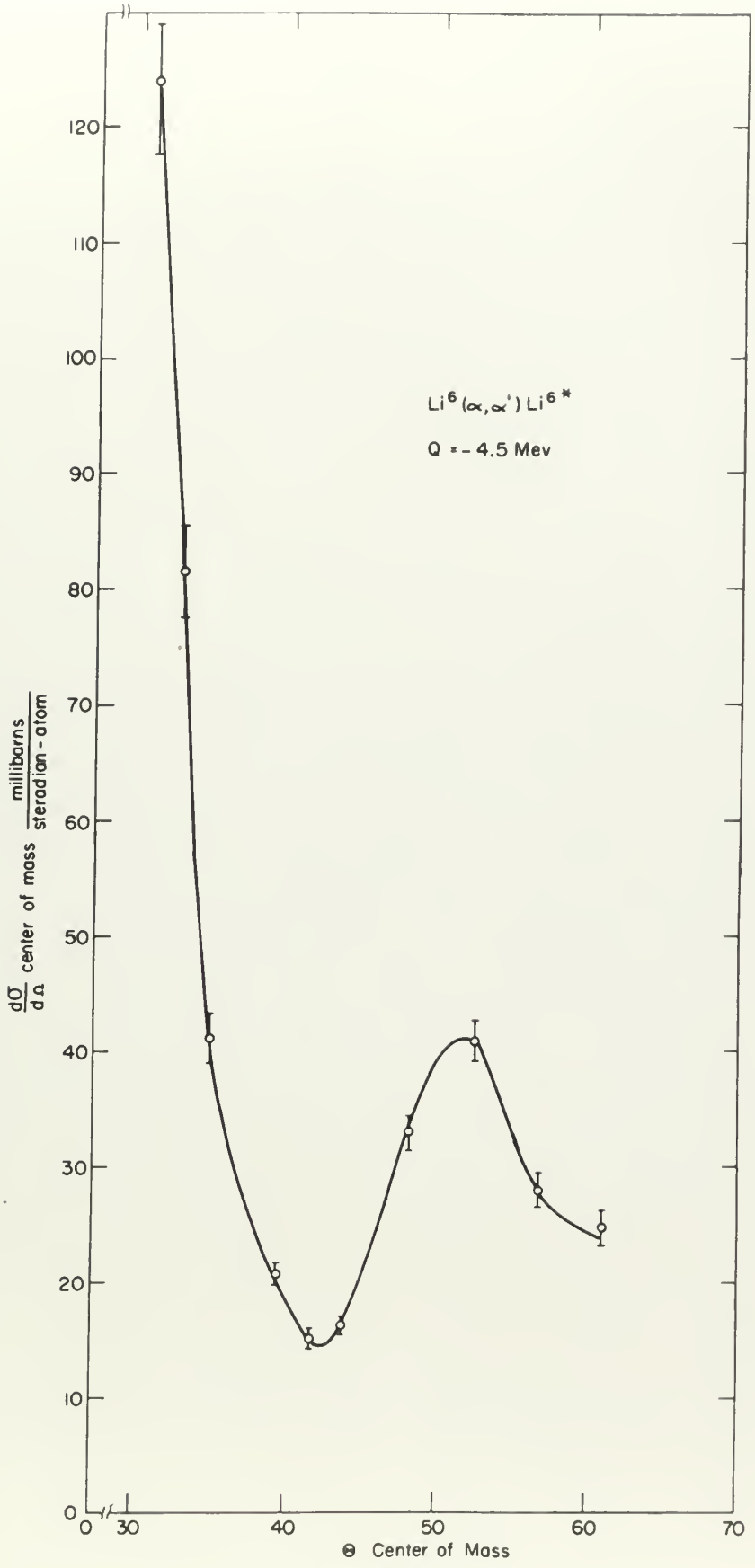
$Li^6(\alpha,\alpha')Li^{6*}$
Q = - 4.5 Mev
$\frac{d\sigma}{d\Omega}$ center of mass $\frac{\text{millibarns}}{\text{steradian - atom}}$
Θ Center of Mass
0
10
20
30
40
50
60
70
80
90
100
110
120
30
40
50
60
70

Figure 14

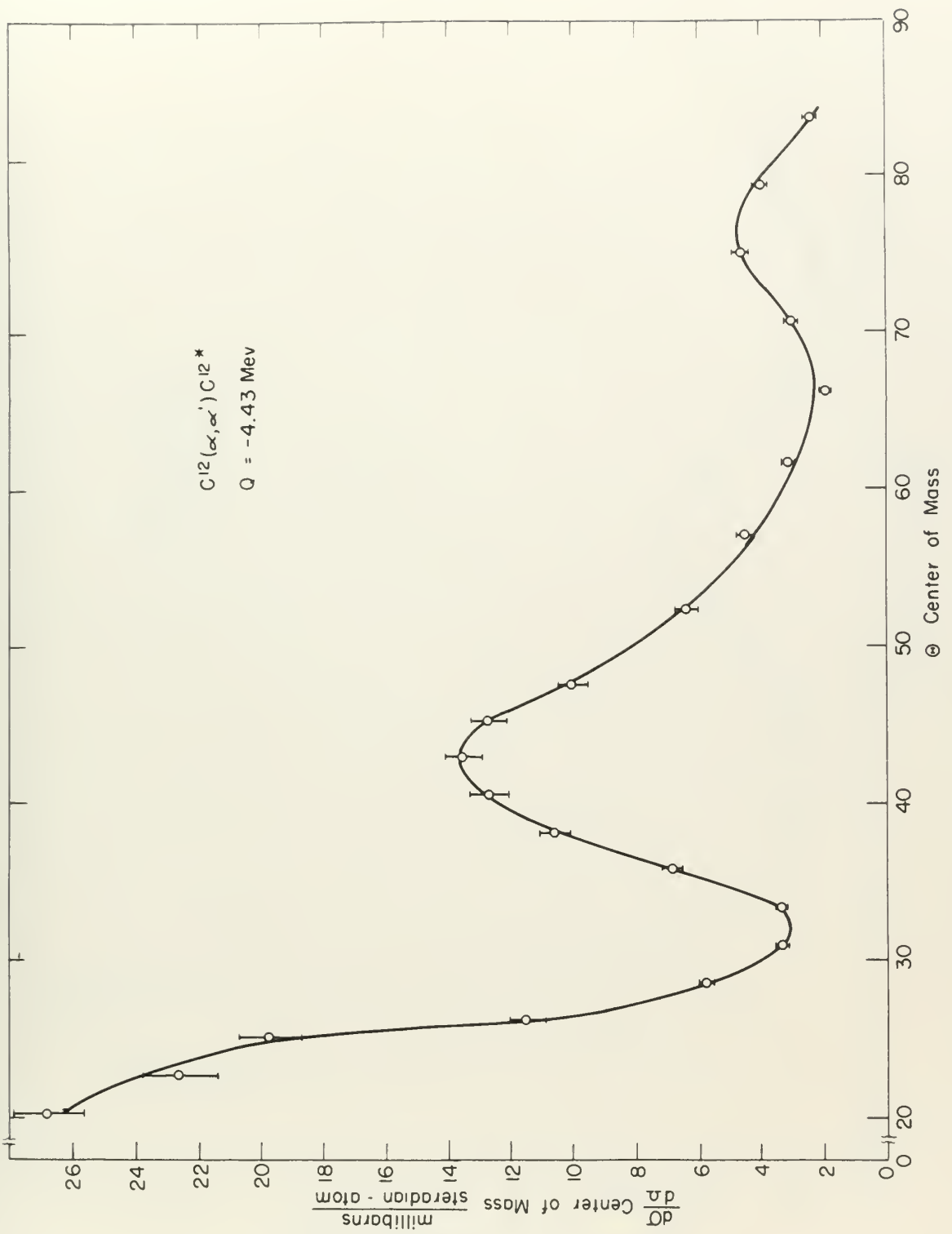
$C^{12}(\alpha,\alpha')C^{12*}$
Q = -4.43 Mev
$\frac{dQ}{d\Omega}$ Center of Mass $\frac{\text{millibarns}}{\text{steradian - atom}}$
Θ Center of Mass
0
2
4
6
8
10
12
14
16
18
20
22
24
26
0
20
30
40
50
60
70
80
90

Figure 15


$C^{12}(\alpha,\alpha')\,C^{12*}$
Q = −7.65 Mev
$\frac{dQ}{d\Omega}$ center of mass $\frac{10^{-1}\text{ millibarns}}{\text{steradian - atom}}$
Θ Center of Mass
0
10
20
30
40
50
60
70
80
90
0
20
30
40
50
60
70

Figure 16

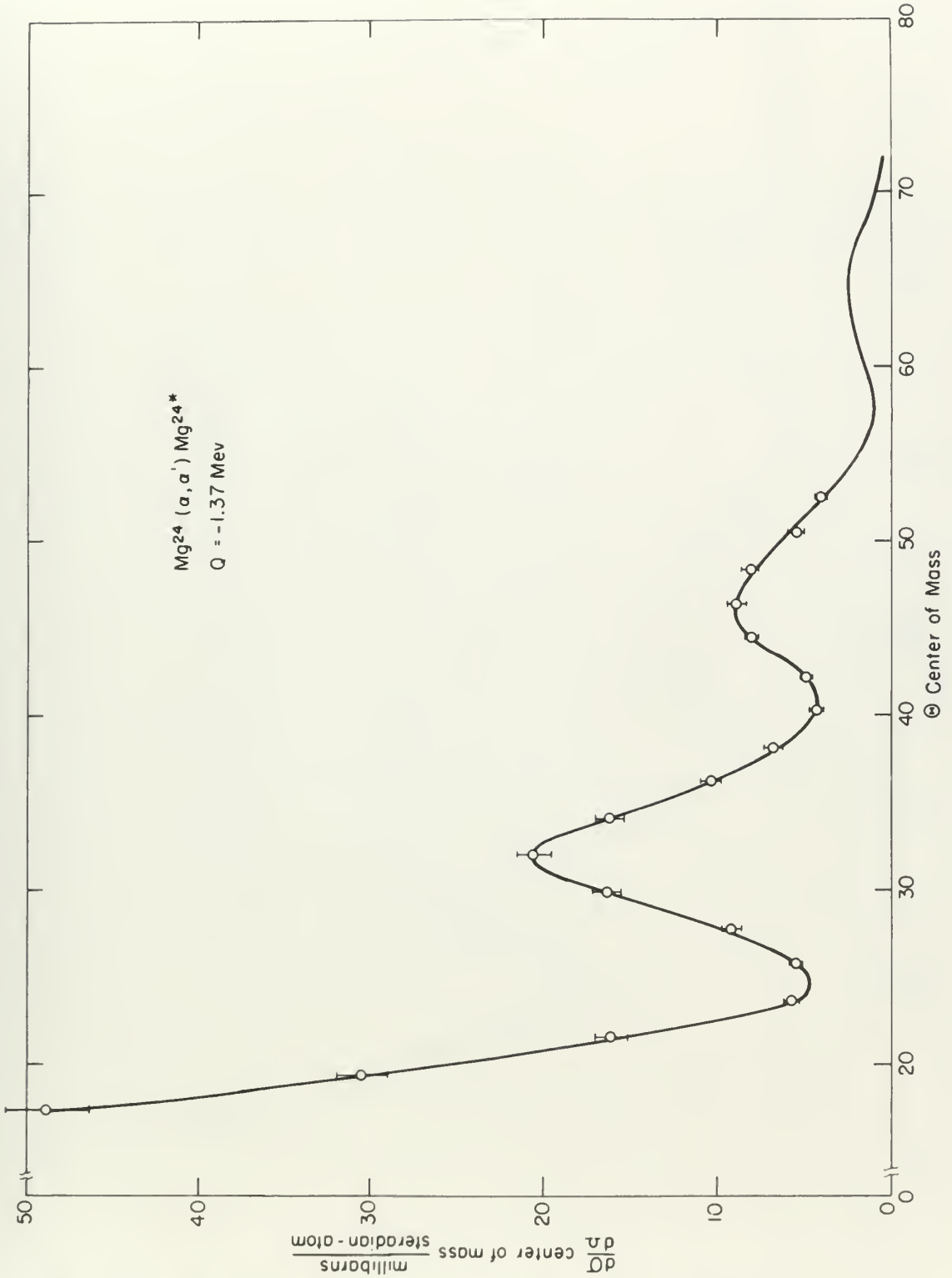
Mg^{24} (a, a') Mg^{24*}
Q = -1.37 Mev
$\frac{d\sigma}{d\Omega}$ center of mass $\frac{\text{millibarns}}{\text{steradian - atom}}$
Θ Center of Mass
0
10
20
30
40
50
60
70
80

Figure 17

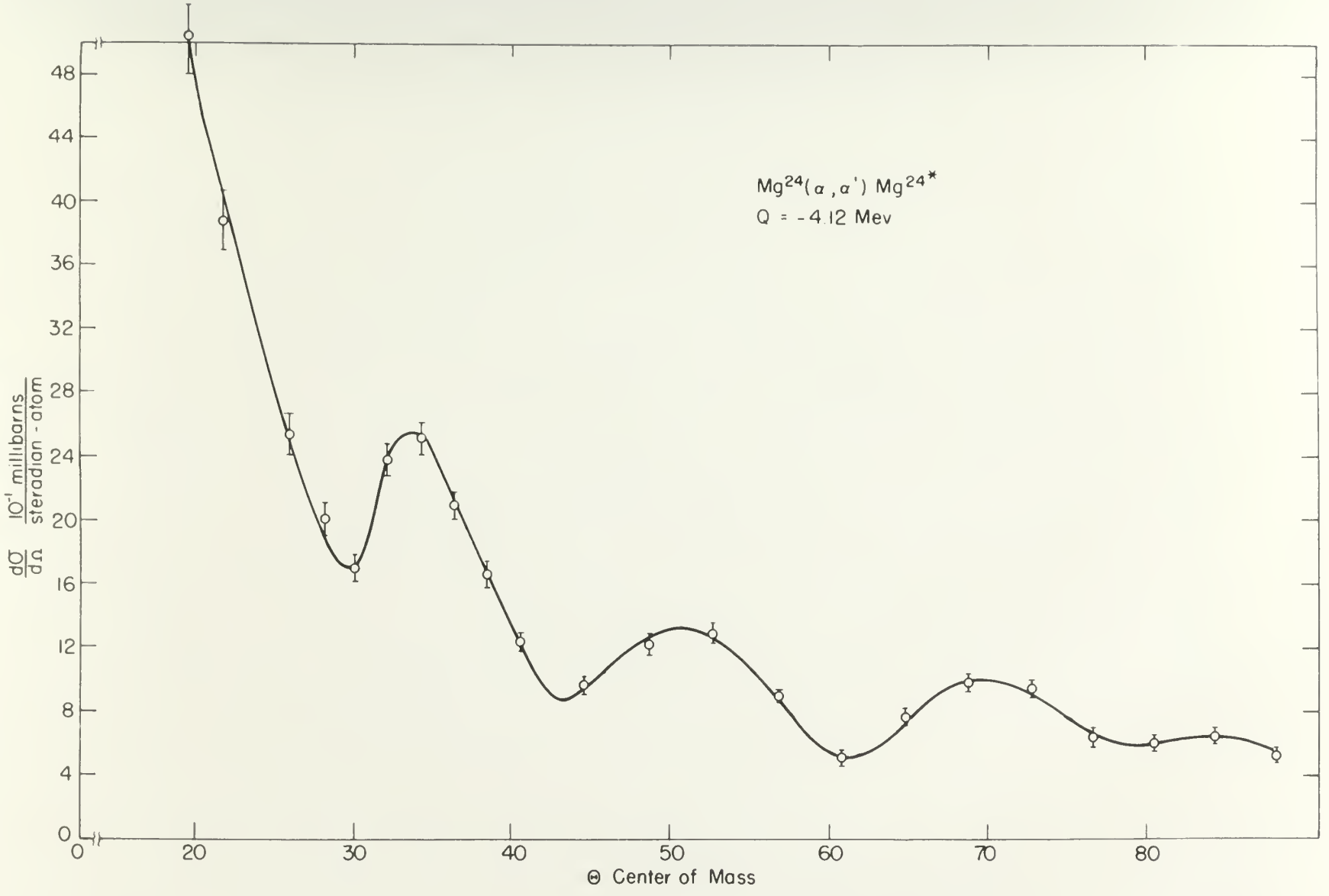
$Mg^{24}(\alpha, \alpha')\ Mg^{24*}$
Q = -4.12 Mev
$\frac{d\sigma}{d\Omega}$ $\frac{10^{-1}\ millibarns}{steradian - atom}$
Θ Center of Mass
0
4
8
12
16
20
24
28
32
36
40
44
48
0
20
30
40
50
60
70
80

Figure 18

Table 1. Angular positions of maxima and minima experimentally observed in the inelastic alpha-particle angular distributions.

Target nucleus	Excitation level (Mev)	Maximum or minimum	Angle C.M.	Intensity millibarns/steradian-atom
Li^6	2.19	min	34.5	33
	2.19	max	44.0	108
	4.5	min	48.5	14
	4.5	max	59	41
C^{12}	4.43	min	38	3
	4.43	max	43	13.5
	4.43	min	66	3.0
	4.43	max	75	4.8
	7.65	max	34.5	9.25
	7.65	min	35	0.75
	7.65	max	46	3.25
	7.65	min	56.5	0.60
	7.65	max	65	1.25

Table 1. Angular positions of maxima and minima experimentally observed in the inelastic alpha-particle diffractionpatterns.

Target nucleus	Excitation level (Mev)	Maximum or minimum	Angle C.M.	Intensity differential cross-section
Li^6	3.19	min	74.7	1
	3.29	max	64.1	108
	4.5	min	60.4	74
	4.6	max	50	42
C^{12}	4.43	min	70	7
	4.43	max	41	13.2
	4.43	min	30	0.4
	4.43	max	75	4.8
	7.65	max	64.1	0.12
	7.65	min	50	0.78
	7.65	max	40	0.08
	7.65	min	34.7	0.02
	7.65	max	25	0.19

Table 1 (cont.)

Target nucleus	Excitation level (Mev)	Maximum or minimum	Angle C.M.	Intensity millibarns/steradian-atom
Mg^{24}	1.37	min	25	4.5
	1.37	max	32	10.5
	1.37	min	40.5	4.0
	1.37	max	46.5	9.0
	1.37	min	57	1.0
	1.37	max	64.5	8.5
	4.12	min	29.5	1.70
	4.12	max	33.5	2.56
	4.12	min	43	0.88
	4.12	max	51	1.32
	4.12	min	60.5	0.52
	4.12	max	69	1.00
	4.12	min	80	0.60

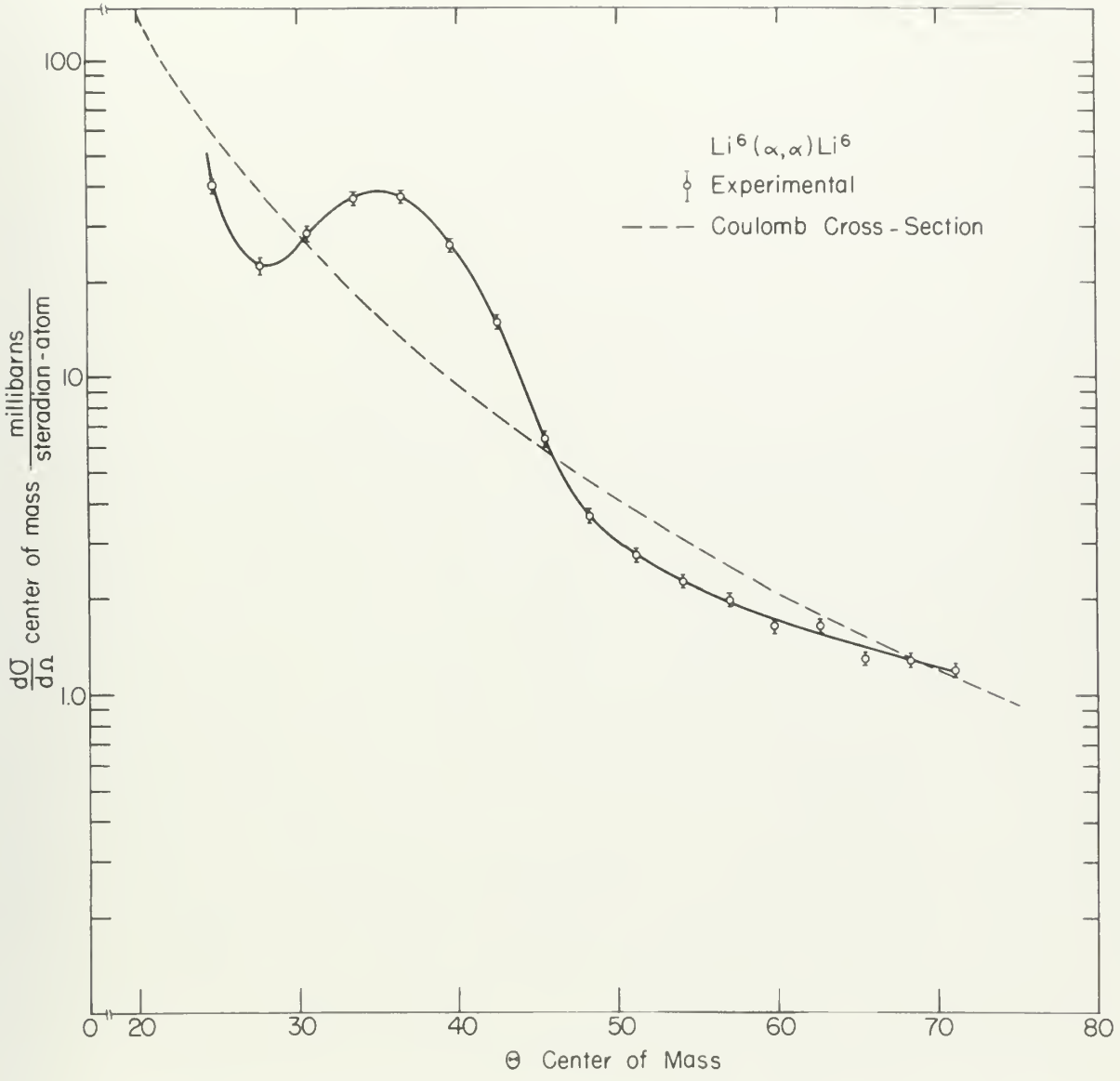
Li⁶(α,α)Li⁶
Experimental
Coulomb Cross-Section
dσ/dΩ center of mass millibarns / steradian-atom
100
10
1.0
0
20
30
40
50
60
70
80
Θ Center of Mass

Figure 10

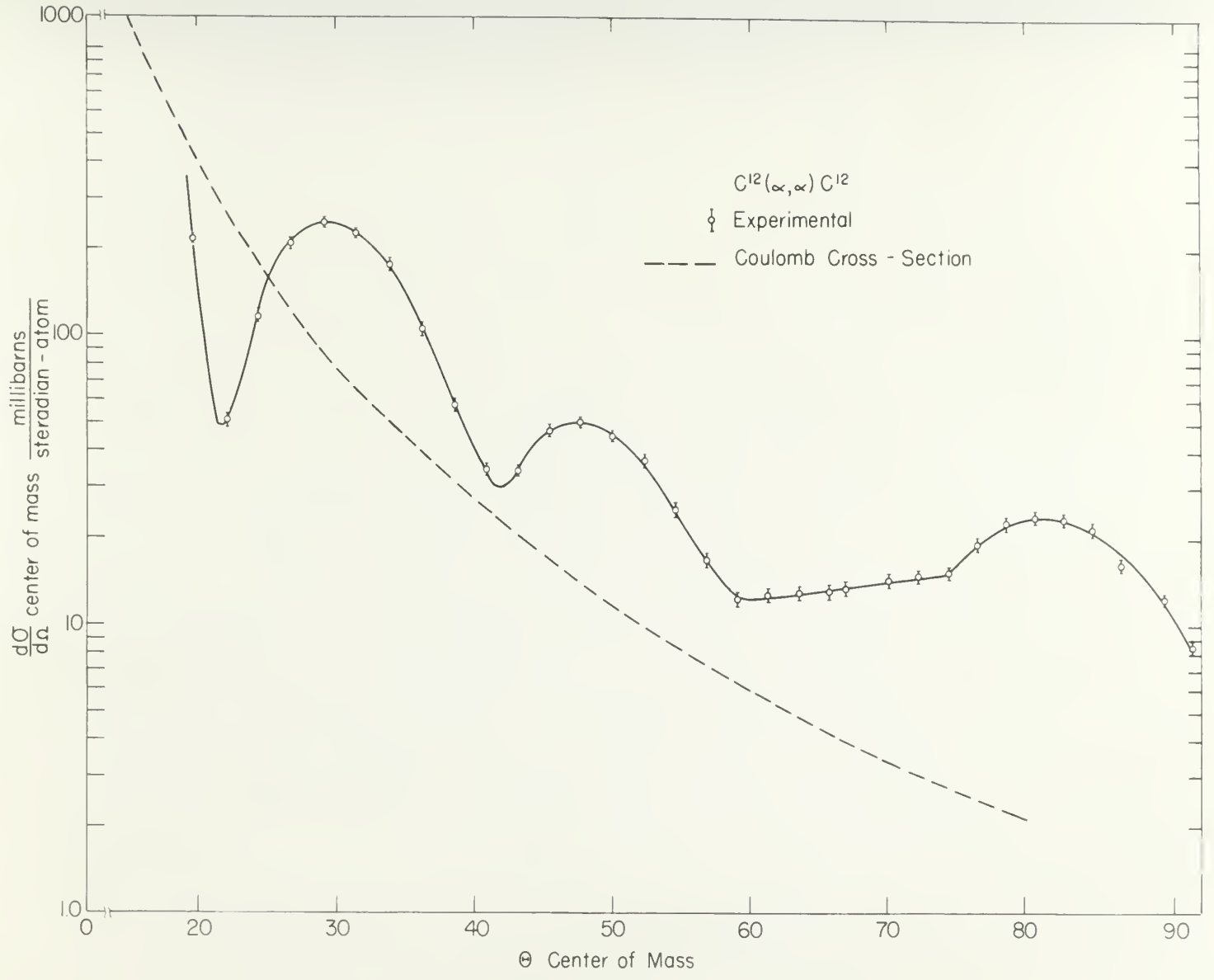
1000
100
10
1.0
0
20
30
40
50
60
70
80
90
Θ Center of Mass
$\frac{d\sigma}{d\Omega}$ center of mass $\frac{\text{millibarns}}{\text{steradian - atom}}$
$C^{12}(\alpha,\alpha)\,C^{12}$
Experimental
Coulomb Cross - Section

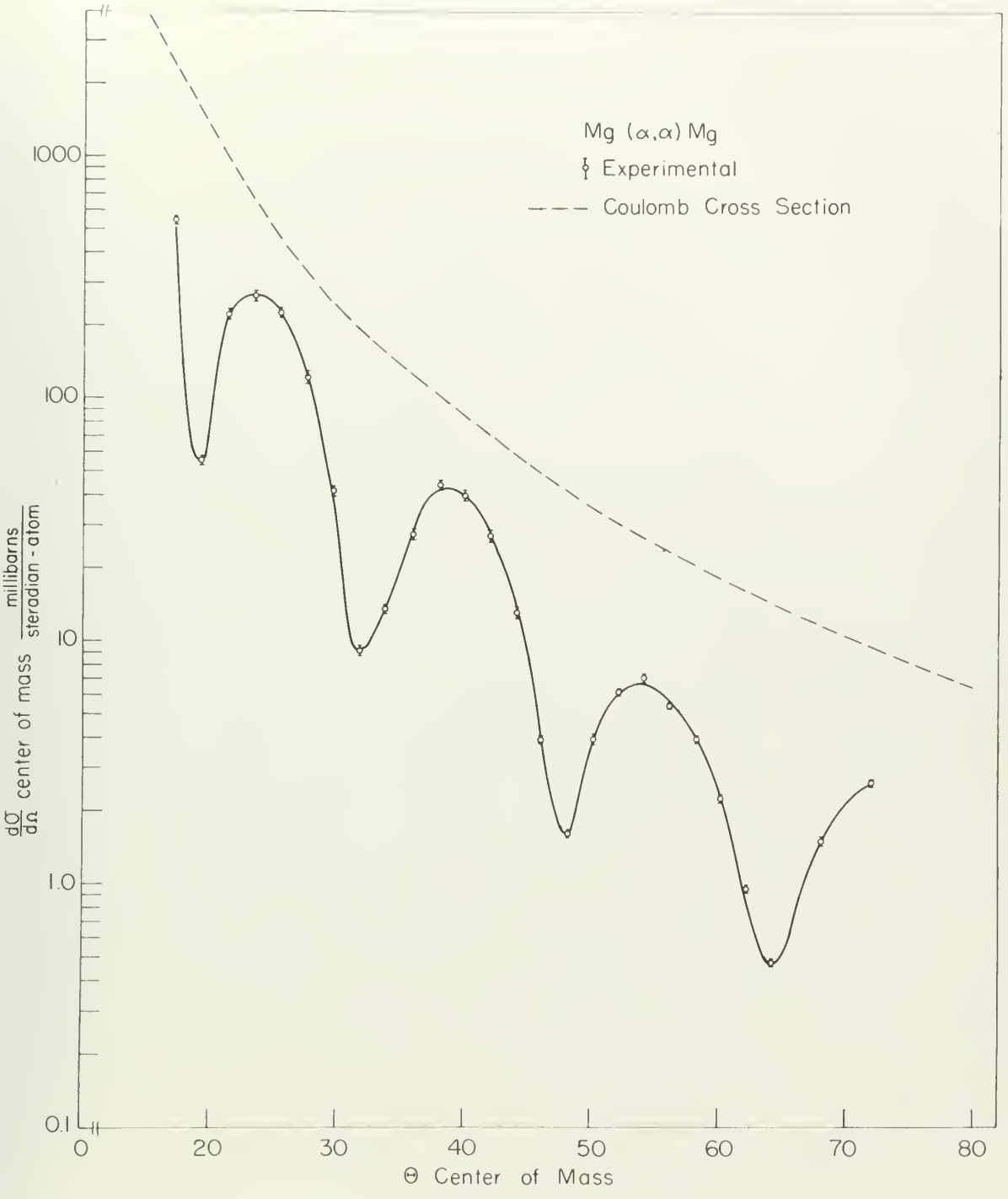
Mg (α,α) Mg
Experimental
Coulomb Cross Section
1000
100
10
1.0
0.1
0
20
30
40
50
60
70
80
Θ Center of Mass
dσ/dΩ center of mass millibarns / steradian - atom

Figure 21

VI. DISCUSSION OF RESULTS

A. INELASTIC SCATTERING PROCESS

The well defined structure evident in the inelastic angular distributions of Figs. 13-18 is suggestive of the theoretical predictions for a direct interaction. This is more definitely indicated when we consider that, in the case of C^{12}, the cross section for scattering at angles greater than 90 degrees was found to be negligible compared with the values observed in the forward quadrant. As mentioned in Sec. I, there are three processes currently accepted as possible mechanisms for the excitation of nuclei by charged particles. Predictions of the theory for each process, when compared with the experimental data, should permit an estimate of the contribution due to each method of excitation.

If excitation occurred by the formation of a compound nucleus, the nuclei involved would be B^{10}, O^{16}, and Si^{28}. A study of the level spacing in these nuclei (A3, E1), at the excitation levels involved, clearly indicates that a statistical treatment is not valid. Even if we did assume that the statistical theory was applicable, any reasonable level density function (W6) predicts inelastic scattering cross sections much smaller than the observed values.

VI. Discussion of results

A. Inelastic scattering process

From a consideration of the energy spread in the incident beam, it is also apparent that the interactions could not involve the excitation of only a single level in the compound nucleus. The possibility still exists that an angular distribution which is not symmetric about 90 degrees in the center-of-mass coordinates could result from a compound nucleus interaction (H3). However, the experimental angular distributions were shown to be insensitive to significant changes in beam energy. It is concluded that no contributions to the observed angular distributions from compound nucleus interactions were experimentally observable.

It is assumed that a contribution to the observed cross sections due to electric excitation would not be of sufficient magnitude to permit detection. This assumption is believed to be valid for the following reasons.

(a) The electric excitation mechanism is most important when the bombarding energies are below the coulomb barrier, a condition not fulfilled in this experiment.

(b) For bombarding energies above the barrier, the electric excitation effect would probably be masked by the large nuclear scattering (H4, M3).

(c) If we optimize conditions of bombarding energy and order of multipole moment involved, the theoretical maximum <u>total</u> cross section for electric excitation is less than most of the <u>differential</u> cross sections obtained for excitation of the individual levels observed.

The early direct interaction models (B5, G1) had considerable success in explaining experimental angular distributions despite their somewhat crude approach. A theory based on the Born approximation (H2) was quite successful in explaining the (d,d') angular distributions obtained in excitation of the 1.38-Mev level in Mg^{24}. The recent theory of Austern et al. (A4) proposes a mechanism by which the reaction proceeds by a direct interaction between the incoming particle and one of the nucleons at the surface of the nucleus rather than with the nucleus as a whole. The theory predicts a differentialcross section for a reaction in which the residual nucleus is left in an excited state. The theory given in the following section closely follows this treatment and was derived (R5) in an attempt to explain the inelastic angular distributions obtained in this experiment.

B. THEORETICAL ANGULAR DISTRIBUTION AND COMPARISON WITH EXPERIMENT

The cross section for the interaction can be written

$$\frac{d\sigma}{d\Omega} = \frac{1}{2J+1} \sum_{M,M'} |f_{M',M}(\theta)|^2$$

where we have averaged over the initial (unprimed) magnetic quantum numbers and summed over the final (primed) ones. Using the Born (plane wave) and impulse (unperturbed nuclear states) approximations (C3)

$$f_{M',M}(\theta) = \int \vec{dr_1} \cdots \vec{dr_A} \vec{dr}\ \psi_{J',M'}(A)\, \mathcal{E}^{-i\vec{k'}\cdot\vec{r}}\, V(r,A)\, \psi_{J,M}(A)\, \mathcal{E}^{i\vec{k}\cdot\vec{r}}$$

in which we have assumed that the spinless alpha particle is a point particle. $\psi_{J,M}(A)$ and $\psi_{J',M'}(A)$ are the initial and final nuclear states and the exchange of particles is neglected. To conserve angular momentum the alpha particle must undergo a change in angular momentum equal, and opposite in direction, to that of the nucleus. In other words, J, J', and ℓ must satisfy the triangular inequalities

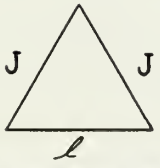

$$J + J' \geq \ell$$
$$J + \ell \geq J'$$
$$J' + \ell \geq J$$

Another selection rule, which results from a consideration of

3. Isomeric effects in scattering from oriented nuclei

REFERENCES

parity, is that ℓ is odd for a nuclear parity change and ℓ is even if the nuclear parity is unchanged in the reaction.

To see the results of the above, we abandon the independent particle model of the nucleus and consider the nucleus as a whole. Then

$$f_{M',M}(\Theta,\varphi) = \int d\vec{r}_N \int d\vec{r}\, \psi^*_{J',M'}(\vec{r}_N)\, e^{-i\vec{k}'\cdot\vec{r}}\, V(\vec{r}-\vec{r}_N)\, \psi_{JM}(\vec{r}_N)\, e^{i\vec{k}\cdot\vec{r}}$$

$$= \int d\vec{r}_N \psi^*_{J'M'}(\vec{r}_N)\, \psi_{JM}(\vec{r}_N)\, e^{i(\vec{k}-\vec{k}')\cdot\vec{r}_N} \int d\vec{x}\, e^{-i\vec{k}'\cdot\vec{x}}\, V(\vec{x})\, e^{i\vec{k}\cdot\vec{x}}$$

where $\vec{x} = \vec{r} - \vec{r}_N$. We set $V(\vec{x}) = V_o \delta(\vec{x})$, and expand the plane wave obtaining

$$f_{M',M}(\Theta,\varphi) = V_o \sum_\ell i^\ell \sqrt{4\pi(2\ell+1)} \int d\vec{r}_N\, \psi^*_{J'M'}(\vec{r}_N)\, \psi_{JM}(\vec{r}_N)\, j_\ell(Kr_N)\, Y^o_\ell(\Theta_N)$$

where $K = |\vec{k}-\vec{k}'| = \sqrt{k^2 + k'^2 - 2kk'\cos\omega}$ and from the selection rule previously discussed, ℓ is restricted to the "triangular values". Separating angular and radial integrals

$$f_{M',M}(\Theta,\varphi) = \sum_\ell \beta(J,J',M,M',\ell) \int_R^\infty r_N^2\, d\vec{r}_N f'(\vec{r}_N) f(\vec{r}_N) j_\ell(Kr_N)$$

where we restrict the integration to the region outside the nucleus. If the integration includes the nuclear volume, the resulting angular distribution has much too little structure to be compared with the experimental data (T3). By assuming that the alpha particle does not penetrate the nucleus we imply a direct "surface" interaction.

$$\mathcal{H}^{J,M}(\theta,\phi) = \int d\vec{R}\, d\vec{r}\, \psi^{J,M}_{\alpha_1 I_1 \alpha_2 I_2}(\vec{R},\vec{r})\, \delta(\vec{r}-\vec{r}_1)\, \psi^{J,M}_{\alpha_1 I_1 \alpha_2 I_2}(\vec{R},\vec{r})$$

$$= \int d\vec{R}\, \psi^{J,M}_{\alpha_1 I_1 \alpha_2 I_2}(\vec{R},\vec{r}_1) \int d\vec{r}\, \delta(\vec{r}-\vec{r}_1)\, \psi^{J,M}_{\alpha_1 I_1 \alpha_2 I_2}(\vec{R},\vec{r})$$

where $\vec{x} = \vec{r} - \vec{r}_1$. We set $\delta(\vec{x}) = \lambda^0 g(\vec{x})$, and evaluate the delta
term explicitly

$$\mathcal{H}^{J,M}(\theta,\phi) = \lambda^0 \sum_{\ell} i^{\ell} \sqrt{4\pi(2\ell+1)} \int d\vec{R}\, \psi^{J,M}_{\alpha_1 I_1 \alpha_2 I_2}(\vec{R},\vec{r}_1)\, Y^{\ell}_0(\hat{x})$$

where $x = |\vec{r} - \vec{r}_1| = \sqrt{R^2 + R_1^2 - 2RR_1 \cos\theta}$. The first two
relation role previously discussed, ℓ is restricted by the
"selection rule". Conservation energy and total isospin

$$\mathcal{H}^{J,M}(\theta,\phi) = \sum_{\ell} \mathcal{H}^{J,M}_{\ell}(I_1,I_2,I_1',I_2',\ell) \int d\hat{R}\, Y^{\ell}_0(\hat{x})\, Y^{\ell}_0(\hat{R})$$

where we restrict the integration to the region outside the
nucleus. If the integration includes the nuclear volume,
the resulting angular distribution has much the little struc-
ture to be compared with the experimental data [21]. By
assuming the ℓ=0 alpha particle does not penetrate the
nucleus we imply a direct "surface" interaction.

If the nuclear wave function falls off sufficiently rapidly outside the nucleus we can approximate it by the value of the integrand at $r_N = R$. Then

$$f_{M',M}(\theta,\phi) = \sum_{\ell} \beta(J,J',M,M',\ell) g(R) j_{\ell}(KR)$$

and if ℓ is restricted by the previous selection rules to a single value

$$f_{M',M}(\theta) = \beta(J,J',M,M',\ell) g(R) j_{\ell}(KR)$$

and

$$\frac{d\sigma}{d\Omega} \propto |j_{\ell}(KR)|^2$$

This restriction of ℓ to a single value will occur only if either J or J' is zero. Otherwise there may be two or more possibilities. These can be further restricted, however, if we use the independent particle model of the nucleus. Assume that the nucleus consists of one or more closed shells with a number of nucleons in the orbital angular momentum state λ outside the last closed shell. Then if we assume two particle interactions between the incident alpha particle and the individual nucleons, $f_{M,M'}(\theta)$ will involve integrals of the form $\int Y_{\lambda m} Y_{\lambda m'} Y_{\ell 0}\, d\Omega$, having the value zero unless $\ell = 0, 2, \ldots, 2\lambda$. This additional selection rule is usually sufficient to eliminate all but a single value of ℓ.

The predictions of this theory are now to be compared with the experimental data. It must be stated that, because of the plane wave approximation, these results are not expected to give accurate angular distributions. The predictions are most accurate at the forward angles and the position of the first maximum is most desirable for determining the value of ℓ involved.

Experimental difficulties prohibited observations at laboratory angles less than 14.8 degrees, an angle greater than the predicted position of the first maxima in most of the interactions. In all but one case studied here, however, the ℓ values can be obtained since the quantum numbers of the levels involved have been determined in other experiments (A3). The theoretical curves were compared with the experimental data using a value of R which gave the best fit with the first observable maximum and minimum.

1. $\underline{Li^6(a,a')Li^{6*}}$. The ground level of Li^6 has J = 1, the 2.19-Mev level J = 3, and the 4.5-Mev level J = 2, all of even parity. In both cases the theory predicts an angular distribution which varies as $|j_2(KR)|^2$. The values of R required to fit the data are quite large. However, this is not considered too serious since the "radius" of Li^6 is a rather nebulous concept. Using the relationship $R = r_0 A^{1/3}$ with $r_0 = 1.5 \times 10^{-13}$ cm, alpha-particle radii of 3.0×10^{-13}

cm and 3.9×10^{-13} cm were required to fit the data for the 4.5-Mev and 5.19-Mev levels. There is some evidence (A6, B8) for a large alpha-particle radius based on (n,a) scattering experiments. However, the values given above are considered excessive. The fit obtained is quite good, however, and is shown in Figs. 22 and 23.

2. $\underline{C^{12}(a,a')C^{12*}}$ $\underline{Q = -4.43 \text{ Mev}}$. The theory predicts an angular distribution varying as $|j_2(KR)|^2$ for excitation from the $J = 0^+$ ground level to the $J = 2^+$ first excited level in C^{12}. Figure 24 shows the fit with experimental observations and also illustrates the sensitivity of the spherical Bessel function to a small change in R. The value of R which gave the best agreement at forward angles required an alpha-particle radius of 2.5×10^{-13} cm for $r_o = 1.5 \times 10^{-13}$ cm. This is not incompatible with the previously mentioned evidence for a large alpha-particle radius. It is noted that the data deviate from the theoretical curve at angles greater than 50 degrees as expected from the discussion of its range of validity.

3. $\underline{C^{12}(a,a')C^{12*}}$ $\underline{Q = -7.65 \text{ Mev}}$. In this case a $|j_o(KR)|^2$ curve is predicted since the ground and second excited levels are both $J = 0^+$. Agreement between theory and experiment are illustrated in Fig. 25 where the fit is seen to be extremely good. The value of R is the same as

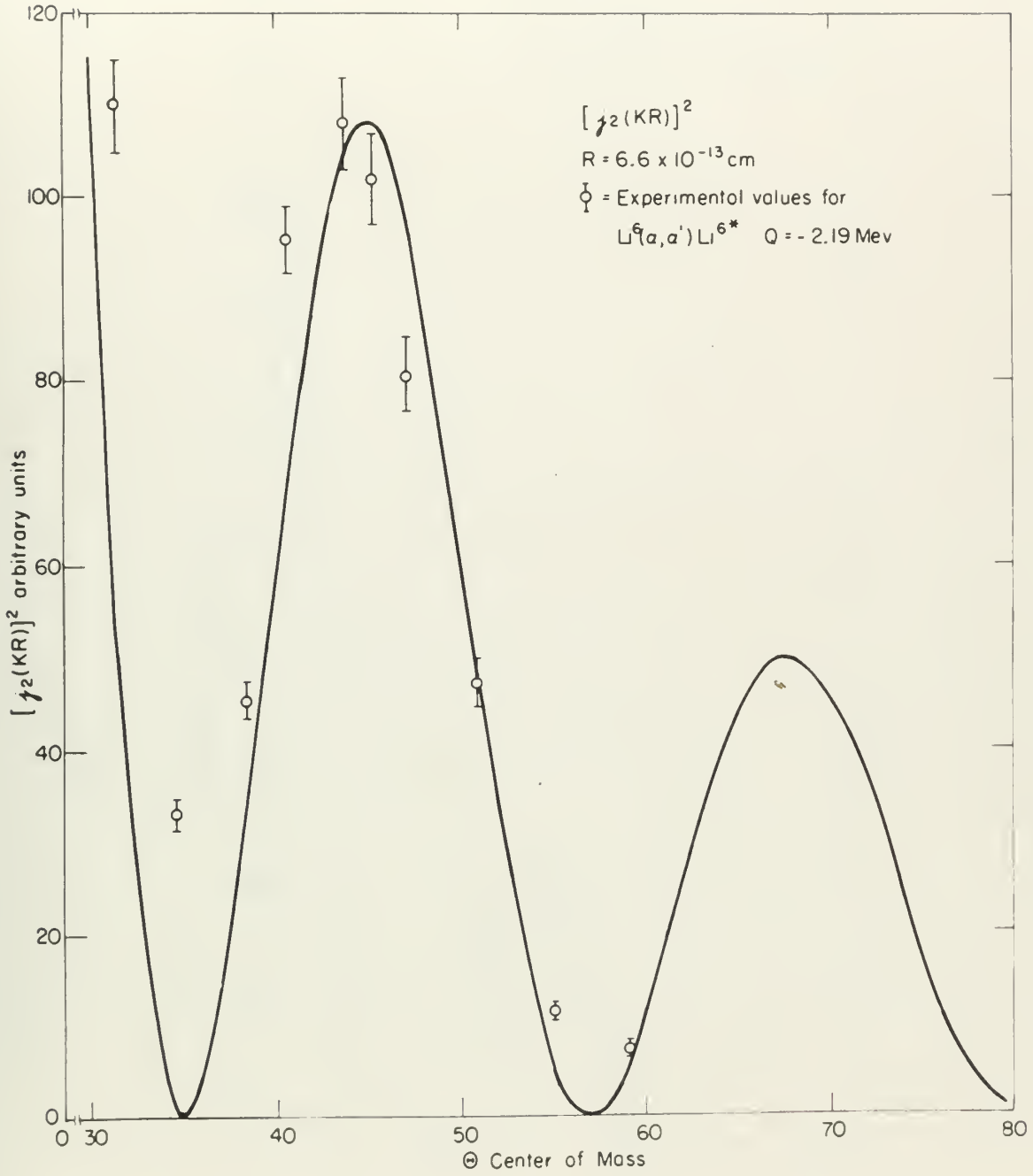
$[j_2(KR)]^2$
R = 6.6 x 10^{-13} cm
= Experimental values for
$Li^6(a,a')Li^{6*}$ Q = - 2.19 Mev
$[j_2(KR)]^2$ arbitrary units
Θ Center of Mass
0
20
40
60
80
100
120
30
50
70

Figure 12

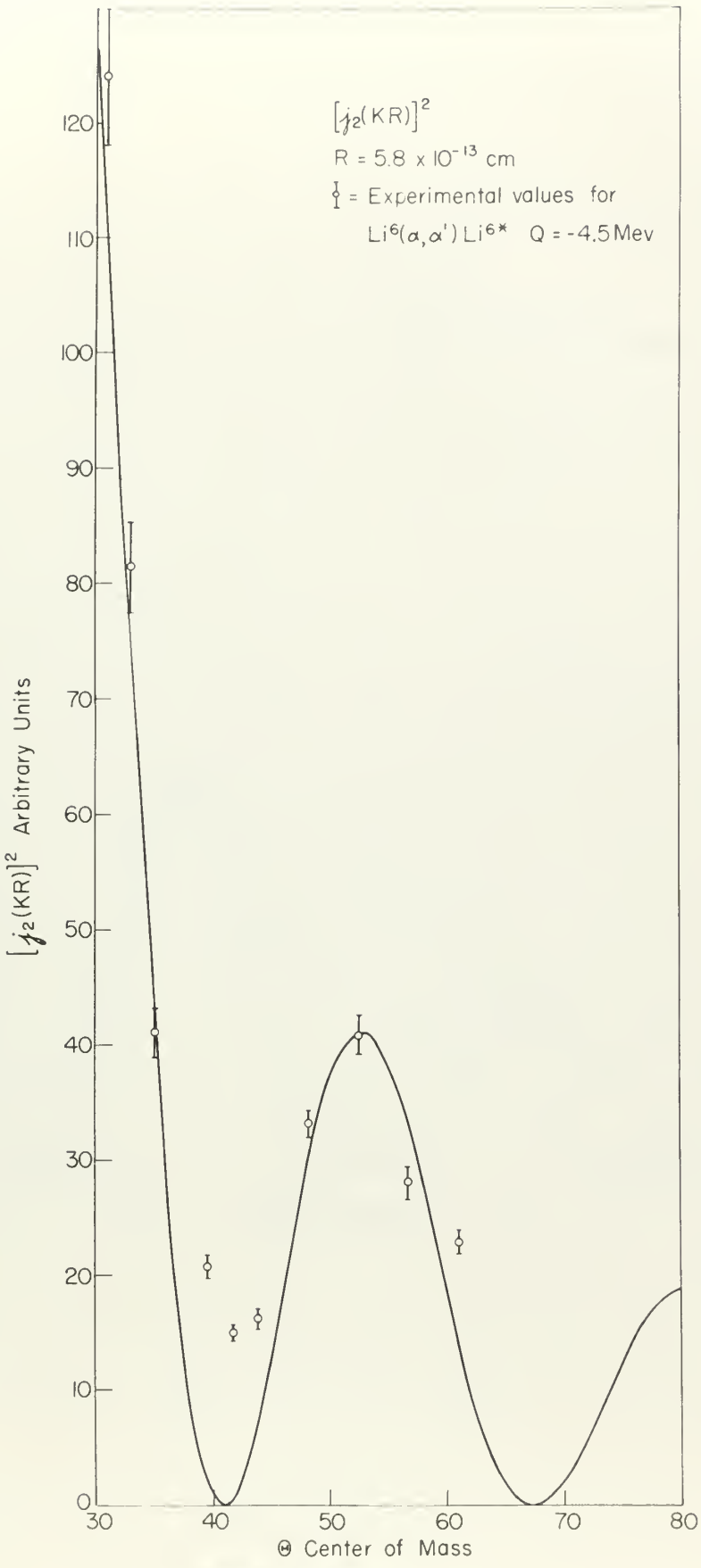
$[j_2(KR)]^2$
R = 5.8 x 10⁻¹³ cm
= Experimental values for
Li⁶(α,α')Li⁶* Q = -4.5 Mev
$[j_2(KR)]^2$ Arbitrary Units
0
10
20
30
40
50
60
70
80
90
100
110
120
30
40
50
60
70
80
Θ Center of Mass

Figure 13

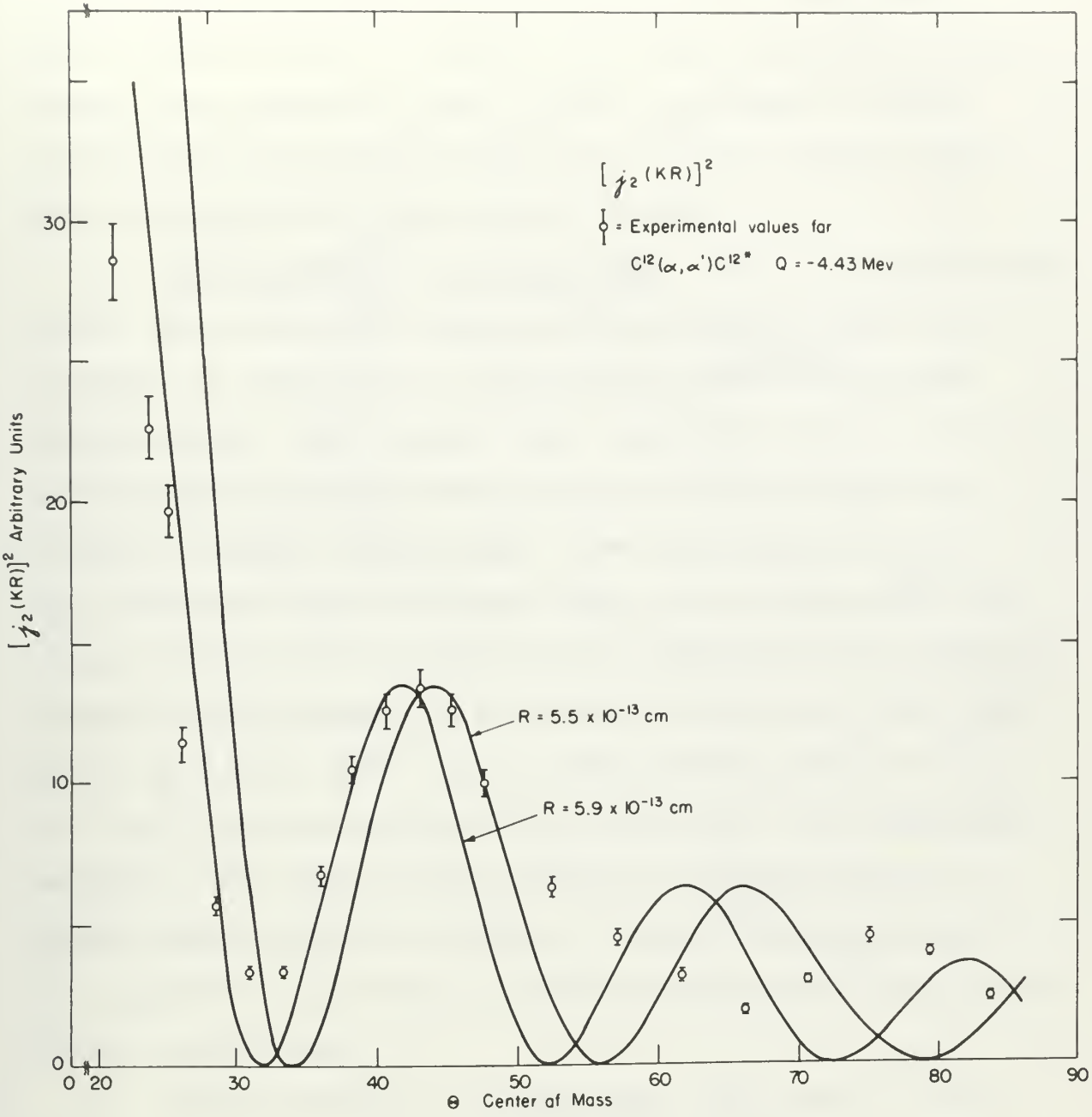
$[j_2(KR)]^2$
= Experimental values for
$C^{12}(\alpha,\alpha')C^{12*}$ Q = -4.43 Mev
R = 5.5 x 10^{-13} cm
R = 5.9 x 10^{-13} cm
$[j_2(KR)]^2$ Arbitrary Units
0
10
20
30
0
20
30
40
50
60
70
80
90
Θ Center of Mass

Figure 24

was used for the first excited level of C^{12}. Since the first maximum shown is actually the first maximum occurring beyond zero degrees for the j_0 curve, agreement at larger angles should be somewhat better than in the previous case. This is illustrated quite well in Fig. 35.

4. $\underline{Mg^{24}(a,a')Mg^{24*}}$ $\underline{Q = -1.37 \text{ Mev}}$. Due to the kinematics of the interaction, the center-of-mass angular range of observation is increased for interactions involving heavier target nuclei. For a ground level spin of $J = 0$ and a $J = 2$ excited level, both of even parity, the theory predicts a $|j_2(KR)|^2$ angular distribution. The experimental data fit the theoretical curve extremely well and this agreement continues past the third maximum of the spherical Bessel function (second maximum shown), as indicated in Fig. 36. With a unit radius $r_o = 1.5 \times 10^{-13}$ cm, an alpha-particle radius of 3.1×10^{-13} cm was required to fit the curve. By bombarding magnesium with 44-Mev alpha particles, Gugelot (H6) has obtained almost identical results. His data are approximated by a $|j_2(KR)|^2$ and require a radius approximately the same as in the present case.

5. $\underline{Mg^{24}(a,a')Mg^{24*}}$ $\underline{Q = -4.12 \text{ Mev}}$. The level of excitation involved in this interaction is actually a doublet (H5). The lower level has been determined to be $J = 4^+$ (A3) for which the theory would predict a $|j_4(KR)|^2$ angular

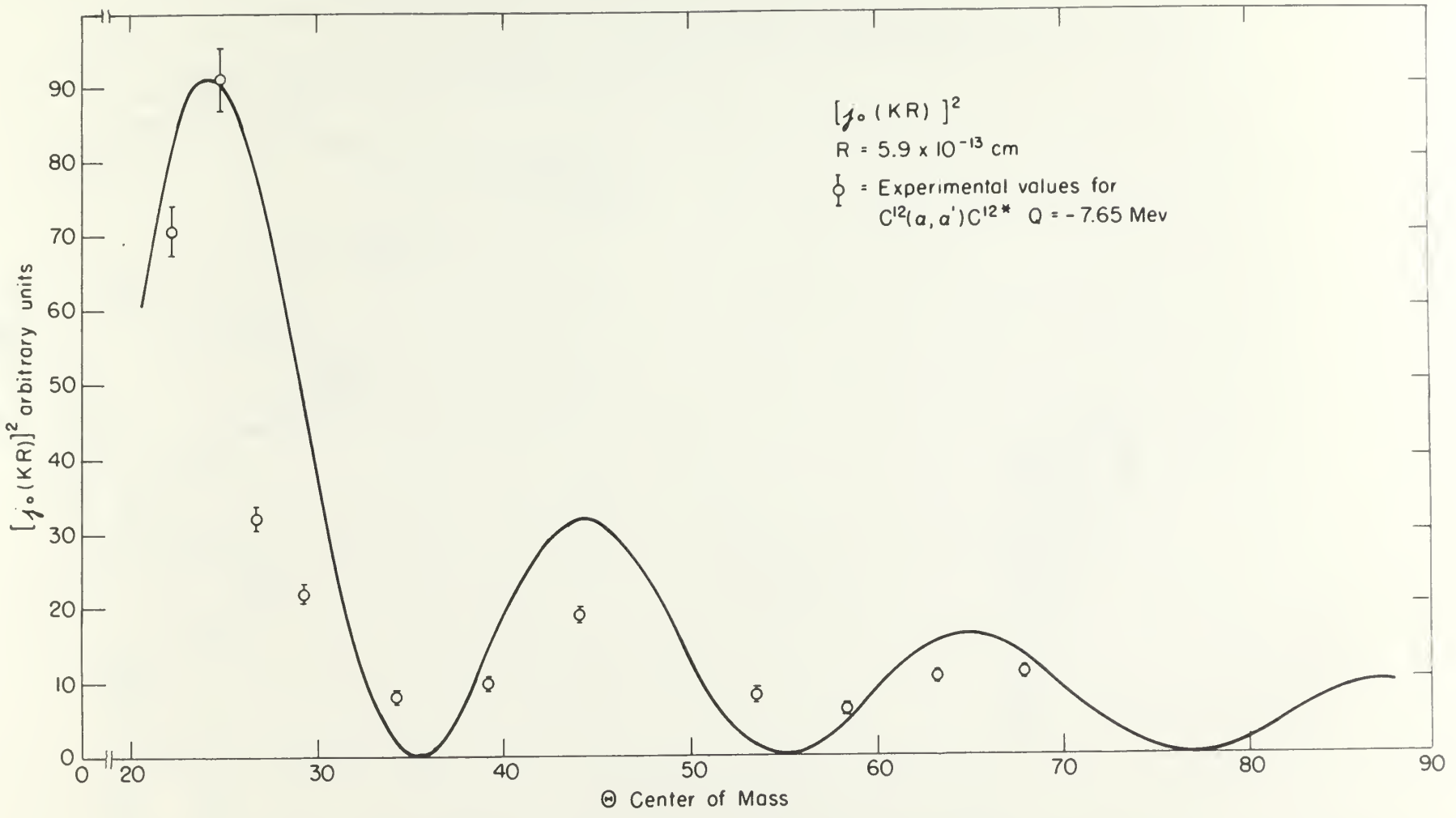
$[j_0(KR)]^2$
R = 5.9 x 10^{-13} cm
= Experimental values for
C^{12}(α, α')C^{12}* Q = - 7.65 Mev
$[j_0(KR)]^2$ arbitrary units
Θ Center of Mass
0
10
20
30
40
50
60
70
80
90

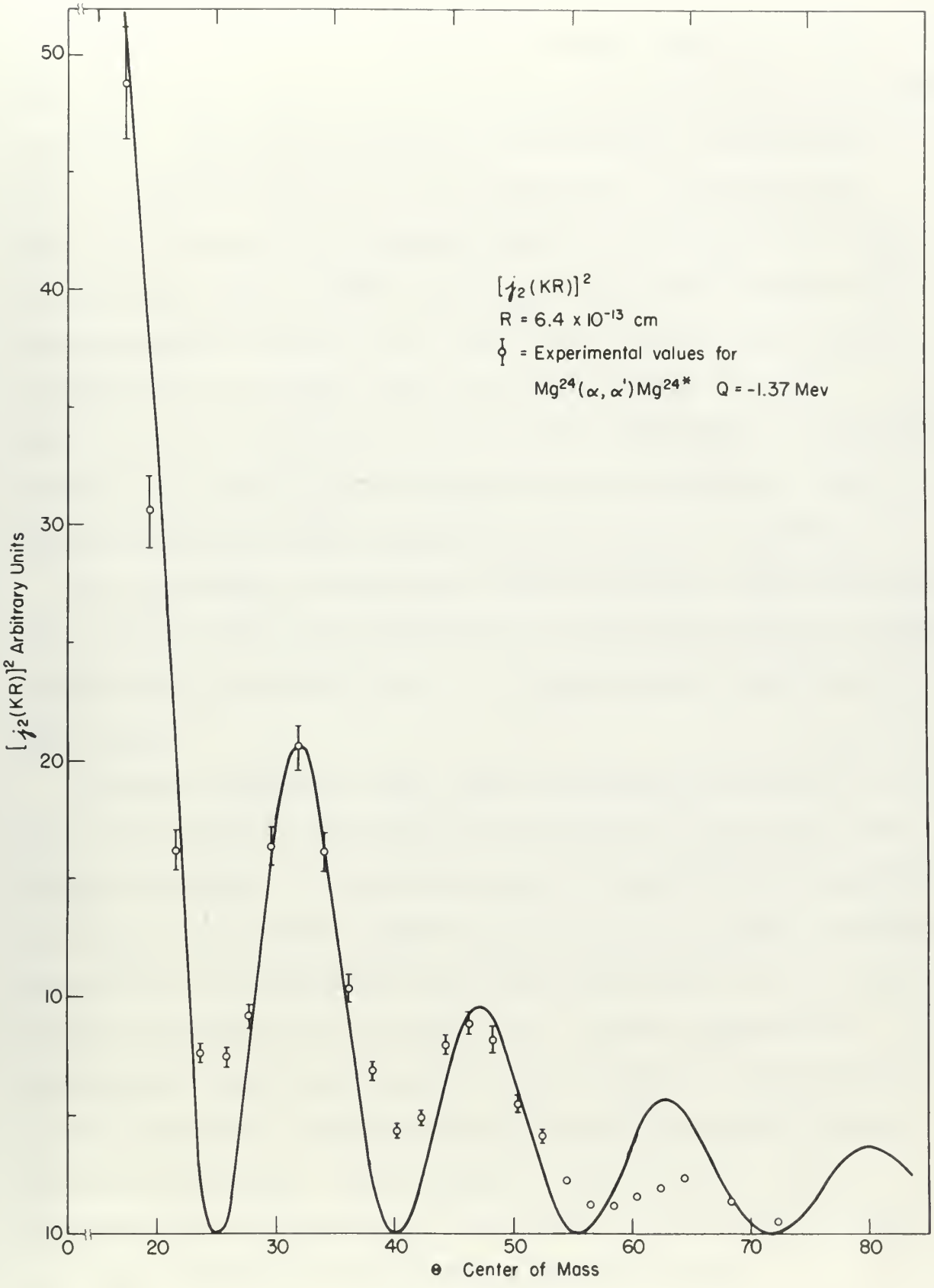
$[j_2(KR)]^2$
R = 6.4 x 10^{-13} cm
= Experimental values for
$Mg^{24}(\alpha, \alpha')Mg^{24*}$ Q = -1.37 Mev
$[j_2(KR)]^2$ Arbitrary Units
θ Center of Mass
50
40
30
20
10
10
0
20
30
40
50
60
70
80

Figure 28

distribution. However, the nuclear radius required to fit the data to this curve is too large to be considered physically possible. The agreement between experimental observations and a $j_2(KR)^2$ spherical Bessel function, illustrated in Fig. 27, is seen to be extremely good. The theoretical curve was obtained using a unit radius $r_o = 1.5 \times 10^{-13}$ cm and an alpha-particle radius of 1.9×10^{-13} cm. This result can be interpreted to indicate that the higher level, having a spin J = 2, is excited and that in this interaction, excitation of the J = 4 level is discriminated against because of the higher angular momentum transfer which would be involved.

The positions of maxima and minima obtained experimentally are compared with the predictions for the direct surface interaction model in Table 2 and it is seen that the agreement is quite good.

With one exception (S2), there is no known evidence to support the direction interaction process in the inelastic scattering of protons. A study was made of the results of many of the (p,p') interactions (B7, B9, F5, F6, G2, R4, W8) and in none of these was it possible to fit the experimental data to the angular distributions predicted for a direct interaction. It appears that the (p,p') interaction proceeds by a process completely different from that which occurs in inelastic alpha-particle scattering. This could be interpreted as due to a difference in diffuseness at the nuclear surface for protons and alpha particles as discussed later in Sec. D.

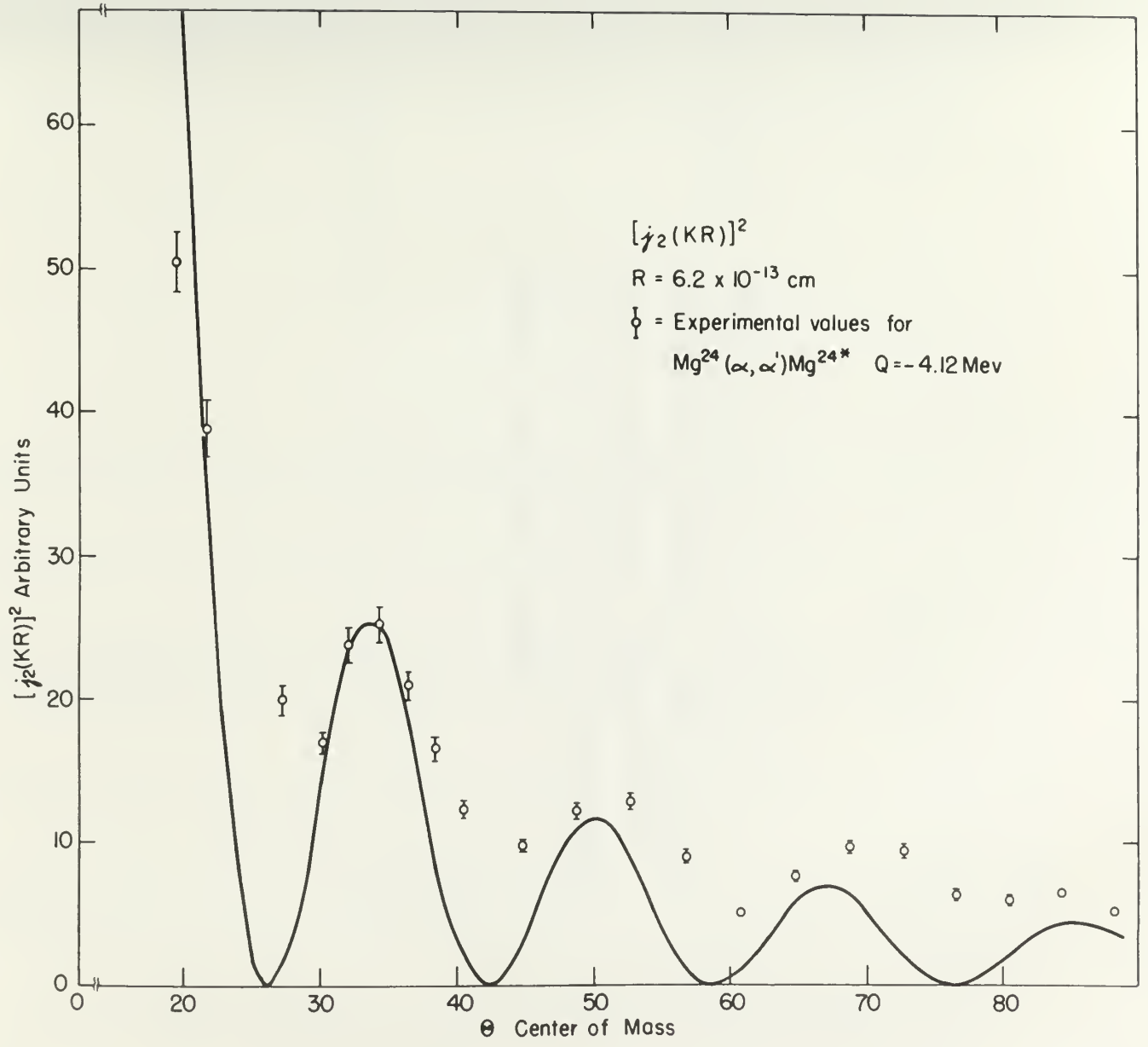
$[j_2(KR)]^2$
R = 6.2 x 10^{-13} cm
= Experimental values for
$Mg^{24}(\alpha,\alpha')Mg^{24*}$ Q = - 4.12 Mev
$[j_2(KR)]^2$ Arbitrary Units
Θ Center of Mass
0
10
20
30
40
50
60
70
80

Table 9. Angular positions of maxima and minima of the inelastic alpha-particle angular distributions compared with theoretical predictions for the direct surface interaction model.

POSITIONS OF MAXIMA AND MINIMA
IN THE INELASTIC ALPHA PARTICLE ANGULAR DISTRIBUTIONS
EXPERIMENTAL DATA
COMPARED WITH
PREDICTIONS OF DIRECT SURFACE INTERACTION MODEL

TARGET NUCLEUS	EXCITATION LEVEL (Mev)	MAXIMUM OR MINIMUM	CENTER OF MASS ANGLE (Deg.)	
			Experiment	Theory
Li^6	2.19	Min	34.5	35
	"	Max	44	45
	4.5	Min	42.5	41
	"	Max	52	53
C^{12}	4.43	Min	32	32
	"	Max	43	42
	"	Min	66	52
	"	Max	75	62
	7.65	Max	24.5	24.5
	"	Min	35	35.5
	"	Max	46	44.5
	"	Min	56.5	55.5
	"	Max	65	65
Mg^{24}	1.37	Min	25	25
	"	Max	32	32
	"	Min	40.5	40
	"	Max	46.5	47
	"	Min	57	55
	"	Max	64.5	63
	4.12	Min	29.5	26.5
	"	Max	33.5	34
	"	Min	43	42.5
	"	Max	51	50.5
	"	Min	60.5	59
	"	Max	69	67
	"	Min	80	77

C. VALIDITY OF THE ISOTOPIC SPIN SELECTION RULE

The alpha-particle spectrum of Fig. 10 and the discussion of Sec. V indicate that there is little or no breakdown of the isotopic spin selection rule in the inelastic scattering interactions observed in this investigation. In the bombardment of Li^6, excitation of the forbidden 3.57-Mev level occurred with a probability of less than 4 percent that of either of the two allowed levels which were strongly excited. Similarly, excitation of the 2.31-Mev level in N^{14}, forbidden by this charge independence selection rule, occurred with a probability less than 6 percent that of the allowed 3.95-Mev level.

The statements of Part A of this section and the agreement between the experimental angular distributions and those theoretically predicted, for the inelastic scattering mechanism described in Sec. VIB, are clearly indicative of a direct surface interaction process.

These facts lend support to the recent proposal of Lane and Thomas (L3) that isotopic spin should be conserved in a direct interaction.

D. ELASTIC SCATTERING

The elastic alpha-particle angular distributions obtained in this experiment, Figs. 19-21, exhibit a structure similar to that observed in the diffraction of light by an opaque body. The reasons for the smooth cross section variation from 60-78 degrees shown in Fig. 20 are not understood. The diffraction pattern is apparently masked by interference with some other process occurring in the interaction and this appears to be worthy of future investigation. A very similar phenomenon was observed in the elastic scattering of deuterons from oxygen (F3) but no analysis of these data was attempted.

Recently, various experimenters have reported the results obtained in the elastic scattering of 10-40-Mev alpha particles by heavy nuclei (F1, G3, W2, W3). The essentially classical analyses of these data (B6, F1, W3) have had some success in qualitatively explaining the observed monotonic decrease of $\sigma/\sigma_{coulomb}$ with increasing angle. These experimental results, however, are in direct contrast to the diffraction patterns observed in the elastic scattering of 18-Mev protons (C4, C5) and 40-Mev alpha particles (I1) by light nuclei: diffraction effects, similar to those obtained in this investigation, have also been noted in other elastic alpha-particle scattering experiments (B10, E1) in which the results were interpreted in terms of an optical scattering model.

The optical model of the nucleus (F8, F9) has been used with varying degrees of success in explaining the diffraction patterns observed in the elastic scattering of charged particles by nuclei (B11). It is of interest that good agreement with experiment (G4, L4) was obtained for such a model in the elastic scattering of 32-Mev protons by aluminum (W9). The real part of the complex potential, necessary to obtain agreement in this case, was represented by the square well potential obtained when one assumes that all of the nuclear charge is essentially on the nuclear surface. By imposing the additional requirement that the target nucleus have a diffuse surface, this form of the complex potential also gave satisfactory agreement with experimental data on the elastic scattering of protons by heavy nuclei. Porter (P1) has estimated this diffuseness to be of the order of 1×10^{-13} cm for the alpha-particle bombardment of heavy nuclei, i.e., approximately twice the value which gives satisfactory agreement when protons are used as the bombarding particles. The diffraction type phenomena occurring in the elastic angular distributions of the present investigation can also be explained in terms of an optical model which is consistent with the model employed in the analysis of the inelastic scattering data.

Large (α,p) and (α,d) cross sections observed in this investigation (Figs. 8 and 28), and others, are interpreted

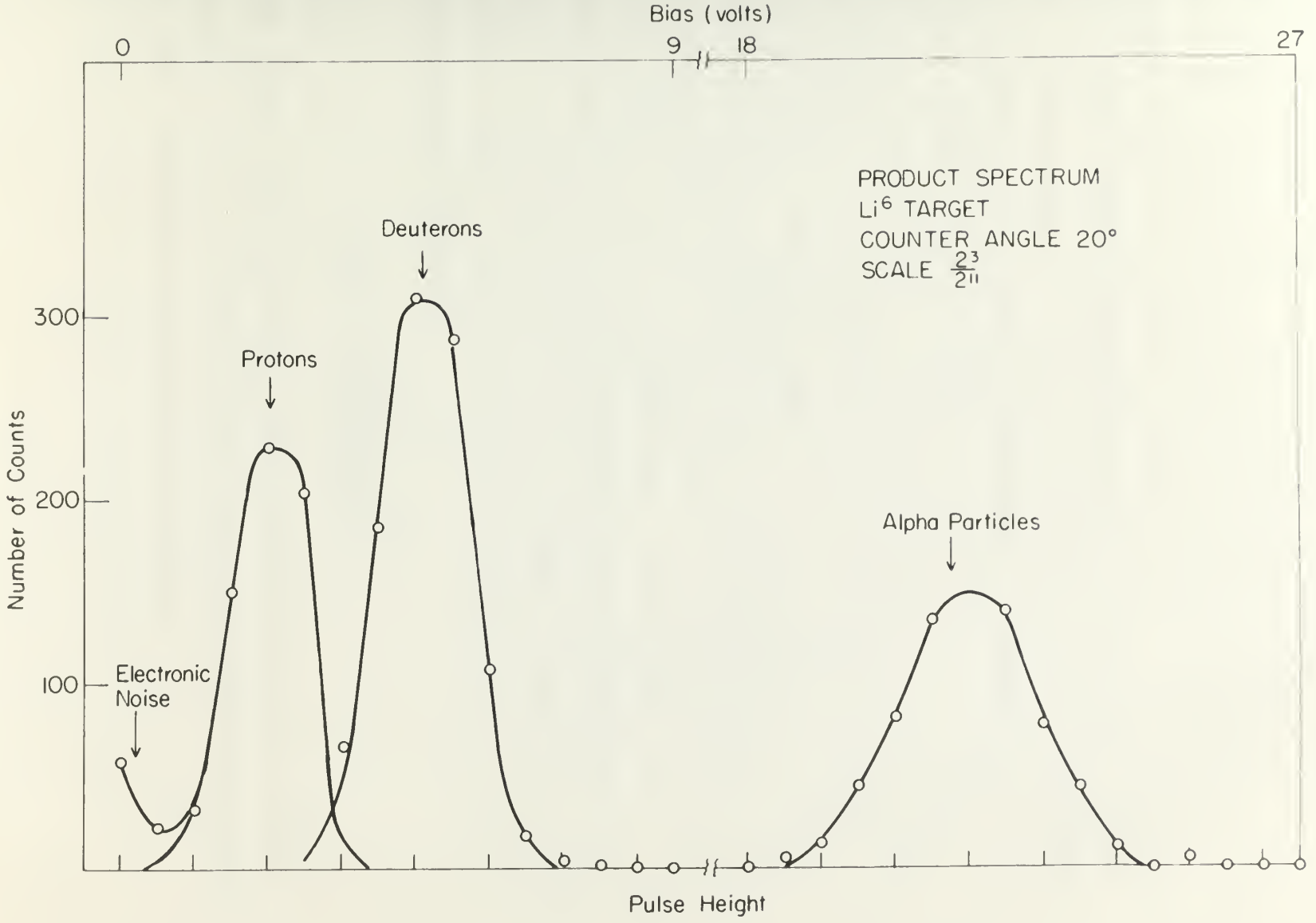
Bias (volts)
0
9
18
27
PRODUCT SPECTRUM
Li⁶ TARGET
COUNTER ANGLE 20°
SCALE 23/211
Deuterons
Protons
Alpha Particles
Electronic Noise
300
200
100
Number of Counts
Pulse Height

to indicate that nuclei are opaque to high-energy alpha particles (Bl[illegible], Pl, W[illegible]). The theoretical treatment of data in the elastic alpha-particle scattering previously mentioned (26) also assumed an opaque nucleus. The argument was that complete absorption occurred for partial waves with ℓ values less than that corresponding to the classical angular momentum for which the distance of closest approach is equal to the sum of the alpha particle and the nuclear radii. In the treatment of the data obtained in the present investigation it is assumed that the nucleus can be represented as being completely opaque out to a radius R, with a diffuse surface of thickness ΔR. This model is similar to the optical model which can be deduced from the results of a recent survey of total reaction cross section data (Bl[illegible]). In Table 3, the elastic angular distributions of the present experiment are compared with those predicted for scattering from an opaque sphere. Positions of the predicted maxima were obtained from the relation

$$\frac{d\sigma}{d\Omega} = \left| \frac{J_1(KR \sin \theta)}{KR \sin \theta} \right|^2$$

which is the exact expression for the scattering from an opaque disc and very closely approximates the angular distributions for scattering from an opaque sphere.

$$\frac{d\Omega}{d\sigma} = \left| \frac{x^2}{J_1'(2x \sin\theta)} \right|^2$$

Table 3. Angular positions of the maxima observed in the elastic scattering angular distributions compared with those predicted for scattering from an opaque sphere.

Natural Mg		C^{12}		Li^{6}	
C.M. Angular Position of Maxima (degrees)		C.M. Angular Position of Maxima (degrees)		C.M. Angular Position of Maxima (degrees)	
Expt.	Opaque Sphere R = 5.4 $\times 10^{-13}$ cm	Expt.	Opaque Sphere R = 4.4 $\times 10^{-13}$ cm	Expt.	Opaque Sphere R = 4.5 $\times 10^{-13}$ cm
24	24	29	29	33.5	33.5
39	41	48	50		
55	55	-	69		
		83	89		

The theoretical curves were fitted using values of R which gave an exact fit at the position of the first experimental maximum. These values of R are compared with the mean values of the interaction radii required to fit the inelastic scattering theory to the experimental data. This comparison yields the following values for the diffuseness ΔR of the nuclear surface: Li^6 - 1.7×10^{-13} cm, C^{12} - 1.3×10^{-13} cm, natural Mg - 0.9×10^{-13} cm. These results are of the order of magnitude estimated by Porter (P1) and are in agreement with results obtained in recent analysis of total reaction cross section data (B17). The increase in diffuseness with decreasing atomic number is not incompatible with the concept that the light nuclei are less concentrated.

The difference in diffuseness of the nuclear surface to protons and to alpha particles was mentioned earlier in this section. It has also been pointed out that angular distributions obtained in the inelastic scattering of protons do not, in general, show the structure characteristic of a direct surface interaction which is observed in this experiment. It is not inconsistent with these considerations to speculate that the relatively thick diffuse edge of the nucleus, as seen by an alpha particle, represents a larger effective direct interaction "surface", to alpha particles

than to protons.

As illustrated in Table 3, the concept of a diffuse surface opaque nucleus, which is consistent with the model assumed for the inelastic scattering process, gives results in close agreement with the elastic scattering data. This cannot be interpreted, however, as verification of the validity of the elastic scattering model, since similar agreement with the data can be obtained using a completely different representation of the elastic interaction. Consider the nucleus as being represented by a square well potential with the coulomb potential cut off at the nuclear radius R_n. In this case a differential scattering cross section $\frac{d\sigma}{d\Omega} \sim |f(\theta)|^2$ is obtained in which

$$f(\theta) = \frac{1}{K^3}\left[V_o \sin KR - (V_o KR + 2e^2 K) \cos KR\right]$$

where $K = \sqrt{k_i^2 + k_f^2 - 2k_i k_f \cos\theta}$

k_i = initial interaction wave number

k_f = final interaction wave number

θ = center-of-mass scattering angle

R = interaction radius

V_o = depth of potential well

This reduces to

$$f(\theta) \simeq \frac{V_o R^2}{K}\left[j_1(KR) - \frac{Ze^2}{KR^2 V_o}\cos(KR)\right]$$

where j_1 is the spherical Bessel function of order one. For any reasonable value for V_o*, it can be shown (W7) that the second term, due entirely to the coulomb effect, has a negligible effect on the angular positions of the maxima, and that the differential cross section may be approximated by

$$\frac{d\sigma}{d\Omega} \simeq \frac{V_o R^2}{K}\left|j_1(KR)\right|^2 .$$

A rigorous treatment of this problem (F5), based on the general phase shift representation of the scattering matrix, has been published complete with tables. The predictions of the above equation are compared with the experimental data in Table 4 where the agreement is seen to be as good as that illustrated in Table 3. From these results, it is concluded that the close agreement with experiment obtained for the opaque nucleus concept is insufficient evidence to validate the use of the model. The fact that the model is consistent with the one employed to describe the inelastic scattering process may be entirely fortuituous. The theoretical curves were fitted using values for R which correspond to the mean values of the interaction radii required to fit the inelastic scattering theory to the experimental data. These radii are comparable with the ones obtained in the computation of total reaction cross sections calculated by Shapiro (S4) for a totally black square well potential.

---

* A reasonable value of 25-30 Mev was used. There is evidence (T5) for a larger well depth.

$$\frac{d\Omega}{} \simeq \frac{}{\lambda^2 E_c} |f^2(\Omega)|$$

Table 4. Angular positions of the maxima observed in the elastic scattering angular distributions compared with those predicted for elastic scattering from a square well potential.

Natural Mg		C^{12}		Li^{6}	
C.M. Angular Position of Maxima (degrees)		C.M. Angular Position of Maxima (degrees)		C.M. Angular Position of Maxima (degrees)	
Expt.	Square well	Expt.	Square well	Expt.	Square well
24	25.6	29	31.6	33.5	34
39	39.5	48	49		
55	54	-	69.6		
		83	91.3		

A recent, and as yet unpublished, elastic alpha-particle scattering experiment was performed to study the angular dependence of $(\frac{d\sigma}{d\Omega})/(\frac{d\sigma}{d\Omega})_{coulomb}$ at 40 Mev over a range of elements from carbon to silver (I1). A composite plot of these data shows the details of the gradual change from the diffraction to the exponential behavior with increasing atomic number. The data obtained in the present investigation are illustrated in this same form in Fig. 79 to facilitate comparison of the behavior at the bombarding energy of 31.5 Mev used in this experiment. The general characteristics of both composite plots are quite similar.

VII. CONCLUSIONS

The data obtained in this investigation and the discussion of Sec. VIA clearly indicate that the mechanisms of compound nucleus formation and electric excitation are not of primary importance in an analysis of the inelastic scattering of 31.5-Mev alpha particles by light nuclei. The angular distributions are similar to those predicted by Austern et al. (A4) for an interaction in which the bombarding particle transfers an amount of energy to a nucleon at the surface of the nucleus,

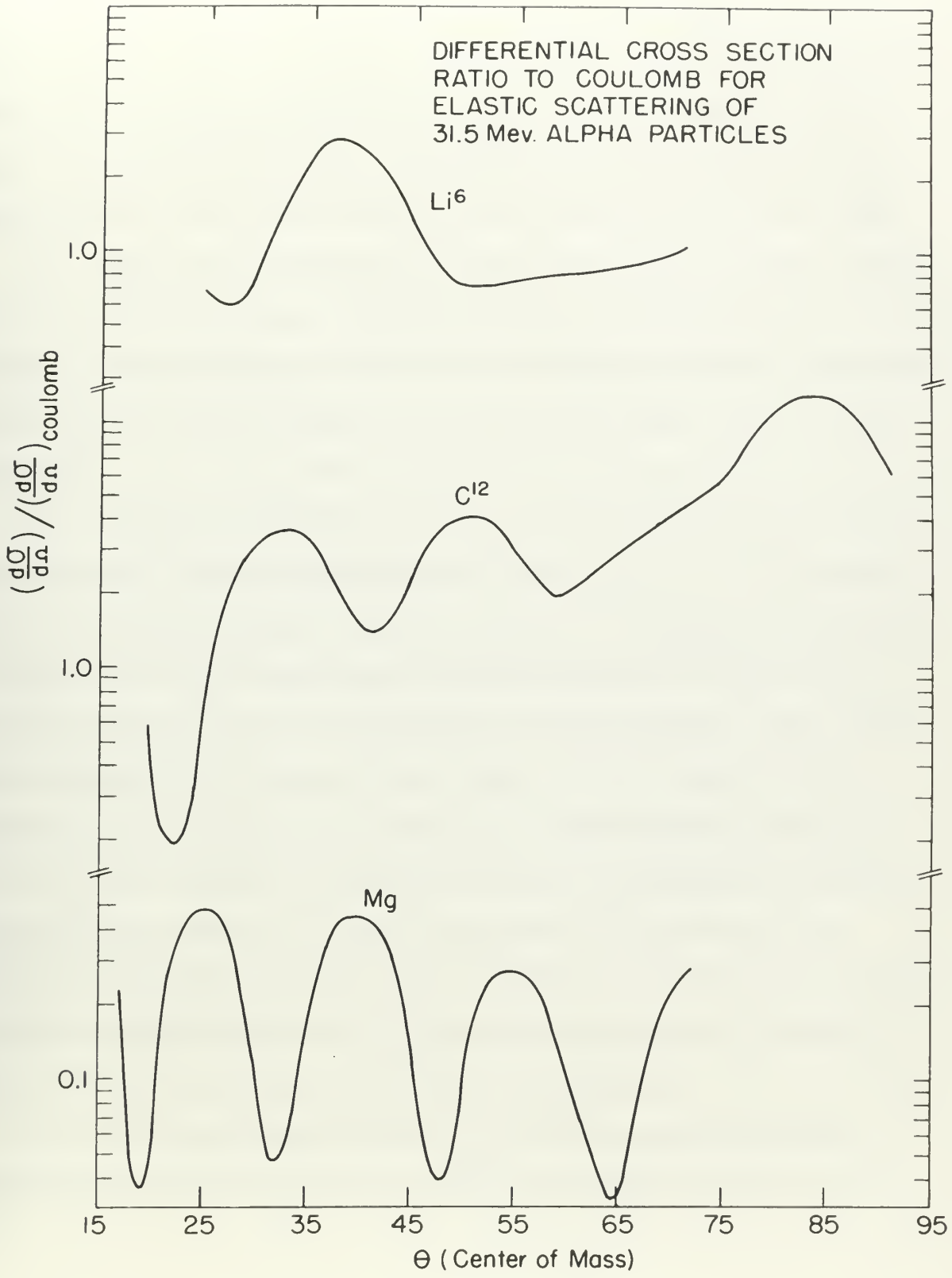
DIFFERENTIAL CROSS SECTION
RATIO TO COULOMB FOR
ELASTIC SCATTERING OF
31.5 Mev. ALPHA PARTICLES
Li6
C12
Mg
1.0
1.0
0.1
(dσ/dΩ)/(dσ/dΩ)coulomb
15
25
35
45
55
65
75
85
95
Θ (Center of Mass)

the so-called direct surface interaction. Experimental agreement with the predictions of a theory based on this model is quite good. Nevertheless, the following statements must be considered as imposing a limit on the validity of this model.

1. The theory assumes an interaction with a single nucleon in the target nucleus. However, from purely kinematic considerations it can be shown (H6) that the momentum transfer involved requires that the energy be transferred to more than a single nucleon.

2. The Born approximation is probably quite good for the interactions under consideration, i.e., $E_\alpha \sim 30$ Mev compared with a maximum coulomb barrier of 8 Mev. Similar agreement obtained with the use of coulomb wave functions would give strong support to the applicability of the model. This will be attempted in the near future (T5) and the effect on the theoretical predictions should be of considerable interest.

3. The electric interaction theory is subject to certain refinements which may or may not affect the magnitude and angular dependence of the cross sections predicted for this method of excitation. One of the most important of these is the use of an arbitrary radius of interaction.

4. It was assumed that the compound nucleus type of interaction did not occur for the following reasons:

(a) The variation of intensity with angle was not smooth but showed a well defined structure.

(b) There was no angular symmetry about 90 degrees.

(c) No back angle maxima were found and the majority of the inelastic scattering was confined to the forward quadrant.

(d) The angular distributions were insensitive to significant variations in the incident beam energy.

(e) The differential cross sections observed were large compared with those previously obtained for interactions known to proceed by compound nucleus formation.

The development of a formal compound nucleus theory, which predicts the inelastic angular distributions resulting from the excitation of discrete levels, could affect the above considerations.

On the basis of the present evidence, however, it is concluded that the inelastically scattered alpha particles, observed in the present investigation, result from a direct interaction at the nuclear surface. Due to experimental limitations, it was not possible to obtain data at angles smaller than 14.8 degrees. As a result, even though good agreement with theory was found at larger angles, it was not possible to verify the position of the first predicted maxima except

(c) The variation of intensity with angle was not
measured over enough a wide distance.

(b) There was no angular dependence of intensity.

(d) The beam might deviate even though the velocity
of the light was unchanged in the
forward direction.

(a) The angular distributions were insensitive to
experimental deviations in the incident beam energy.

(e) The difference(s) cannot reasonably be accounted for
large contrast with those experimentally obtained
for interactions known to proceed by compound
nuclear formation.

The development of a formal nucleonic chemical theory, which
predicts the likely modes of disintegration resulting from
the excitation of transmute isotopes, would clarify the consi-
derations.

On the basis of the present evidence, however, it is con-
cluded that the doubly charged particles resulting from a direct
capture of the neutron possess, due to coulombic repulsion,
higher energies than the singly charged ones. It was not possible
to verify the prediction of the theory concerning energy

in one level of C^{12}. If these experimental difficulties can be overcome, it is possible that (α,α') angular distributions can yield valuable information about the properties of a number of nuclei in which the quantum numbers of the energy levels are as yet undetermined.

In the two cases investigated, it was seen that the excitation of levels prohibited by the isotopic spin selection rule occurred with a probability of less than about 5 percent that of the allowed levels. These experimental results lend support to the statement that isotopic spin is conserved in direct interactions (L3).

The diffraction phenomena, occurring in the angular distributions of elastically scattered alpha particles, are suggestive of the use of an optical model in the description of elastic nuclear events. The large (α,p) and (α,d) cross sections observed in this experiment can be interpreted as requiring the use of a large absorption coefficient in the complex scattering potential employed in the optical model. Both statements are compatible with the results of others (B6, B19, P1, S4, W9). The elastic angular distributions can be interpreted in terms of a model consistent with the one employed in describing the inelastic scattering data, although this evidence is insufficient to verify the validity of the model. The results of this experiment support the increasing

evidence that the elastic scattering of alpha particles can be described in terms of an optical model in which the imaginary potential is extensive and rather intense.

The conclusions which can be drawn from the data obtained in this experiment are summarized as follows:

1. The inelastic alpha-particle scattering proceeds primarily by a direct surface interaction process, with the possibility of some small contributions from compound nucleus formation or electric excitation.

2. It is possible to obtain useful information about the properties of the energy levels of nuclei from a study of the (α,α') angular distributions.

3. Isotopic spin is conserved in these interactions.

4. The (p,p') and (α,α') reactions proceed by completely different processes.

5. The elastic alpha-particle scattering can be interpreted in terms of a potential square well scattering center or in terms of an optical model and a complex scattering potential.

APPENDIX I

THE CONVERSION OF EXPERIMENTAL ANGULAR DISTRIBUTION DATA TO THE CENTER-OF-MASS COORDINATE SYSTEM

Experimental data must be converted from the laboratory to the particle or center-of-mass frame of reference for comparison with theoretical angular distribution predictions. The form of the corrections to be applied to the experimental data is summarized by Schiff (S3). A compilation of these corrections, suitable for interpolation, has been prepared (M5) and a nomogram, suitable for rough but rapid conversion, has been published (F7). To eliminate an additional source of error in the results of the present experiment, conversion to the particle coordinate system was accomplished using correction curves plotted from the exact formulae. The following symbols are used in this appendix, where the required corrections are derived from elementary principles:

m_1 mass of bombarding particle

m_2 mass of target nucleus

m_3 mass of observed particle

m_4 mass of residual nucleus

$v_1 \ldots v_4$ the velocities of $m_1 \ldots m_4$ measured in the laboratory frame of reference

v_c velocity of the center of mass measured in the laboratory coordinate system

$V_1 \ldots V_4$ the velocities of $m_1 \ldots m_4$ measured in the center-of-mass system

Q the reaction Q value as calculated from the mass tables and expressed in Mev

E_o the total initial kinetic energy measured in the laboratory

E the total initial kinetic energy of the system measured in the center of mass

θ_o the laboratory angle of observation of particle m_3

θ the center-of-mass angle corresponding to the laboratory angle θ_o.

$d\omega$ the unit solid angle measured in the laboratory coordinates

$d\Omega$ the unit solid angle measured in the center-of-mass coordinates

γ defined by equation (4)

$g(\theta_o)$ defined by equation (12)

1. RELATIONS BETWEEN ANGLES IN THE LABORATORY AND CENTER OF MASS

In the laboratory the bombarding particle of mass m_1 moving with velocity v_1 collides with a target nucleus of mass m_2 at rest. The center of mass of the two particles moves with a velocity v_c so that the linear momentum of the system is $m_1 v_1 = (m_1 + m_2) v_c$. Therefore

$$v_c = a v_1 \quad \text{where } a = \frac{m_1}{m_1 + m_2} \tag{1}$$

In the center of mass, prior to the collision the velocity of m_1 is

$$V_1 = (v_1 - v_c) = v_1(1 - a)$$

Since m_2 is initially at rest in the laboratory system, the center-of-mass velocity of m_2 is simply

$$V_2 = -v_c$$

The center of mass is, by definition, stationary in the center-of-mass frame of reference. Therefore, in the center-of-mass coordinates, the total linear momentum is zero. After the collision, this requires that

$$m_3 V_3 = m_4 V_4 \quad \text{or} \quad V_4 = \frac{m_3}{m_4} V_3$$

where m_3 and V_3 refer to the scattered or observed particle and m_4 and V_4 refer to the residual particle.

From energy conservation considerations

$$\tfrac{1}{2}m_1v_1^2 + \tfrac{1}{2}m_2v_2^2 = \tfrac{1}{2}m_3v_3^2 + \tfrac{1}{2}m_4v_4^2 - Q$$

which reduces to

$$\tfrac{1}{2}m_1v_1^2\left(\frac{m_2}{m_1 + m_2}\right) = \tfrac{1}{2}m_3v_3^2\left(1 + \frac{m_3}{m_4}\right) - Q$$

However

$$\tfrac{1}{2}m_1v_1^2\left(\frac{m_2}{m_1 + m_2}\right) = \left(\frac{m_2}{m_1 + m_2}\right)E_o = E$$

the total initial center-of-mass kinetic energy of the system, therefore

$$v_3^2 = \frac{E + Q}{\tfrac{1}{2}m_3\left(\dfrac{m_3 + m_4}{m_4}\right)} \qquad (9)$$

In Fig. 30 the uniform motion v_c of the center of mass in the laboratory system is superimposed on the angular and velocity relations in the center-of-mass coordinate system. It is seen that laboratory velocities can be obtained by vectorially adding v_c to the center of mass

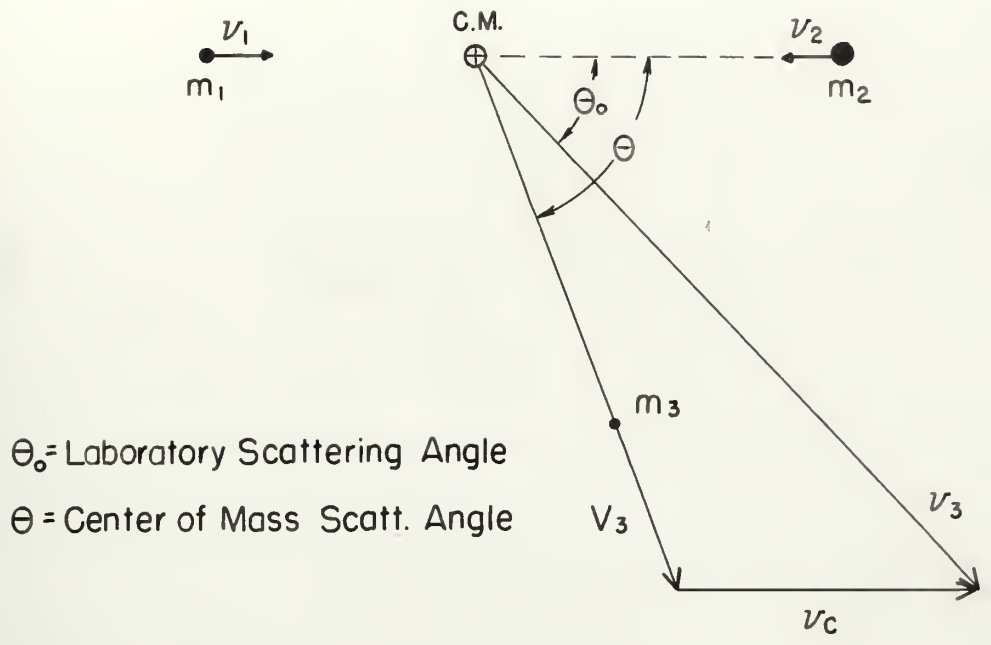

Figure 30

Applying the law of sines to Fig. 30

$$\frac{\sin \Theta_o}{V_3} = \frac{\sin (\Theta - \Theta_o)}{v_c}$$

or

$$\sin (\Theta - \Theta_o) = \frac{v_c}{V_3} \sin \Theta_o \qquad (3)$$

Considering only nonrelativistic interactions, where $Q = (m_1 + m_2 - m_3 - m_4)$ is small compared with the rest energy m_i of any of the particles involved, it is assumed that $m_1 + m_2 \simeq m_3 + m_4$. Substituting v_c from equation (1) and V_3 from equation (2)

θ_o = Laboratory Scattering Angle

θ = Center of Mass Scatt. Angle

Figure 30

Applying the law of sines to Fig. 30

$$\frac{\sin \theta_o}{V_3} = \frac{\sin (\theta - \theta_o)}{V_c}$$

or

$$\sin (\theta - \theta_o) = \frac{V_c}{V_3} \sin \theta_o \qquad (1)$$

Considering only nonrelativistic interactions, where $Q = (m^1 + m^2 - m^3 - m^4)$ is small compared with the rest energy m^1 of any of the particles involved, it is assumed that $m^1 + m^2 \simeq m^3 + m^4$. Substituting V_c from equation (1) and V_3 from equation (2)

$$\frac{v_c}{V_3} = \left[\frac{m_1 m_3}{m_2 m_4} \frac{E}{E + Q}\right]^{1/2} \equiv \gamma \qquad (4)$$

and equation (3) reduces to the useful form

$$\sin (\theta - \theta_o) = \gamma \sin \theta_o \qquad (5)$$

In the case of scattering, $m_3 = m_1$ and $m_4 = m_2$ so that

$$\gamma = \frac{m_1}{m_2}\left[\frac{E}{E + Q}\right]^{1/2}$$

By use of the trigonometric identity for the difference of two angles, equation (5) reduces to

$$\tan \theta_o = \frac{\sin \theta}{\gamma + \cos \theta} \qquad (6)$$

which is identical with equation 18.4 of Schiff (53) and can be conveniently represented as shown in Fig. 31.

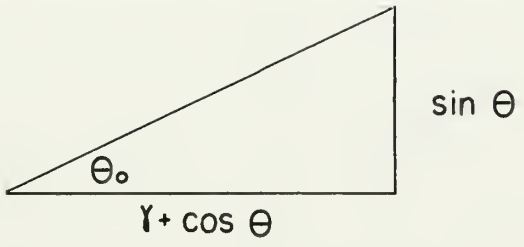

Figure 31

Equation (5) can then be plotted for each value of γ determined by the energy levels of the target nucleus as illustrated in Fig. 32. The conversion from laboratory to center-of-mass angle can be obtained directly from the curve with an accuracy of better than ± 0.05 degree.

Figure 31

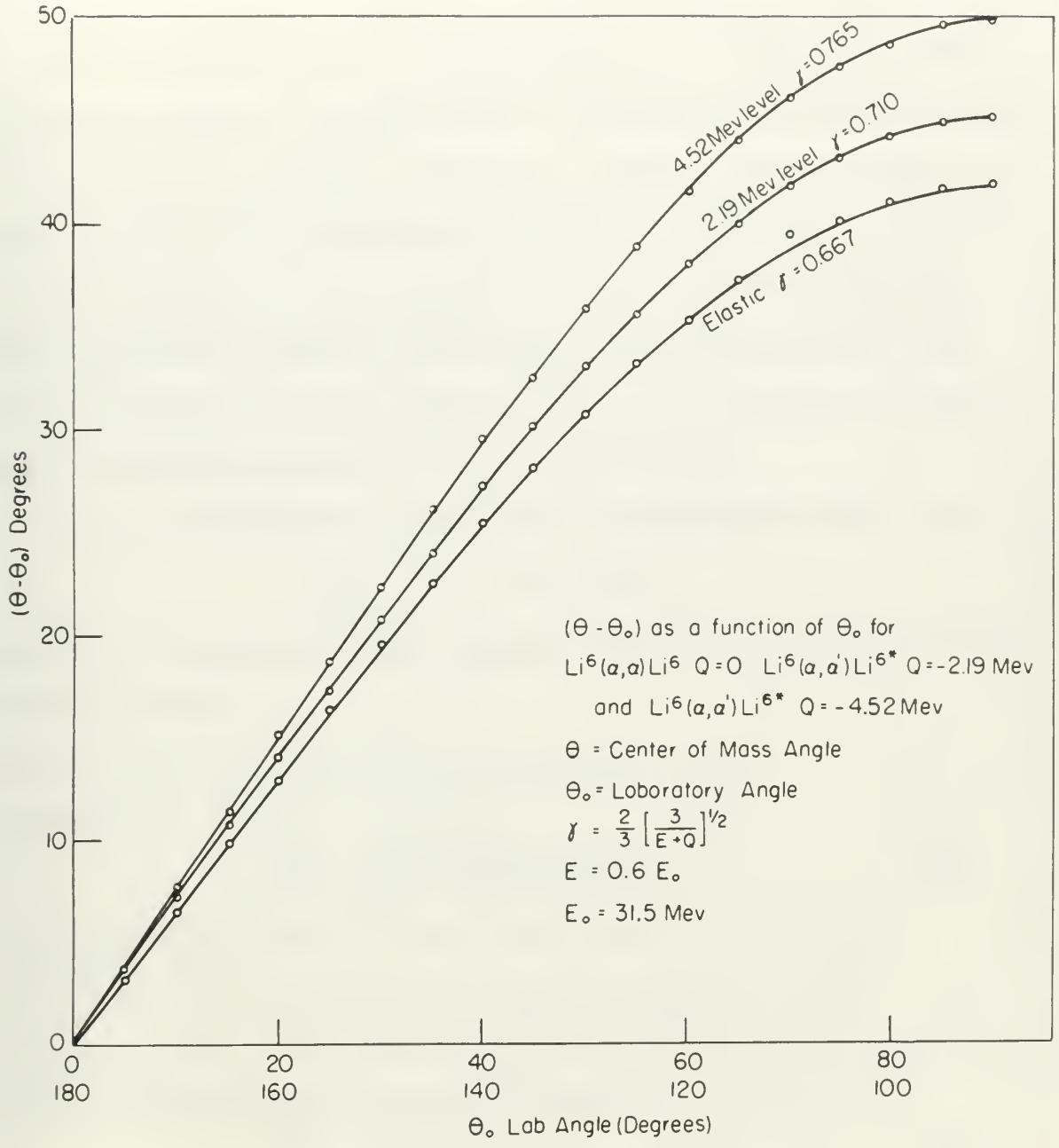
50
40
30
20
10
0
(θ-θ₀) Degrees
4.52Mev level γ=0.765
2.19Mev level γ=0.710
Elastic γ=0.667
(θ - θ₀) as a function of θ₀ for
Li⁶(α,α)Li⁶ Q=0 Li⁶(α,α')Li⁶* Q=-2.19 Mev
and Li⁶(α,α')Li⁶* Q=-4.52 Mev
θ = Center of Mass Angle
θ₀ = Loboratory Angle
γ = 2/3 [3/(E+Q)]^1/2
E = 0.6 E₀
E₀ = 31.5 Mev
0
180
20
160
40
140
60
120
80
100
θ₀ Lab Angle (Degrees)

Figure 32

8. RELATION BETWEEN LABORATORY AND CENTER-OF-MASS DIFFERENTIAL CROSS SECTIONS

At a forward angle of observation, the finite counter aperture subtends a larger solid angle in the center-of-mass coordinates than in the laboratory system. This effect is most important in reactions involving light nuclei since it is due entirely to the velocity of the center of mass in the laboratory frame of reference. The relation between the differential cross section in the two reference frames can be obtained directly from its definition.

In the laboratory system, the differential solid angle is

$$d\omega = 2\pi \sin \theta_o \, d\theta_o$$

since φ is common to both reference frames. In the center-of-mass system

$$d\Omega = 2\pi \sin \theta \, d\theta$$

therefore

$$\frac{d\omega}{d\Omega} = \frac{\sin \theta_o \, d\theta_o}{\sin \theta \, d\theta} \tag{7}$$

From Fig. 31

$$\cot \theta_o = \gamma \csc \theta + \cot \theta \tag{8}$$

and by differentiation of equation (8)

$$\frac{d\theta_o}{d\theta} = \frac{\sin^2 \theta_o}{\sin^2 \theta}(1 + \gamma \cos \theta) \tag{9}$$

6. RELATIVE ACTIVE ELEMENTS OF CENTRE-OF-MASS DIFFERENTIAL CROSS SECTIONS

If a Coriolis force of acceleration, the Earth geodetic aperture subtends a large solid angle in the centre-of-mass coordinates than in the laboratory system. This effect is most important in receiving inverting light nuclei since it is due entirely to the velocity of the centre of mass in the laboratory frame of reference. The relation between the differential cross section in the two reference frames can be obtained directly from its definition.

In the laboratory system, the differential cross angle is

$$d\omega = 2\pi \sin\theta^{0} \, d\theta^{0}$$

where θ is measured in both reference frames. In the centre-of-mass system

$$d\Omega = 2\pi \sin\gamma \, d\gamma$$

therefore

$$\frac{d\omega}{d\Omega} = \frac{\sin\theta^{0} \, d\theta^{0}}{\sin\gamma \, d\gamma} \qquad (7)$$

From fig. 12

$$\cot\theta^{0} = \frac{1}{\tan\gamma} + \cot\gamma \qquad (8)$$

and by differentiation of equation (8)

$$\frac{d\theta^{0}}{d\gamma} = \frac{\sin^{2}\gamma}{\sin^{2}\theta^{0}}\left(1 + \frac{1}{\cos\gamma}\right) \qquad (9)$$

Figure 33 can be obtained directly from equation (8):

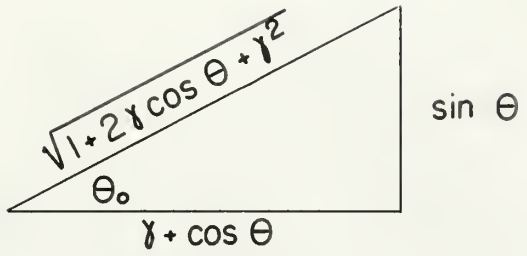

Figure 33

and Fig. 34 is obtained directly from equation (5):

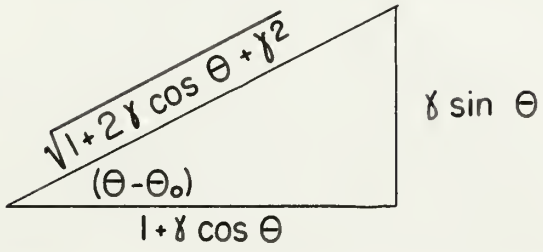

Figure 34

Substituting equation (9) into equation (7)

$$\frac{d\omega}{d\Omega} = \frac{\sin^3 \theta_o}{\sin^3 \theta}(1 + \gamma \cos \theta) \qquad (10)$$

It is necessary to obtain the value of $(\theta - \theta_o)$ in converting from laboratory to center-of-mass angle. Equation (10) is easily expressed in terms of $(\theta - \theta_o)$ by use of the following relation obtained from Fig. 33:

Figure 33

Figure 34

$$\sin \theta_o = \frac{\sin \theta}{\sqrt{1 + 2\gamma \cos \theta + \gamma^2}} \qquad (11)$$

Substitution of equation (11) into equation (10) yields

$$\frac{d\omega}{d\Omega} = \frac{\sin^2 \theta_o}{\sin^2 \theta} \cos (\theta - \theta_o) \equiv g(\theta_o) \qquad (11)$$

The intensity in the center-of-mass system is found by multiplying the measured intensity by the factor g which for a given reaction depends on γ and θ_o. A plot of $g(\theta_o)$, computed for three levels of excitation of the Li^6 nucleus, is illustrated in Fig. 35.

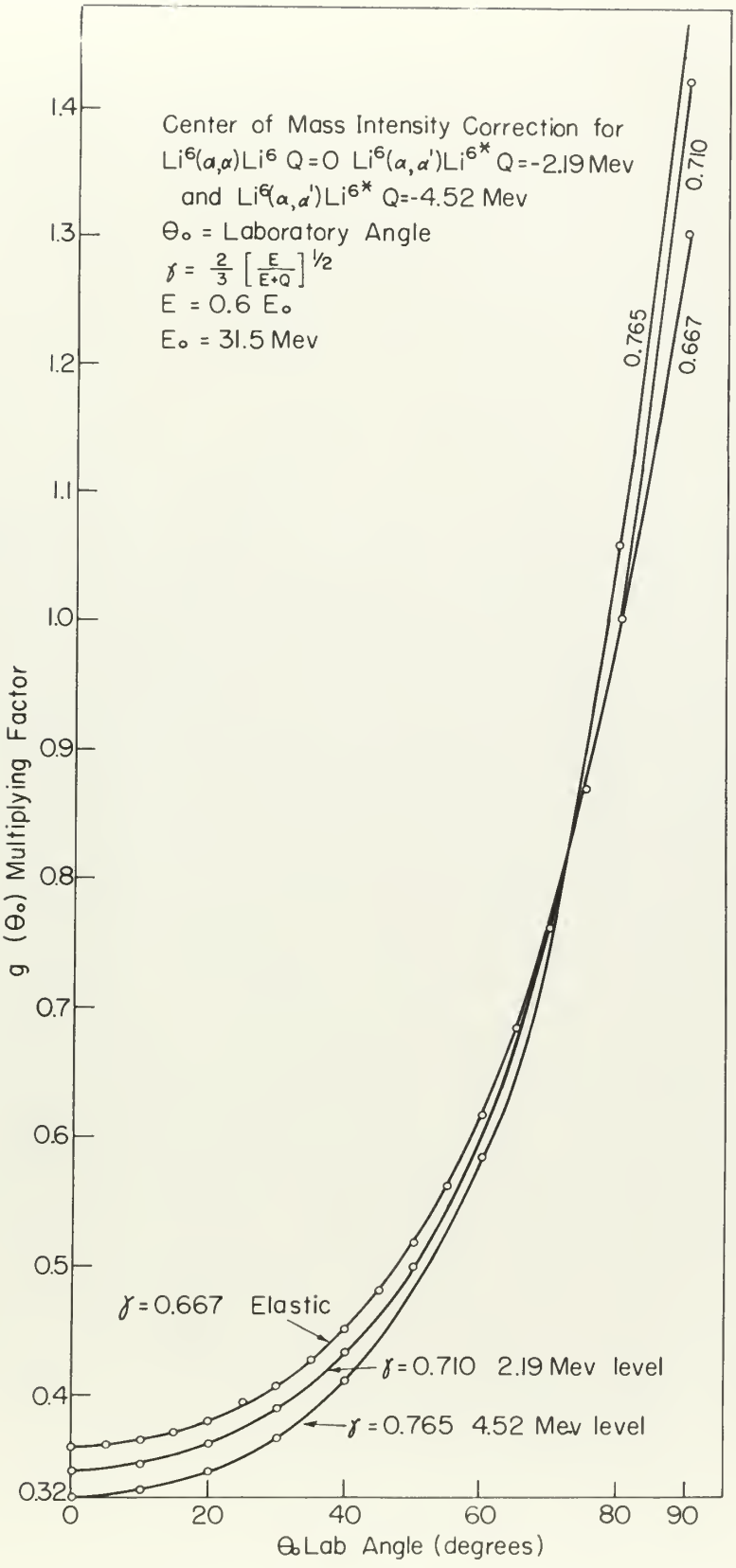
Center of Mass Intensity Correction for
Li⁶(α,α)Li⁶ Q=0 Li⁶(α,α')Li⁶* Q=-2.19 Mev
and Li⁶(α,α')Li⁶* Q=-4.52 Mev
Θ₀ = Laboratory Angle
γ = 2/3 [E/(E+Q)]^1/2
E = 0.6 E₀
E₀ = 31.5 Mev
0.765
0.710
0.667
γ = 0.667 Elastic
γ = 0.710 2.19 Mev level
γ = 0.765 4.52 Mev level
g (Θ₀) Multiplying Factor
Θ₀ Lab Angle (degrees)
1.4
1.3
1.2
1.1
1.0
0.9
0.8
0.7
0.6
0.5
0.4
0.32
0
20
40
60
80
90

Figure 15

BIBLIOGRAPHY

A1 F. A. Aschenbrenner, Phys. Rev. 98, 657 (1955), and Ph.D. Thesis, M.I.T., May 1954.

A2 W. A. Aron, B. G. Hoffman, and F. C. Williams, AECU 663, Radiation Laboratory, Univ. of Calif. May 1951.

A3 F. Ajzenberg and T. Lauritsen, Revs. Modern Phys. 27, 77 (1955).

A4 N. Austern, S. T. Butler, and H. McManus, Phys. Rev. 92, 350 (1953).

A5 R. K. Adair, Phys. Rev. 87, 1041 (1952).

A6 R. K. Adair, Phys. Rev. 86, 155 (1952).

B1 H. A. Bethe, Revs. Modern Phys. 9, 69 (1937).

B2 E. S. Bieler, Proc. Roy. Soc. (London), A105, 434 (1924).

B3 P. R. Dyerly and W. E. Stephens, Phys. Rev. 81, 473 (1951).

B4 E. Bleuler, A. K. Stebbins, and D. J. Tendam, Phys. Rev. 90, 460 (1953).

B5 A. B. Bhatia and K. Huang, reported by R. Huby, Nature, 166, 554 (1950).

B6 J. S. Blair, Phys. Rev. 95, 1218 (1954).

B7 C. J. Baker, J. N. Dodd, and D. H. Simmons, Phys. Rev. 85, 1051 (1952).

B8 S. Bashkin, F. P. Mooring and B. Petree, Phys. Rev. 84, 378 (1951).

B9 W. E. Burcham, W. M. Gibson, A. Hossain, and J. Rotblat, Phys. Rev. 92, 1268 (1953).

[47] F. A. Kaempffert, Phys. Rev. 36, 632 (1930), and Ph.D. Thesis, M.I.T., May 1926.

[48] M. A. Kron, M. O. Hoffman, and R. C. Williams, AFCO 660, Radiation Laboratory, Chic. or Calif. Nov 1951.

[49] F. Ajzenberg and T. Lauritsen, Rev. Modern Phys. 27, 77 (1955).

[50] E. Juncosa, I. S. Dutter, and E. Goldsack, Phys. Rev. 85, 360 (1952).

[51] E. E. Adair, Phys. Rev. 58, 191 (1940).

[52] R. R. Adair, Phys. Rev. 59, 918 (1941).

[53] E. A. Deeds, Phys. Rev. 61, 47 (1942).

[54] E. A. Diebert, Proc. Roy. Soc. (London), A158, 414 (1937).

[55] P. E. Dyesly and O. C. Kemmeny, Phys. Rev. 73, 471 (1948).

[56] E. Diedzer, E. K. Steinbrin, and P. A. Tendam, Phys. Rev. 90, 490 (1953).

[57] A. P. Bradie and E. Feather, reported by E. Eddy, Proc. Roy. Soc. 126, 554 (1930).

[58] J. E. Glair, Phys. Rev. 75, 1718 (1949).

[59] C. J. Baker, J. H. Cook, and D. G. Kimmeny, Phys. Rev. 92, 1021 (1953).

[60] W. Hamish, P. T. Elmerley and E. Perkins, Phil. Mag. 44, 348 (1953).

[61] C. E. Mortimer, H. T. Clinton, A. Hemmerly, and C. Goldsack, Phys. Rev. 85, 1000 (1952).

B10 E. Bleuler and D.J. Tendam, Phys. Rev. 99, 1605 (1955).

B11 "Statistical Aspects of the Nucleus", a conference held at the Brookhaven National Laboratory, Jan. 24-26, 1955.

B12 M. G. Blosser and T. E. Stanley, Phys. Rev. 100, 1340 (1955).

C1 B. L. Cohen, Phys. Rev. 98, 1545 (1955).

C2 E. D. Courant, Phys. Rev. 82, 703 (1951).

C3 G. Chew, Phys. Rev. 80, 196 (1950).

C4 B. L. Cohen and R. V. Neidigh, Rev. Sci. Instr. 25, 955 (1954).

C5 B. L. Cohen and R. V. Neidigh, Phys. Rev. 93, 282 (1954).

D1 S. Devons, Proc. Roy. Soc. (London), A178, 127 (1939).

D2 B. C. Diven and G. M. Almy, Phys. Rev. 80, 407 (1950).

E1 R. M. Eisberg, G. Igo, and H. E. Wegner, Phys. Rev. 99, 1606 (1955).

E2 P. M. Endt and J. C. Kluyver, Revs. Modern Phys. 26, 95 (1954).

F1 G. W. Farwell and H. E. Wegner, Phys. Rev. 95, 356 (1954).

F2 Y. Fujimoto and A. Hossain, Phil. Mag. 46, 543 (1955).

F3 R. G. Freemantle, D. J. Prowse, and J. Rotblat, Phys. Rev. 96, 1668 (1954); R. G. Freemantle, W. M. Gibson, D. J. Prowse, and J. Rotblatt, Phys. Rev. 92, 1668 (1953); W. E. Burcham, W. M. Gibson, A. Hossain, and J. Rotblatt, Phys. Rev. 92, 1668 (1953).

F4 H. Feshbach, C. E. Porter, and V. F. Weisskopf, Phys. Rev. 96, 448 (1954).

F5 A. J. Ferguson, "The Elastic Scattering of Charged Particles b Nuclei", AEC of Canada, Ltd. AECL 157, August 1954.

F6 R. G. Freemantle, D. J. Prowse, A. Hossain, and J. Rotblatt, Phys. Rev. 96, 1370 (1954).

F7 F. J. M. Farley, Nucleonics, 12, 56 (October 1954).

F8 S. Fernbach, R. Serber, and T. B. Taylor, Phys. Rev. 75, 1352 (1949).

F9 N. C. Francis and K. M. Watson, Am. J. Phys. 21, 653 (1953).

G1 E. Guth, Phys. Rev. 68, 280 (1945).

G2 H. E. Gove and H. F. Stoddart, Phys. Rev. 86, 572 (1952).

G3 H. E. Gove, Phys. Rev. 99, 1353 (1955).

G4 P. C. Gugelot, Phys. Rev. 87, 525 (1952).

G5 H. Geiger and E. Marsden, Proc. Roy. Soc. (London), A82, 495 (1909).

H1 J. W. Haffner, Ph.D. Thesis, M.I.T., 1955.

H2 R. Huby and H. C. Newns, Phil. Mag. 42, 1441 (1951).

H3 W. Hauser and H. Feshbach, Phys. Rev. 87, 366 (1952).

H4 R. Huby and H. C. Newns, Proc. Phys. Soc. (London), A64, 618 (1951).

H5 H. J. Hausman, A. J. Allen, J. S. Arthur, R. F. Bender, and C. J. McDole, Phys. Rev. 88, 1296 (1952).

H6 Private communication, E. Henley, Univ. of Washington.

I1 "Elastic Scattering of 40-Mev Alpha Particles from Light Elements", G. Igo, H. E. Wegner, and R. M. Eisberg; preprint to be published in Physical Review.

L1 M. S. Livingston, J. Appl. Phys. 15, 7 (1944).

L2 M. S. Livingston and H. A. Bethe, Revs. Modern Phys. 9, 263 (1937).

L3 A. M. Lane and R. G. Thomas, "The Compound Nucleus Theory of Nuclear Reactions", to be published.

L4 R. E. LeLevier and D. S. Saxon, Phys. Rev. 87, 40 (1952).

M1 Private communication, D. W. Miller, Indiana University.

M2 H. McManus and W. T. Sharp, Phys. Rev. 87, 188 (1952).

M3 C. J. Mullin and E. Guth, Phys. Rev. 82, 141 (1951).

M4 M. A. Melkanoff, S. A. Moszkowski, J. Nodvik, and D. S. Saxon, University of California, unpublished.

M5 M. Moskow, Master's Degree Essay, Johns Hopkins University, May 1948.

P1 C. E. Porter, Phys. Rev. 99, 1400 (1955).

P2 J. Prentki, Cahiers de Phys. 55, 37 (1955). Contains a review of theories for the excitation of nuclei by charged particles.

R1 E. Rutherford, Phil. Mag. 21, 669 (1911).

R2 V. K. Rasmussen, D. W. Miller, and M. B. Sampson, Phys. Rev. 100, 181 (1955).

R3 W. Reizler, Proc. Roy. Soc. (London), A134, 154 (1931).

R4 E. H. Rhoderick, Proc. Roy. Soc. (London), A201, 348 (1950).

R5 Private communication, L. S. Rodberg, M.I.T.

[1] R. C. Buck, Sets and Boolean rings, Pacific J. Math. 4 (1954), 541–554.

[2] R. C. Buck and E. F. Buck, Equal-valued neighborhoods of continuous functions, Proc. Amer. Math. Soc. 15 (1964), 744–749.

[3] L. Gillman and M. Jerison, Rings of Continuous Functions, Van Nostrand, Princeton, N.J., 1960.

[4] E. Hewitt, Rings of real-valued continuous functions. I, Trans. Amer. Math. Soc. 64 (1948), 45–99.

[5] I. Kaplansky, Topological representation of algebras, Trans. Amer. Math. Soc. 68 (1950), 62–75.

[6] J. Nagata, Modern General Topology, Wolters-Noordhoff, Groningen; North-Holland, Amsterdam; Interscience, New York, 1968.

[7] M. H. Stone, Boundedness properties in function-lattices, Canad. J. Math. 1 (1949), 176–186.

[8] M. H. Stone, Applications of the theory of Boolean rings to general topology, Trans. Amer. Math. Soc. 41 (1937), 375–481.

[9] M. H. Stone, Algebraic characterizations of special Boolean rings, Fund. Math. 29 (1937), 223–303.

[10] M. H. Stone, Boolean algebras and their application to topology, Proc. Nat. Acad. Sci. U.S.A. 26 (1940), 280–283.

[11] M. H. Stone, Applications of the theory of Boolean rings to general topology, Trans. Amer. Math. Soc. 41 (1937), 375–481.

[12] M. H. Stone, Boundedness properties in function-lattices, Canad. J. Math. 1 (1949), 176–186.

S1 H. F. Stoddart and R. E. Cove, Phys. Rev. 97, 908 (1955).

S2 G. Schrank, P. C. Gugelot, and I. D. Layton, Palmer Physical Laboratory, Princeton University, September 27, 1954 (unpublished).

S3 L. I. Schiff, "Quantum Mechanics", pp. 87-101, McGraw-Hill Book Co., Inc., 1949.

S4 M. M. Shapiro, Phys. Rev. 90, 171 (1953).

T1 C. J. Taylor, W. K. Jentschke, M. E. Remley, F. S. Eby, and P. G. Kruger, Phys. Rev. 84, 1034 (1951).

T2 E. Bleuler and D. J. Tendam, Bull. Am. Phys. Soc. 30, No. 4, 26 (1955).

T3 This computation was done by W. Tobocman, Institute for Advanced Study, Princeton University.

T4 H. A. Tolhoek and P. J. Brussard, Physica, XXI, 449 (1955).

T5 Private communication, W. Tobocman, Institute for Advanced Study, Princeton, University.

W1 N. S. Wall, Ph.D. Thesis, M.I.T. 1953.

W2 H. E. Wegner, R. M. Eisberg, and G. Igo, Phys. Rev. 99, 825 (1955).

W3 N. S. Wall, J. R. Rees, and K. W. Ford, Phys. Rev. 97, 726 (1955).

W4 V. F. Weisskopf, and D. H. Ewing, Phys. Rev. 57, 472 (1940).

W5 T. R. Wilkins, Phys. Rev. 60, 365 (1941).

W6 J. M. Blatt and V. F. Weisskopf, "Theoretical Nuclear Physics", John Wiley and Sons, N. Y., 1954.

W7 Private communication, N. S. Wall.

W8 G. A. Wrenshall, Phys. Rev. 81, 58 (1949).

W9 R. D. Woods and D. S. Saxon, Phys. Rev. 95, 577 (1954).

BIOGRAPHICAL NOTE

The author was born August 19, 1920 in Indianapolis, Indiana. He was called to active duty as a member of the U. S. Naval Reserve in 1940, commissioned an Ensign in 1943 and subsequently served on board the USS BRAINE (DD630) in the South Pacific until 1945. In December 1945 he was assigned as Operations Officer, Commander Destroyer Squadron 4 and later served as Executive Officer, USS GEARING (DD710). In 1947, in accordance with the U. S. Navy Five Term Program, he was enrolled as an undergraduate at Purdue University and in 1949 was awarded the B.S. degree with Highest Distinction.

He attended the U. S. Naval Postgraduate School, Annapolis, Md. during the academic year 1950-51, as a student in the Ordnance Engineering (Special Physics) curriculum, and was enrolled in the M.I.T. Graduate School, Department of Physics, in June 1951. After obtaining the degree of Master of Science at M.I.T. in June 1953 he was assigned as Commanding Officer, USS C. T. O'BRIEN (DE421). In September 1954 he returned to M.I.T. and was enrolled in the Graduate School of Physics under the provisions of The Advanced Science Program sponsored by the Office of Naval Research.

Publication: "The Radionuclides of Arsenic Produced by Deuteron Bombardment of Germanium", Phys. Rev. 95, 748 (1954), with Lt. J. F. Fagan, Jr.

Thesis
W268 Watters 36226
Angular distributions of alpha particles scattered by light nuclei.